

Study on Particle Breakage of Sands Subjected to Various
Confining Stress and Shear Strain Levels

by

Chien-wen Huang

Supervised by:

Professor Mitsutoshi Yoshimine

A thesis submitted to the Tokyo Metropolitan University

Department of Civil and Environmental Engineering

In partial fulfilment of the requirements for the degree of

Doctor of Philosophy

2015

TABLE OF CONTENTS

TABLE OF CONTENTS	II
ACKNOLEGEMENT	V
ABSTRACT	VII
NOTATIONS	VIII
LIST OF TABLE	X
LIST OF FIGURES	XI
CHAPETER 1 INTRODUCTION	1
1.1 Research Background	1
1.2 Aim and Objectives.....	3
1.3 Organization of the Report.....	4
CHAPTER 2 LITERATURE REVIEW	7
2.1 General Remarks.....	7
2.2 Basic Concept of Particle Breakage.....	7
2.2.1 Particle Breakage Mechanism.....	7
2.2.2 Factors Affecting Particle Breakage	7
2.2.3 Methods of Quantifying Particle Breakage.....	10
2.3 Effect of fines content in Sand.....	12
2.3.1 Effect of fines on undrained Behavior	12
2.3.2 Effect of fines on steady state line (SSL)/ Critical State Line (CSL) ...	13
2.3.3 Intergranular Void Ratio.....	14
2.4 Constitutive Models of Soil in Particle Breakage.....	15
CHAPTER 3 EXPERIMENTAL METHODOLOGY	17
3.1 General Remarks.....	17
3.2 Soil Tested	17
3.2.1 Toyoura Sand	18
3.2.2 JCA Sand.....	18
3.2.3 Takasegawa Sand	18
3.2.4 Inagi Sand	19
3.3 Laboratory Test Procedures	23
3.3.1 Consolidated Drained Triaxial Compression Tests.....	23
3.3.1.1 Triaxial Test Apparatus.....	23
3.3.1.2 Sample Preparation	28
3.3.1.3 Consolidation	29
3.3.1.3 Shearing	30
3.3.2 Minimum and Maximum Density Tests.....	30
3.3.2.1 Test Apparatus	31
3.3.2.2 Sample Preparation	31

3.3.2.3 Test Procedure	32
3.2.2.4 Potential Sources of errors	34
3.3.3 Water absorption of fine aggregates.....	35
3.3.3.1 Test Apparatus	35
3.3.3.2 Sample Preparation	36
3.3.3.3 Test Procedure	36
3.3.4 Micro Experimentation	37
3.3.4.1 General Remarks.....	38
3.3.4.2 Microscopic photographs.....	39
3.3.4.3 Potential Sources of errors	40
3.4 Summary	40
CHAPTER 4 EXPERIMENTAL RESULT ANALYSIS	45
4.1 General Remarks.....	45
4.2 Drained Behavior of Materials.....	45
4.2.1 Stress-Strain Response.....	45
4.2.2 Investigation of Grain size distribution.....	51
4.2.3 Investigation of Particle Breakage	57
4.2.3.1 Increment of fines content	58
4.2.3.2 Marsal's Breakage Index (B_g).....	61
4.2.3.3 Hardin's Breakage Index (B_r)	63
4.2.3.4 Lee & Farhoomand's Breakage Index (D_{15}).....	65
4.2.3.5 D_{50} breakage index.....	67
4.2.3.6 Summary	68
4.3 Brittleness Degree of Sands	76
4.3.1 Introduction.....	76
4.3.2 Determination of Brittleness degree (B_d) value	77
4.3.2.1 Prediction of brittleness degree (B_d) value.....	77
4.3.2.2 Summary	81
4.4 Density Evaluation Based on Test Method for Minimum and Maximum densities of sands	82
4.4.1 Effect of low water content on Minimum and Maximum Densities	82
4.4.1.1 Toyoura sand.....	82
4.4.1.2 JCA sand	84
4.4.1.3 JCA sand (250 μ m-150 μ m).....	85
4.4.1.4 Takasegawa sand	87
4.4.1.5 Inagi sand.....	89
4.4.1.6 Summary of analysis.....	90
4.5 Water Effects Related to Particle Breakage.....	94

4.5.1 Effect of water content and water absorption on densities of sands	94
4.5.2 Determination of minimum dry density- water content relationship....	96
4.5.3 Determination brittleness degree - water absorption relationship	100
4.6 Summary	104
5.1 General Remarks.....	105
5.2 Selection of the constitutive model.....	105
5.2.1 Modified bounding surface hypoplasticity	105
5.2.2 Intergranular void ratio (e_s).....	106
5.2.3 Brittleness degree of soils	107
5.3 Determination of Parameters and input formats	108
5.3.1 Parameter determination of constitutive model	108
5.3.3 Critical state parameters.....	109
5.3.3 Determination of other parameters	110
5.4 Comparison of Predicted Results and Measured Results	111
5.4.1 Experimental Verification	111
5.4.2 Effect of fines on Monotonic loading behavior	114
5.4.2.1 Numerical Modelling	114
5.4.3.2 Results of Numerical Analyses	115
5.5 Summery	131
CHAPTER 6 CONCLUSIONS	134
6.1 General.....	134
6.2 Summary and Conclusions	134
6.3 Recommendations for Future Research	137
References.....	139

To my beloved Grandmother, Father and Mother

ACKNOLEGEMENT

I wish to express my sincere gratitude to my supervisor Professor Mitsutoshi Yoshimine who has been a constant source of ideas, guidance and support throughout the candidature. I especially appreciate his enthusiasm for the subject matter and for tirelessly providing me with critical review of this thesis, which were essential in the development of this study. He is a wise mentor. He clarified my thoughts, and led me through the choices to a course of action that was completely my own. Instead of a destination, he had given me a path of direction.

I thank all of my committee members, Professor Kazuo Nishimura, Professor Atsushi Ueno and Professor Yoshiya Oda, for simultaneously encouraging, guiding, and supporting my research ideas and me. I believe that I am tremendously fortunate to have consulted with outstanding individuals and scholars, and am deeply appreciative to each of them for their important contributions. I am also acknowledge to Professor Kimitaka Uji at the Department of Civil and Environmental Engineering, TMU, for help with academic arrangement. Special thanks go to Professor Motoyuki Inoue whose knowledge, energy, and enthusiasm were critical to this effort.

I wish to dedicate this thesis to my grandmother, Yuki Huang for her encouragement throughout my life and study. I have been extremely fortunate in my life to have grandmother who has shown me unconditional love and support. She always tells me “ learn something from school and 勉強します“. She plays an important role in the development of my identity and shaping the individual that I am today.

I am grateful for the love, encouragement, and tolerance of my parents, Teng-lieh Huang and Li-ser Wu for the support, who have made all the differences in my life. Without their patience and sacrifice, I couldn't have completed this thesis. I also wish to thank my fiancés, Tun-jen Tsai for his support and understanding. His wish and love has provided me a power in overcoming many obstacles in my studies. A special word of thanks also goes to my sister, Chiung-I Huang, and a cousin, Sue Huang, for their continuous support, encouragement during the study.

Finally, I wish to express my thanks to the staff at Department of Civil and Environmental Engineering, Tokyo Metropolitan University for the friendship and support. The financial support received from Tokyo Metropolitan Government is gratefully acknowledged.

Last but not least, I would like to express my gratitude to anyone that should be here and has been forgotten and left out. This has certainly been a great experience.

ABSTRACT

In recent decades, the importance of particle breakage has been recognized in failure phenomena of saturated or near-saturated sandy soils, i.e., ground deformation, landslide, and liquefaction. When sand particles are damaged by abrasion, shearing-off of asperities especially sharp corners or edges, and splitting under higher stress conditions, the particle breakage can change the original physical properties of soils. It alters the stiffness and strength, compresses the volume of the materials, and leads to hazards in practical applications such as bearing capacity reduction of piles and settlement of earth structures.

In this research, I investigated particle breakage by performing a series of triaxial tests on the different types of sand ranging from brittle to stiff materials. The tested materials were consolidated at various confining pressure and sheared up to different axial strain levels. From the experimental results, I quantified the degree of particle breakage in terms of breakage indices. Through these process, I can obtain the degree of particle breakage by triaxial test under a given stress and strain levels.

Despite the fact that triaxial test has be considered as one of the most versatile and widely performed for evaluating the particle breakage phenomenon, the disadvantage of this experimental method is the high expense and large time consuming in practice. Thus, I tried to select alternative methods for assessing particle breakage instead of triaxial compression tests. To find more efficient and less time-consuming approaches to evaluate the particle breakage, I presented a relevant mechanism between particle breakage and water effects. The mechanism is consistent with the experimental results in terms of triaxial compression tests and the minimum and maximum densities of sands associated with differences in mineralogy, particle shape and grain size distribution of the tested materials. Through these experimental results, I propose a conceptual equation to calculate brittleness degree of soils that is useful and reasonable for practical works. This concept was applied to a bounding surface hypoplasticity model for stress-strain behavior of granular soils to examine the effect of particle breakage. The concept of intergranular void ratio was introduced to quantify particle breakage. The increment of fines content (ΔF_c), brittleness degree (B_d) and intergranular void ratio (e_s) are linked and correlated to stress-strain response in the model. The results of model simulation exhibit significant reduction of stiffness and undrained strength of sandy materials due to increase of the potential of particle breakage.

NOTATIONS

- a_p = Water absorption (%)
 B_d = Brittleness degree (1/kPa)
 B_g = Particle breakage index (Marsal 1967)
 B_r = Relative breakage (Hardin 1985)
 B_p = Breakage potential (Hardin 1985)
 B_t = Total breakage (Hardin 1985)
 $d\varepsilon_v^p$ = Volumetric strain increment
 $d\varepsilon_q^p$ = Deviatoric strain increment
 dp = Increment of mean effective stress
 $d\varepsilon_q$ = Increment of mean effective mean stress
 d_{rji} = Stress ratio increments
 d_p = Mean stress increment
 D = Grain size
 D_{15} = 15% diameter
 D_{15i} = Initial 15% size of the materials
 D_{15a} = 15% size of the materials after testing
 D_{50} = Mean grain size
 D_{50i} = Initial 50% size of the materials
 D_{50a} = 50% size of the materials after testing
 D_r = Relative density (dimensionless)
 D_{rmax} = Maximum relative density
 D_{rmin} = Minimum relative density
 e = Void ratio / global void ratio
 e_0 = Void ratio at $p' = 0$ kPa
 e_c = Void ratio at critical state
 e_{ini} = Initial void ratio $p' = 0$ kPa
 e_s = Intergranular void ratio
 F_c = Fines content in decimal
 G = Elastic shear modulus
 G_0 = Material constant for elastic shear modulus
 h_r = Model constant
 H_r = Plastic shear modulus
 I_p = State pressure index,
 K = Elastic bulk modulus
 K_r = Plastic bulk modulus
 M = Failure stress ratio
 M_b = Virtual failure stress ratio

M_d = Dilatancy stress ratio
 M_p = Phase transformation stress ratio
 p' = Effective mean stress
 p_a = Atmospheric pressure
 p'_c = Effective mean stress at critical state
 p'_{ini} = Initial confining pressure
 p_m = Preexisting maximum mean pressure
 q = Deviator stress
 R_f = Stress ratio at failure in compression
 S_{ij} = Deviatoric stress tensor
 ΔF_c = Increment of fines content
 ϵ_a = Axial strain
 ρ_s = Density of solid constituent
 ρ_{dmax} = Maximum dry density
 ρ_{dmin} = Minimum dry density
 ΔW_k = Difference between W_{ki} and W_{kf}
 W_{ki} = Percent by weight retained for each grain size fraction before test
 W_{kf} = Percent by weight retained for each grain size fraction after test
 η = Stress ratio
 κ = Model parameter
 λ = Material constant
 ξ = Material constant
 ν = Poisson's ratio
 ω = Water content (%)
 ω_s = Low water content (%)

LIST OF TABLE

Table 3.2-1 Physical properties of tested sands	20
Table 4.2-1 Summary of test results on four types of sand (1/6)	70
Table 4.2-2 Summary of test results on four types of sand (2/6)	71
Table 4.2-3 Summary of test results on four types of sand (3/6)	72
Table 4.2-4 Summary of test results on four types of sand (4/6)	73
Table 4.2-5 Summary of test results on four types of sand (5/6)	74
Table 4.2-6 Summary of test results on four types of sand (6/6)	75
Table 4.3-1 Summary of brittleness degree for each sands.....	81
Table 4.5-1 Summary of sands with D_{min} at $\omega_s = 0.5\%$	97
Table 5.3-1 Parameters used in model simulation (Wang et al. 2002).....	110
Table 5.3-2 Constants of critical state line for Toyoura sand (Wang et al. 2002).....	110

LIST OF FIGURES

Figure 1.2-1 Significance of research	4
Figure 1.3-1 Organization for body chapters	6
Figure 2.2-1 Definitions of particle breakage index (Revised by Lade et al.; 1996)...	12
Figure 3.2-1 Grain size distribution curves of tested soils.....	20
Figure 3.2-2 Microscope photographs of tested materials - Toyoura Sand	21
Figure 3.2-3 Microscope photographs of tested materials - JCA Sand.....	21
Figure 3.2-4 Microscope photographs of tested materials - Takasegawa sand.....	22
Figure 3.2-5 Microscope photographs of tested materials - Inagi Sand	22
Figure 3.3-1 Schematic diagram of triaxial testing system.....	24
Figure 3.3-2 A photo of the overall view of the triaxial loading system	25
Figure 3.3-3 A photo of the pressure transducer	25
Figure 3.3-4 A photo of the axial loading device.....	26
Figure 3.3-5 A photo of a top plate and a base plate.....	26
Figure 3.3-6 A photo of vacuum system combined with cell pressure system	27
Figure 3.3-7 A photo of (a) pulse motor controller and (b) deformation indicator.....	28
Figure 3.3-8 photos of sample preparation	29
Figure 3.3-9 A photo of side of the specimen after CD triaxial test	30
Figure 3.3-10 A photo of the assembly of the apparatus for the minimum and maximum densities of the sands	31
Figure 3.3-11 Photos of low water content on maximum density (a) drop target water content to material (b) mix the oven-dried soil thoroughly to provide an even distribution of particle sizes (c) pour material to mold (d) tamp the mold (f) trim excessive material by straight knife (f) remove the collar and then scraped the sand level	34
Figure 3.3-12 A photo of The assembly of the apparatus for water absorption of fine aggregates	36
Figure 3.3-13 Photos of water absorption of fine aggregates (a) placed materials in the mold (b) tamped the materials into the mold with 25 drops of the tamper (c) lifted the mold vertically	37
Figure 3.3-14 photos of KEYENCE VHX-2000 microscope.....	38
Figure 3.3-15 Microscope photographs of Toyoura sand before and after CD tests ...	41
Figure 3.3-16 Microscope photographs of JCA sand before and after CD tests.....	42
Figure 3.3-17 Microscope photographs of Takasegawa sand before and after CD tests	43
Figure 3.3-18 Microscope photographs of Inagi sand before and after CD tests	45
Figure 4.2-1 Stress-strain curves at 4 MPa confining pressure	46
Figure 4.2-2 Stress-strain curves at 3MPa confining pressure	47

Figure 4.2-3 Stress-strain curves at 2 MPa confining pressure	47
Figure 4.2-4 Stress-strain curves at 1 MPa confining pressure	48
Figure 4.2-5 Variation of deviator stress with confining pressure for various sands at 20% axial strain.....	49
Figure 4.2-6 Variation of deviator stress with confining pressure for various sands at 15% axial strain.....	49
Figure 4.2-7 Variation of deviator stress with confining pressure for various sands at 10% axial strain.....	50
Figure 4.2-8 Variation of deviator stress with confining pressure for various sands at 5% axial strain.....	50
Figure 4.2-9 Grain size distribution curves of Toyoura sand under a confining pressure of 1MPa to 4 MPa o at 20% axial strain-before and after CD triaxial tests	53
Figure 4.2-10 Grain size distribution curves of JCA sand under a confining pressure of 1MPa to 4 MPa at 20% axial strain-before and after CD triaxial tests.....	54
Figure 4.2-11 Grain size distribution curves of Takasegawa sand under a confining pressure of 1MPa to 4 MPa at 20% axial strain-before and after CD triaxial tests	54
Figure 4.2-12 Grain size distribution curves of Inagi sand under a confining pressure of 1MPa to 4 MPa at 20% axial strain-before and after CD triaxial tests	55
Figure 4.2-13 Grain size distribution curves of Toyoura sand under 4MPa confining pressure at various axial strains-before and after CD triaxial tests.....	55
Figure 4.2-14 Grain size distribution curves of JCA sand under 4MPa confining pressure at various axial strains-before and after CD triaxial tests.....	56
Figure 4.2-15 Grain size distribution curves of Takasegawa sand under 4MPa confining pressure at various axial strains-before and after CD triaxial tests	56
Figure 4.2-16 Grain size distribution curves of Inagi sand under 4MPa confining pressure at various axial strains-before and after CD triaxial tests.....	57
Figure 4.2-17 Increment of fines content versus confining pressure at an axial strain of 20%	59
Figure 4.2-18 Increment of fines content versus confining pressure at axial strain at a confining pressure of 4 MPa.....	59
Figure 4.2-19 Increment of fines content versus confining pressure for Inagi sand....	60
Figure 4.2-20 Increment of fines content versus axial strain for Inagi sand.....	60
Figure 4.2-21 Marsal's breakage index versus confining pressure at an axial strain of 20%	62
Figure 4.2-22 Marsal's breakage index versus confining pressure axial strain at a confining pressure of 4 MPa.....	62
Figure 4.2-23 Hardin's breakage index versus confining pressure at an axial strain of	

20%	64
Figure 4.2-24 Hardin's breakage index versus axial strain at a confining pressure of 4 MPa	65
Figure 4.2-25 D_{15} 's breakage index versus confining pressure at an axial strain of 20%	66
Figure 4.2-26 D_{15} 's breakage index versus axial strain at a confining pressure of 4 MPa	66
Figure 4.2-27 D_{50} 's breakage index versus confining pressure at an axial strain of 20%	67
Figure 4.2-28 D_{50} 's breakage index versus confining pressure at axial strain at a confining pressure of 4 MPa	68
Figure 4.3-1 Increment of fines content and $\sigma_3'/p_a \times \varepsilon_1$ relationship	78
Figure 4.3-2 Marsal's breakage index and $\sigma_3'/p_a \times \varepsilon_1$ relationship	79
Figure 4.3-3 Hardin's breakage index and $\sigma_3'/p_a \times \varepsilon_1$ relationship	79
Figure 4.3-4 Lee & Farhoomand's breakage index and $\sigma_3'/p_a \times \varepsilon_1$ relationship	80
Figure 4.3-5 D_{50} 's breakage index and $\sigma_3'/p_a \times \varepsilon_1$ relationship	80
Figure 4.4-1 Dry density versus water content (Toyoura Sand)	83
Figure 4.4-2 Relative density versus water content (Toyoura Sand)	84
Figure 4.4-3 Dry density versus water content (JCA Sand)	85
Figure 4.4-4 Relative density versus water content (JCA Sand)	85
Figure 4.4-5 Dry density versus water content (JCA Sand, 250 μm -150 μm)	86
Figure 4.4-6 Relative density versus water content (JCA Sand, 250 μm -150 μm)	87
Figure 4.4-7 Dry density versus water content (Takasegawa sand)	88
Figure 4.4-8 Relative density versus water content (Takasegawa sand)	88
Figure 4.4-9 Dry density versus water content (Inagi sand)	89
Figure 4.4-10 Relative density versus water content (Inagi sand)	90
Figure 4.3-11 Water content and maximum density relationship	92
Figure 4.3-12 Water content and minimum density relationship	93
Figure 4.3-13 Water content and maximum relative density relationship	93
Figure 4.3-14 Water content and minimum relative density relationship	93
Figure 4.4-1 Minimum relative density and brittleness degree relationship	98
Figure 4.4-2 Brittleness degree and water content relationship – Marsal's breakage index	98
Figure 4.4-3 Brittleness degree and water content relationship – Hardin's breakage index	99
Figure 4.4-4 Brittleness degree and water content relationship – Lee and Farhoomand's breakage index	99
Figure 4.4-5 Brittleness degree and water content relationship – D_{50} 's breakage index	

.....	100
Figure 4.4-6 Brittleness degree and water absorption relationship - increment of fines content.....	101
Figure 4.4-7 Brittleness degree and water absorption relationship - Marsal's breakage index.....	102
Figure 4.4-8 Brittleness degree and water absorption relationship - Hardin's breakage index.....	102
Figure 4.4-9 Brittleness degree and water absorption relationship – Lee and Farhoomand's breakage index	103
Figure 4.4-10 Brittleness degree and water absorption relationship – D_{50} 's breakage index.....	103
Figure 5.4-1 Comparison between model prediction and test results for stress path on Toyoura sand under different confining pressure	113
Figure 5.4-2 Comparison between model prediction and test results for stress-strain response on Toyoura sand under different confining pressure.....	113
Figure 5.4-3 Simulated Results under various brittleness degree (B_d), for selected value of initial void ratio $e_{mi} = 0.7$ and a confining pressure of 3MPa. (a) stress-strain response; (b) stress path; (c) e_s -axial strain; (d) $e_s - (p')$; (e) fines content- axial strain; (f) fines content- mean effective stress	118
Figure 5.4-4 Simulated Results under various brittleness degree (B_d), for selected value of initial void ratio $e_{mi} = 0.7$ and a confining pressure of 1MPa. (a) stress-strain response; (b) stress path; (c) e_s -axial strain; (d) $e_s - (p')$; (e) fines content- axial strain; (f) fines content- mean effective stress	119
Figure 5.4-5 Simulated Results under various brittleness degree (B_d), for selected value of initial void ratio $e_{mi} = 0.7$ and a confining pressure of 0.3MPa. (a) stress-strain response; (b) stress path; (c) e_s -axial strain; (d) $e_s - (p')$; (e) fines content- axial strain; (f) fines content- mean effective stress	120
Figure 5.4-6 Simulated Results under various brittleness degree (B_d), for selected value of initial void ratio $e_{mi} = 0.7$ and a confining pressure of 0.1MPa. (a) stress-strain response; (b) stress path; (c) e_s -axial strain; (d) $e_s - (p')$; (e) fines content- axial strain; (f) fines content- mean effective stress	121
Figure 5.4-7 Simulated Results under various brittleness degree (B_d), for selected value of initial void ratio $e_{mi} = 0.8$ and a confining pressure of 3MPa. (a) stress-strain response; (b) stress path; (c) e_s -axial strain; (d) $e_s - (p')$; (e) fines content- axial strain; (f) fines content- mean effective stress	123
Figure 5.4-8 Simulated Results under various brittleness degree (B_d), for selected value of initial void ratio $e_{mi} = 0.8$ and a confining pressure of 1MPa. (a) stress-strain response; (b) stress path; (c) e_s -axial strain; (d) $e_s - (p')$; (e) fines	

content- axial strain; (f) fines content- mean effective stress	124
Figure 5.4-9 Simulated Results under various brittleness degree (B_d), for selected value of initial void ratio $e_{ini} = 0.8$ and a confining pressure of 0.3MPa. (a) stress-strain response; (b) stress path; (c) e_s -axial strain; (d) $e_s - (p')$; (e) fines content- axial strain; (f) fines content- mean effective stress	125
Figure 5.4-10 Simulated Results under various brittleness degree (B_d), for selected value of initial void ratio $e_{ini} = 0.8$ and a confining pressure of 0.1MPa. (a) stress-strain response; (b) stress path; (c) e_s -axial strain; (d) $e_s - (p')$; (e) fines content- axial strain; (f) fines content- mean effective stress	126
Figure 5.4-11 Simulated Results under various brittleness degree (B_d), for selected value of initial void ratio $e_{ini} = 0.9$ and a confining pressure of 3MPa. (a) stress-strain response; (b) stress path; (c) e_s -axial strain; (d) $e_s - (p')$; (e) fines content- axial strain; (f) fines content- mean effective stress	128
Figure 5.4-12 Simulated Results under various brittleness degree (B_d), for selected value of initial void ratio $e_{ini} = 0.9$ and a confining pressure of 1MPa. (a) stress-strain response; (b) stress path; (c) e_s -axial strain; (d) $e_s - (p')$; (e) fines content- axial strain; (f) fines content- mean effective stress	129
Figure 5.4-13 Simulated Results under various brittleness degree (B_d), for selected value of initial void ratio $e_{ini} = 0.9$ and a confining pressure of 0.3MPa. (a) stress-strain response; (b) stress path; (c) e_s -axial strain; (d) $e_s - (p')$; (e) fines content- axial strain; (f) fines content- mean effective stress	130
Figure 5.4-14 Simulated Results under various brittleness degree (B_d), for selected value of initial void ratio $e_{ini} = 0.9$ and a confining pressure of 0.1MPa. (a) stress-strain response; (b) stress path; (c) e_s -axial strain; (d) $e_s - (p')$; (e) fines content- axial strain; (f) fines content- mean effective stress	131

CHAPTER 1 INTRODUCTION

1.1 Research Background

Globally, each year, natural disasters such as earthquakes, landslides, tsunamis, floods, hurricanes, volcanoes, and wildfires cause thousands of deaths and trillions of dollars in damages. Man-made disasters have been highlighted in the last decade that over billions dollars from disruption of commerce and destruction of infrastructure to engineering failure. Such significant warnings lead us to aware that identifying the actual treats, prevention and mitigation play a critical role in disaster preparedness and rehabilitation.

Many researches has been performed on subject of the effect of particle breakage in sands on stress-strain conditions when it is subjected to conditions capable of triggers. They concluded granular materials associated with natural slopes, embankments, deep foundations, railroad ballasts, tunnels, as well as in other geotechnical engineering applications, may experiences static and dynamic loading to cause particle breakage. (Miura, 1985, Yasufuku and Hyde, 1995; Leung et al., 1996, Hattori et al., 1998; Ohta et al. 2001; Lobo-Guerrero et al., 2006).

For example, soil particles in the underlying layers of earth dam are subjected to significant stress magnitude and the stresses imposed on the particles exceed their strength, it may cause the particles to break and the increase in fines content decreased hydraulic conductivity of the soil in earth dam. Consequently, this would slow pore-water pressure dissipation and the pore pressure distribution in the earth dam.

Following the devastating 1995 Kobe earthquake, natural hazards, i.e. 1999 Taiwan Chi-Chi, and 2011 Tohoku earthquake induced the complex interaction between the extrinsic and intrinsic thresholds, as in the case of earthquake-induced rapid landslides or particle-breakage-induced liquefaction. Common triggers landslides are intense rainfall, seismic shaking, volcanic eruption, or flood erosion. Because particle breakage and the resulting increase in fines content led to increased soil contraction and liquefaction susceptibility, as the heavy rainfall occurs, the dissipation of pore water pressure within liquefied sloped ground after seismic shaking may generate a landslide and large ground deformation. Huang et al., 2012 observed the slope failures of cut slope with crushable particle in Fudosawa, the branch of Takase River in Nagano prefecture. Due to the extreme weather, slope failure along Fudosawa created and supplied a huge amount of debris into Takase reservoir (Huang et al., 2012).

In this dissertation, the purpose of this research mainly is looking for a low cost and less time-consuming approach to evaluate the particle breakage. We tried to select alternative methods for assessing particle breakage to substitute triaxial tests. Therefore, in this research, firstly, the development of particle breakage under various types of loading path was studied by experimental investigations. In this programme, a multiple of consolidated drained (CD) triaxial compression tests has been performed, analyzed and compared on four types of sands to examine the method of particle breakage as well as associated changes in mineralogy, particle shape, grain size distribution, stress and strain level. We observed the microscope photographs of particle breakage and effect of damage on particle shape. Through these experimental results, we examined the degree of particle breakage in terms of Lee & Farhoomand's breakage index (1967); Marsal's breakage index (1967), Hardin's breakage index (1985); D_{50} 's breakage index and increment of fines content (ΔF_C) (Nakata et al., 1998).

Furthermore, I adopted relative density in strict accordance with the JGS procedures for determining minimum and maximum densities, and observed low water content limits to evaluate the influence of minimum and maximum densities on four types of sands as well as associated changes in material characteristics and grain size distribution. The last but not least, the effect of water absorption on particle breakage phenomena were discussed and proposed a functional relationship between particle breakage with stress-strain and water effect.

Regarding to the numerical studies, by using constitutive models and the critical state soil mechanics framework as a background for the analysis of these comparisons, a series of concluding remarks considering the soils behavior has been drawn. Constitutive models for sand that incorporates the effect of particle breakage was emphasized the change of stress-location of the critical state in intergranular void ratio-logarithm of the mean effective stress (e_s -log(p')) space when particle breakage occurs. This approach differs from earlier research where a unique and static critical state line was assumed. The basic difference between two approach being the question on after particle breakage occurs, do soils knows breakage that it has suffered.

In this research, I presented experimental results on four types of sand and quantified the degree of particle breakage in terms of increment of fines content. Based on observations from increment of fines content, I proposed a conceptual equation to calculate brittleness degree associated with stress and strain levels. I then applied to a bounding surface hypoplasticity model for stress-strain behavior of sandy materials to examine the effect of particle breakage. Besides, the concept of intergranular void ratio

was introduced to link and correlate to stress-strain response in the model. I examined how particle breakage affects engineering properties, such as density, stress-strain behavior and stress response in terms of model simulation.

1.2 Aim and Objectives

In this dissertation, the purpose of this research mainly is looking for a low cost and less time-consuming approached to evaluate the particle breakage. I tried to select alternative methods for assessing particle breakage to substitute triaxial tests. This was separated into three distinct elements:

1. Laboratory testing was carried out to performed, analyzed and compared on four types of sands to examine the methods of particle breakage.
2. Detailed data analysis was undertaken to evaluate alternative factors that affect particle breakage.
3. Model simulation was adopted to evaluate the effects of particle breakage on shear response of sands.

To meet this aim the following objectives were set, the significant of research is shown in Figure 1.2-1:

- (1)To investigate the particle breakage behavior under consolidated drained triaxial compression test and then quantify the magnitude of particle breakage.
- (2)To consider and perform some other factors that may affect particle breakage and select an alternative method to substitute triaxial tests for assessing particle breakage.
- (3)New and simple linear concept of brittleness degree was proposed to estimate fines content.
- (4)New concept was applied to a bounding surface hypoplasticity model for stress-strain behavior of granular soils to examine the effect of particle breakage. The concept of intergranular void ratio was introduced to quantify particle breakage.
- (5)The increment of fines content, brittleness degree and intergranular void ratio are linked and correlated to stress-strain response in the model.

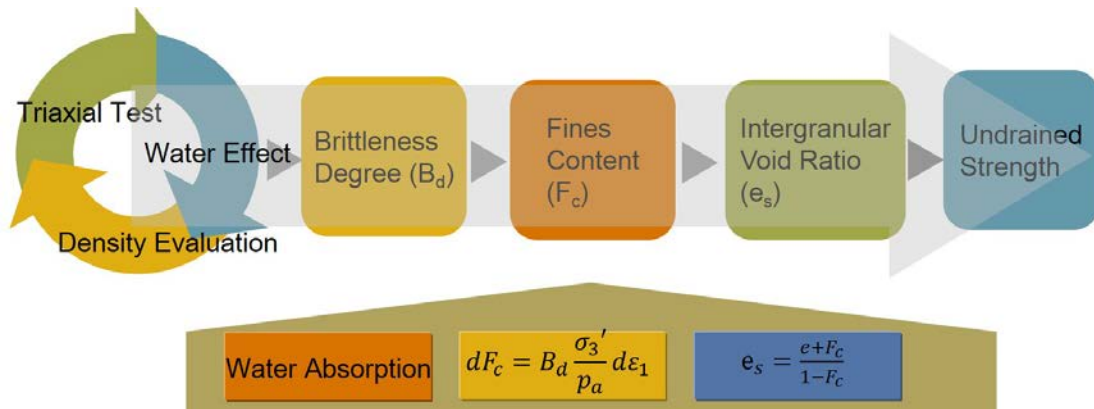


Figure 1.2-1 Significance of research

1.3 Organization of the Report

This thesis is organized in six chapters and the contents of each chapter are briefly summarized below. The dissertation process is shown in Fig. 1.3-1.

Chapter 1 is the introduction of this study which emphasized the importance of conducting experimental study on particle breakage of granular materials in geotechnical issues. Following the introduction, Chapter 2 contains the literature review where general background theory for the behavior of sands is presented with attention to the various factors affecting particle breakage, mechanism of particle breakage, and methods of quantifying particle breakage. The effect of water action phenomenon on particle breakage is also focused in the context of practical technology for evaluating degree of particle breakage. Besides experimental researches, challenges of analytical approaches were reviewed and reported, which attempted to overcome the problems encountered with the presence of particle breakage. Especially three literatures were carefully reviewed, namely, basic concepts of constitutive laws, existing numerical failure shape functions and yield surface by Wang et al., intergranular void ratio criteria by Thevanayagam, and an approach of developing a constitutive model respective of fines content by Rahman, since these concepts play important role in the proposal of new model in Chapter 5.

Chapter 3 describes the details of four tested materials used in this study and the testing program including consolidated-drained (CD) triaxial tests and test method of minimum and maximum density of soils, as well as measuring water absorption of fine aggregates. The specifications of the materials used were represented by grain size distributions and particle shape observed through microscope. Instrumentation and data acquisition system of the high pressure triaxial device are also introduced along with the

details of the testing procedure including the sample preparation processes used for the formation of the specimens.

Chapter 4 reports the experimental results obtained from CD triaxial tests, minimum and maximum density tests of soils and water absorption tests for fine aggregates. A total of 129 CD triaxial tests, 83 minimum density tests and 68 maximum density tests, as well as 32 water absorption tests were conducted on the four different sands which have different particle shape and different grain size distribution. In the series of triaxial tests, consolidated at various confining pressure and sheared up to different axial strain levels. The test results are carefully examined including the stress-strain relationship and grain size distribution curves before and after each shear test to reveal the nature of particle breakage. The amount of particle breakage were evaluated and quantified by various particle breakage indices in terms of Marsal's breakage index, Hardin's breakage index, Lee and Farhoomad's breakage index, as well as the shift of mean particle diameter (D_{50}) and the increment of fines content (ΔF_c). Besides the effects of water action to the particles were investigated for four types of material by examining the influence of low water contents on the minimum and maximum densities. Water absorption of the selected materials are also measured to examine the effects of water action. Finally, water effects related to particle breakage is then summarized and a conceptual equation based on increment of fines content (ΔF_c) and brittleness degree (B_d) associated with stress and strain levels is then proposed and discussed in this chapter.

In Chapter 5, a constitutive model of sands is proposed. The proposed procedure for incorporating brittleness degree (B_d) of soils into the bounding surface hypoplasticity model for granular soils and the concept of intergranular void ratio (e_s) is described step by step. Undrained shear behavior of sands with different brittleness degree (B_d) - values was predicted using the proposed constitutive model. It was shown that brittleness of particles has significant effect on undrained stress-strain relationship of the sands. When B_d - value was higher, the stiffness and undrained strength considerably decreased. This numerical study confirms that brittleness of particles should be carefully and properly considered in engineering designs.

Lastly Chapter 6 gives the conclusions of this study and recommendations for future research.

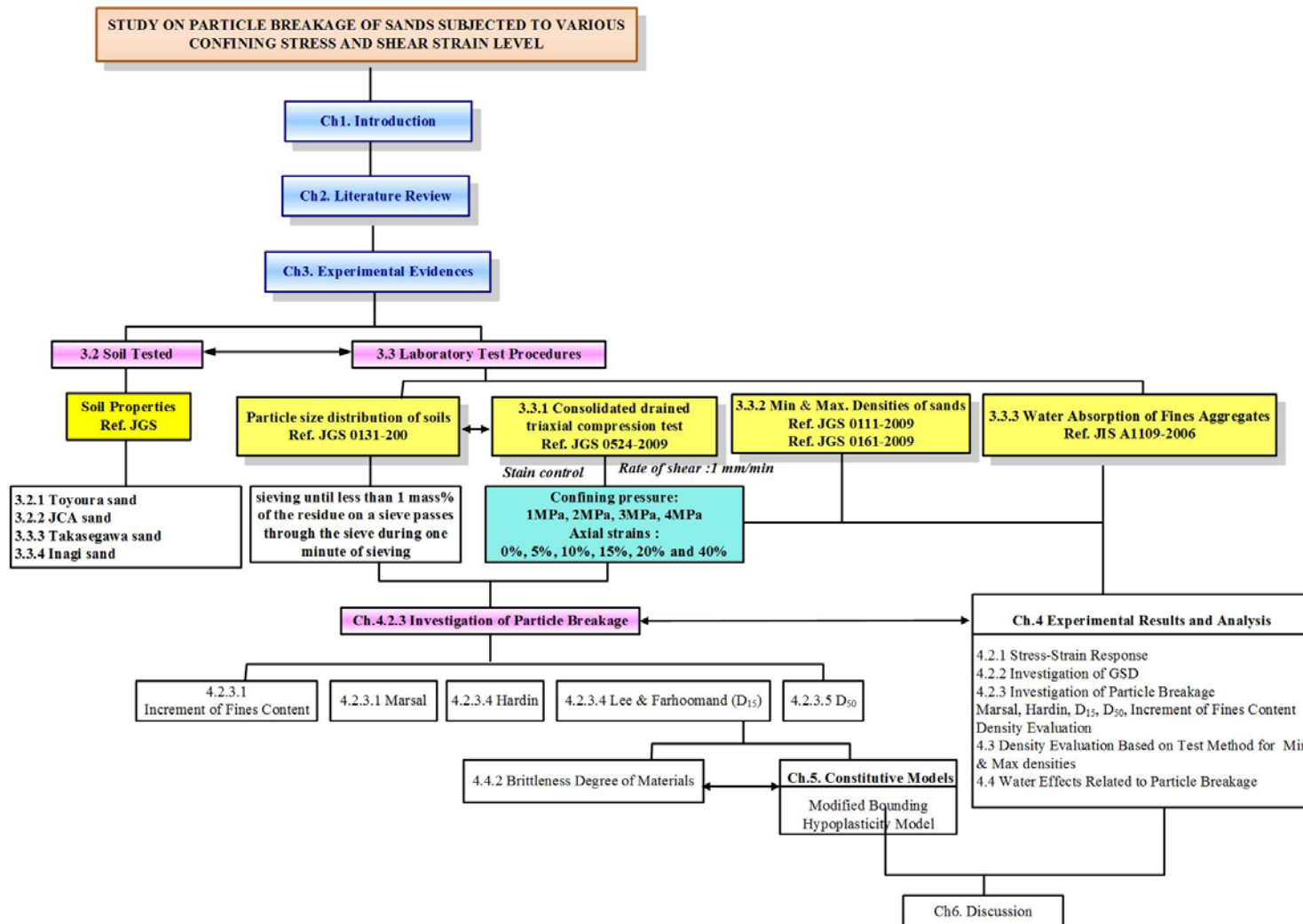


Figure 1.3-1 Organization for body chapters

CHAPTER 2 LITERATURE REVIEW

2.1 General Remarks

A review of the theoretical background and literature relevant to this study is presented in Chapter 2. In this dissertation, the literature review and the research are linked between experimental evidence and modelling simulation. A review of particle breakage phenomenon of sands associated changes in mineralogy, particle shape, grain size distribution stress and strain level are presented. All literatures are presented in three different parts. Part one focuses on basic concept of particle breakage with special attention to particle breakage mechanism, factors affecting particle breakage, and methods of quantifying particle breakage. Part two discusses the effect fines on undrained behavior and critical state soil mechanics affect by the present of fines. Part three discusses about the basic concepts of constitutive law for granular soils and existing models of sand with particle breakage irrespective of fines content.

2.2 Basic Concept of Particle Breakage

2.2.1 Particle Breakage Mechanism

Previous studies have investigated particle breakage mechanism on different aspects in terms of soil response, particle hardness and grain size distribution. Accordingly, when the particles subjected to stresses, the dominant modes of particle breakage have been presented as disintegrative fracture, attrition, abrasion or particle splitting and so on. (Marsal 1967; Hardin 1985; Rahim 1989; Coop 1990; Pestana and Whittle 1995; Nakata et al. 2001a, 2001b; Chuhan et al. 2002; Mesri and Vardhanabhuti, 2009). In general, particle breakage reduces the particle size of materials when particles sheared with neighboring particles under stress conditions (compression or shearing). The development of the particle breakage evolves at the center or near the contact points with other surrounding particles. It has been pointed out that particle shapes may change significantly with materials characteristics, stiffness, strength anisotropy, stress conditions and strain level.

2.2.2 Factors Affecting Particle Breakage

It has been point out that particle breakage occurs when the stresses imposed on particle exceed their strength (Lade, 1996). According to the previous publication, there are several factors that affect the amount of particle breakage in a soil including particle

density, strength, angularity, grain size distribution, stress level, strain level, and anisotropy (Hall and Gordon, 1963; Vesic and Barksdale, 1963; Bishop, 1966; Lee and Farhoomand, 1967; Hardin, 1985; Coop and Lee, 1993; Lade et al., 1996; Yamamuro and Lade, 1996; McDowell and Bolton, 1998; Coop et al., 2004; Tarantino and Hyde, 2005; Lobo-Guerrero and Vallejo, 2005; Valdes and Caban, 2006; Erzin and Yilmaz, 2008; Melboucil et al., 2008). The summary of factors are shown in the followings:

1. Soil mass properties

(1) Particle size distribution

Hall and Gordon (1963) performed drain triaxial compression tests on gravelly soils and reported that more particle breakage occurred during the tests, especially during the shear stage, and that uniformly graded soil produced considerably more particle breakage than well-graded soil. Both monotonic tests (Marsal, 1967) and cyclic tests (Indraratna et al., 2000, 2003) on ballast specimens have indicated well-graded soils do not break down as easily as uniform soils. As the relative density increases, the amount of particle breakage decreases. In a well-graded soil, more particles surround individual grains reducing the average contact stress and decreasing particle breakage (Lee and Farhoomand, 1967; Lade et al., 1996).

(2) Initial void ratio

Decreasing void ratio decreases particle breakage because smaller void ratios generally yield a larger number of particle contact and a better distribution of stresses produced by neighboring particles (Lade et al., 1996; McDowell and Bolton, 1998; Nakata et al., 2001a).

(3) Stiffness

A stiffer specimen would suffer more particle damage by sustaining larger stresses during constant volume-undrained shear (Nakata et al., 2005).

2. Particle properties

(1) Mineralogy

For example, Coop and Lee (1993) concluded that, for different mineralogies of sands, there is a unique relationship between the amount of particle breakage that occurs upon shearing to a critical state and the mean normal effective stress.

(2) Hardness

Increasing the mineral hardness decreases the amount of particle crushing. The harder or stronger particle materials show smaller amounts of breakage for a given stress (Marsal, 1967; Hardin, 1985; Lade et al., 1996; McDowell and Bolton, 1998; Fedá, 2002).

(3) Shape

According to Lee and Farhoomand (1967); Hardin (1985), and Lade et al. (1996), increasing the particle angularity increases particle breakage. Angular particles break more easily because stresses can concentrate along their narrow dimension, thus fracturing the particle. Stresses can also concentrate at angular contact points, causing the points to fracture.

(4) Size

Lade et al. (1996) presented that as the particle size increases, particle crushing also increases. This is due to the fact that larger particles contain more flaws or defects, and they have a higher probability of the defect being present in the particles that will break. Smaller particles are generally created from larger particles fracturing along these defects. As the breakdown process continues, there are fewer defects in the subdivided particles.

3. External Parameter

(1) Time

The quantity of particle breakage is also a function of time. Even under constant stress states of sufficient magnitude, particle breakage continues with time, but at decreasing rates. This time effect shows up externally as creep of the soil, as presented and discussed in detail by Yamamuro and Lade(1993) ; Leung et al. (1996); Takei et al. (2001); McDowell and Khan (2003); Karimpour and Lade (2010).

(2) Mode of loading

A number of studies have reported that the amount of particle breakage is related to the mode of loading during triaxial testing on granular soils at high pressure and shearing. For example, Vesic and Barksdale (1963) conducted a drained triaxial compression test on a medium-grained sand and observed that the amount of particle breakage increased with increasing confining pressure. Furthermore, Bishop (1966) identified that more breakage occurs during the shearing stage of a triaxial test than during the consolidation stage. Yamamuro and Lade (1996) also concluded that more

particle breakage occurs during shearing than during isotropic compression.

(3) Effective confining stress

Increasing effective confining stress increases particle breakage (Lade et al., 1996).

(4) Shear displacement

Increasing shear displacement increases particle damage (Agung et al., 2004; Coop et al., 2004; Lobo-Guerrero and Vallejo, 2005).

(5) Water

A number of studies have reported that the amount of particle breakage is related to the effect of water action. For example, Nobari and Duncan (1972) performed investigation of the factors that influence the collapse of rockfill upon flooding. They found that the initial water content was the most important factor determining the amount of collapse upon flooding. Miura and Yamanouchi (1975) also observed that soil particles crack more easily at higher water content. Das (2002) described that the decrease of dry densities with the increase of water content can be attributed to the capillary tension effect. The capillary tension in the water inhibits the tendency of the soil particles to move around and be densely compacted.

(6) Temperature

Temperature can affect the particle damage susceptibility of some minerals (Nakata et al., 2003; Chester et al., 2004).

2.2.3 Methods of Quantifying Particle Breakage

The amount of particle breakage has been investigated in numerous studies. For example, a number of studies have attempted to quantify the degree of particle breakage (Lee and Farhoomand, 1967; Marsal, 1967, Miura and O'Hara, 1979; Hardin, 1985; Lade et al., 1996). Empirical methods by which to quantify the particle breakage consider changes in specific particle size, e.g., Lee and Farhoomand's relative breakage, the entire grain size distribution before and after loading, e.g., Hardin's relative breakage, and surface area increment, i.e. Miura and O'hara's particle breakage. In this study, I adopted several techniques in order to examine the degree of particle breakage (Lee and Farhoomand, 1967; Marsal, 1967; Hardin, 1985). Having compared the various alternative methods, I adopt the particle breakage index, B_g , used in a number of studies. The definitions of breakage index is depicted in Figure 2.2-1.

Marsal (1967) developed an index of particle breakage, B_g (%), under the assumption that the percentage of particles retained in large size sieves will decrease and the percentage of particles retained in small size sieves will increase (Indraratna and Salim 2002). In this technique, the change (ΔW_k) in weight of the percentage retained, which is equal to the weight of the percentage retained after the test (W_{kf}) minus that retained before the test (W_{ki}), was plotted for each grain size fraction with respect to the corresponding aperture size (Indraratna and Salim 2002). Marsal's breakage index falls in the category of increase in percent passing a single sieve size. When the increase in percent passing is stationary at only one diameter over the range of initial particle size as in Figure 2.2-1, Marsal's breakage index is equal to the increasing in percent passing the sieve suffering the greatest increase (Hardin, 1985).

As shown in Figure 2.2-1, Hardin (1985) defined the relative breakage, B_r (B_t/B_p), as the integral of the changes in the grain size distribution curve for all sizes greater than $74 \mu\text{m}$ (No. 200 U.S. sieve size) caused by a given loading for a given soil, where the B_p is the area under the grain size distribution curve between $D > 74 \mu\text{m}$ and a vertical line defining the upper limit of the silt size, i.e., $D = 74 \mu\text{m}$ (Hardin, 1985; Sadrekarimi and Olson, 2010). Moreover, B_t is defined as the area under the initial grain size distribution curve and the final grain size distribution curve. The relative breakage has a lower limit of zero and a theoretical upper limit of unity (Lade et al, 1996; Sadrekarimi and Olson, 2010).

Lee and Farhoomand (1967) proposed the concept of particle breakage when investigating earth dam filter materials according to Terzaghi's design criteria of drains and filters. They defined relative crushing, $B_g = D_{15i}/D_{15a}$, as the ratio of the initial 15% size of the materials, D_{15i} , to the 15% size of the materials after testing, D_{15a} . Since particle size is plotted on a log scale, the ratio is determined by the horizontal distance between grain size distribution curves at 50% finer as shown in Figure 2.2-1.

Here, D_{50} , which is the grain size corresponding to 50% of the materials by weight, is commonly used to describe the general shape of the grain size distributions. Recently, the change in D_{50} has been used to assess the rate of particle breakage and after the tests. For example, Ghanbari et al. (2008) investigated the particle breakage phenomenon in rockfill samples under large-scale direct shear test and CD triaxial test. The breakage index of D_{50} is defined as the ratio of the D_{50i} of materials before test to the D_{50a} of materials after test, i.e., D_{50i}/D_{50a} . Since particle size is plotted on a log scale, the ratio is determined by the horizontal distance between grain size distribution curves at 15% finer as shown in Figure 2.2-1.

The degree of particle breakage was measured in terms of the increment of fines content (the percentage of particles finer than 75 μm in diameter), ΔF_c , which is the change between the fines content of the sheared specimen and the original specimen as shown in Figure 2.2-1 (Nakata et al., 1998).

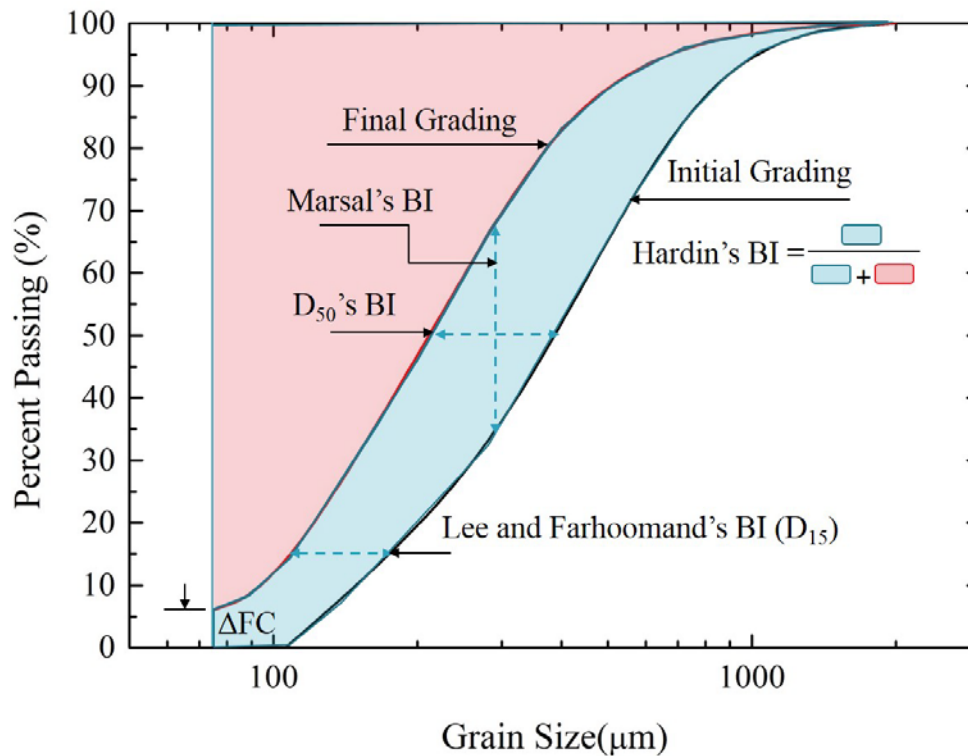


Figure 2.2-1 Definitions of particle breakage index (Revised by Lade et al.; 1996)

2.3 Effect of fines content in Sand

2.3.1 Effect of fines on undrained Behavior

Pitman et al. (1994) performed monotonic test on Ottawa C-109 sand mixed with crushed non-plastic silica fines did use a systematical variation in the fines content. These tests suggested that the behavior of the Ottawa sand became more dilative as the fines content was increased, with less strain-softening response being observed. At a fines content of 40%, the stress path indicates only strain hardening towards the steady state. The steady state line in void ratio-effective stress space also changes with a change in fines content. For a fines percentage of less than 20% the steady state line location moves down, and for a fines percentage of larger than 20% the steady state line location moves up towards the 0% fine location.

Lade and Yamamuro (1997) study the effect of non-plastic fines on the static

liquefaction behavior of four different clean base sands. The result shows that the test specimens reached a lower peak stress and exhibited more contractive behavior as the fines content of the sand was increased.

2.3.2 Effect of fines on steady state line (SSL)/ Critical State Line (CSL)

The effects of small amounts of low-plasticity fines on the critical state line (CSL) of sands were first investigated by Been and Jefferies (1985). A number of studies on the influence of fines content on the undrained monotonic response of sands have been published in recent years (Lade and Yamamuro, 1997; Thevanayagam, 1998; Thevanayagam et al., 2002; Ni et al., 2004).

Been and Jefferies (1985), based on the test results on Kogyuk 350 sand with different fines contents, suggested that the slope of the steady state line in void ratio-effective stress space increases with increasing fines content, which is consistent with a trend towards greater compressibility with increasing fines content.

Zlatovic and Ishihara (1995) reported that the SSLs for Toyoura sand with fines move downwards with increase in fines content in e - $\log(p')$ space up to a fines content around 30%, but moves upwards for fines content $>30\%$. Thevanayagam and Mohan (2000) investigated the undrained response of silty sands. They reported that for the same host sand, a unique SSL exists for silty sands in the e_s versus p' plane at all fines contents and that this SSL is expected to coincide with the SSL for the host sand. Thevanayagam et al. (2002) and Ni et al. (2004) have shown that the addition of non-plastic fines to sand causes a clear downward translation of the CSL in e - $\log(p')$ space, which implies that the overall dilativeness decreases with increasing fines content for a given void ratio.

Yang et al. (2006) investigated the Steady State Lines (SSL) for sand-silt mixture with various fines contents (0, 5, 10, 15, 20, 30, 50, 70, and 94%) from drained and undrained compression tests. It was observed that the location of the SSL in the e - $\ln p'$ space was different for each mixture and depended on the fines content in the mixture. The slopes of SSL are similar with the fines content that was less than the Transition Fines content (TFC). Bouckovalas et al. (2003) proposed an ideal effect of the non-plastic silt content and effective stress on the SSL of sandy soil and observed the same effect as observed by Been and Jefferies (1985).

2.3.3 Intergranular Void Ratio

The concept of an inter-granular void ratio has been investigated by a number of researchers and it is pertinent to note that inter-granular void ratio has also been referred to by different names in the literature: void ratio at granular phase (Mitchell 1976), skeleton void ratio (Kuerbis et al., 1988), granular void ratio (Georgiannou et al., 1990), inter-granular void ratio (Thevanayagam, 1998). For consistency, the term “inter-granular void ratio” is used in this thesis. Kuerbis et al. (1988) may be the first who used inter-granular void ratio as comparison basis for soil strength behavior. They found the inter-granular void ratio was increasing with increasing non-plastic fines. But they found that measured soil response showed more dilative tendency instead of contractive tendency as $e_{skeleton}$ increases with increase in fines content which is contradictory to normal behavior. Thus, it was realized that the inter-granular void ratio calculated from above formula is not applicable for entire range (0% to 40%) of fines content.

They suggested that fines particle may simply be occupying void in the sand skeleton and therefore, the measured behavior is controlled by the force chain in sand skeleton. Thus, by neglecting the volume of fines they defined skeleton void ratio, $e_{skeleton}$ and defined by the following expression:

$$e_{skeleton} = \frac{V_T G_s \rho_w - (M_T - M_{silt})}{(M_T - M_{silt})} \quad (2.1)$$

where V_T = total volume of specimen, G_s = specific gravity of sand, ρ_w = density of water, M_T = total mass of specimen and M_{silt} = mass of silt in specimen.

Georgiannou et al. (1990) observed effective stress paths in triaxial compression were almost identical for a constant inter-granular void ratio as shown in Figure 2. 16 and undrained brittleness increased with increasing inter-granular void ratio for Ham river sand with Speswhite kaolin. They calculated inter-granular void ratio by considering the volume of clay equal to zero, and they called it as “granular void ratio, e_{gr} ”.

They expressed granular void ratio as:

$$e_{gr} = \frac{\text{volume of voids} + \text{volume of clay}}{\text{volume of granular phase}} \quad (2.2)$$

Following the work of Georgiannou et al. (1990), Ovando-Shelley and Pérez (1997)

found that intergranular void ratio is also a very significant parameter for Coatzacoalcos River sand with fines.

Thevanayagam (1998) found that the SS point related to sand with non plastic fines are located close to a single SSL when plotted in e_s - $\log(p')$ space. He simplified the concept of inter-granular void ratio significantly by considering silty sand consists of two sub-components: coarse particles and fines particles. When coarse particle to coarse particle contacts dominate soil behaviors, he defined intergranular void ratio as:

$$e_s = \frac{e+F_c}{1-F_c} \quad (2.3)$$

where e_s = inter-granular void ratio, e = global void ratio and F_c = fines content in decimal with respect to total dry weight of solid.

2.4 Constitutive Models of Soil in Particle Breakage

Many constitutive models have been developed by different researchers to describe the stress strain behavior of soils. Some of these models have been developed into finite element models for the solution of real applications, whereas others have been developed for triaxial plane simulations. The most popular models for monotonic and cyclic loading conditions are those based on bounding surface and classical plasticity.

Simulation of particle breakage in sands is one of the major challenges in constitutive modeling of geotechnical materials. Following the terminology introduced in Chapter 2, particle breakage refers to the range of phenomena that would be characterized under static and cyclic loading. It has been known that several researchers have proposed empirical methods to quantify the particle breakage and a number of models has been developed based on those empirical methods in to three categories (Gerolymos, 2007): (a) semi-empirical expressions based on grain size distribution before and after testing by Leslie (1963), Lee and Farhoomand (1967), Marsal (1967), Miura and O'Hare (1979), Hardin (1985), Fukumoto (1992) and Nakata et al. (1999). (b) Critical state models in which the size of the yielding surface is related to the amount of particle breakage (Gerolymos, 2007; Nakata et al. (1999); Nakata et al. (2001). (c) The compressibility models, based on a statistic function and work equation, i.e. McDowell et al. (1996) and; based on water – induced phenomenon by Oldecop and Alonso (2001).

The fundamental stress-strain relationship of granular materials under static and cyclic loading conditions have been made over 30 years by many researchers, i.e.,

Prevost (1981), Dafalias (1986), Wang et al.(1990); Manzari and Dafalias (1997); Zienkiewicz et al. (1999); Li (2002); Yang et al. (2003); Park and Byrne (2004); Dafalias and Manzari (2004); Taiebat and Dafalias (2008); Anandarajah (2008); Yin et al. (2010);Yin and Chang (2013).

For example, Wood et al. (1994) presented a simple sand model for describing density dependent and pressure-dependent response of sands. The strain softening under drained conditions can be reproduced by combining a simple monotonic hardening relationship with a link between the current peak strength and a state parameter. It is assumed that the available peak stress ratio is linked with the current value of the state parameter through an empirical relationship.

Bounding surface models for soils are primary based on the work of Dafalias and Popov (1975) and Krieg (1975). In these models a bounding (or ultimate) surface is first determine in the principal stress space. For stress states inside the bounding surface plastic deformation can occur, the level of which is set by distance of the stress point from an image point on the bonding surface. The distance sets the magnitude of the plastic modulus at that point. The model incorporate flow rules and hardening due to plastic isotropic and deviatoric shear strain (Woodward, 2001).

Among them, Wang et al. (1990) developed the bounding surface hypoplasticity model for granular soils. According to the theory, the strain rate direction depends on current state of stress and stress rate direction. This model has been successfully applied to simulate a fully nonlinear site response for cyclic and monotonic loading (Li et al. 1992, 1998; Arulanandan et al., 2000). However, the model demonstrated by Wang et al. (1990) had several limitations. For instance, the model does not prescribe a zero dilatancy at the limit of critical state (Gerolymos, 2007). To overcome the limitations, the modified bounding surface hypoplasticity model was developed based on the original framework of Wang et al. (1990). The modified model is effective-stress-based model written in tensor form for general loading conditions and is applicable to fully couple static and dynamic problems for both loose sands and dense sands. This model was also implemented to incorporate into the finite element program, FLAC, to solve static, dynamic and soil structure interaction problems (Li et al., 1999; Wang et al. 2002).

CHAPTER 3 EXPERIMENTAL METHODOLOGY

3.1 General Remarks

This chapter discusses in details the development of laboratory testing system to study the manner in which particle breakage occurred when the stresses imposed on soil particles in various sands including a series of CD triaxial test, the minimum and maximum densities of sands, and water absorption of fine aggregates.

A programme of multiple CD triaxial tests (JGS 0524-2009) had been carried out to investigate stress-strain response and particle breakage of granular materials. Additionally, the grain size distribution curves were obtained for each sand after particle breakage, and the results were compared to the corresponding original curves. Furthermore, a series of minimum and maximum density of sands were also conducted on four sand specimens to investigate the sensitivity of slight water content and water absorption ability. Finally, the particle shape with different morphology was examined by microscope photography. The understanding gained from these were then used in the interpretation of the particle breakage and water action which are presented and discussed in Chapter 4. The test methods used to determine the density of soil particles, the minimum and maximum densities of sands, particle size distribution of soils and water absorption of fine aggregates are specified in JGS 0111-2009, JGS 0161-2009, JGS 0131-2009 and JIS A1109-2006, respectively.

In this chapter the materials, test apparatus are reviewed. The testing procedure for the consolidated drained triaxial compression test, low water content affect minimum and maximum density of soils, and water absorption test of fine aggregates are described including the materials, pressures and loading used. Data acquisition and processing are discussed in this chapter along with the test apparatus.

It should be noted that the knowledge on the experimental methodology is not only a prerequisite for the experiment techniques used in this study, but also it is required for proper and consistent interpretation of data from the literature. In Chapter 4, a large data base is developed for theoretical development of brittleness degree, B_d . The data collected from interpreted based on the knowledge of current experiment methodology.

3.2 Soil Tested

I selected four types of sand, which were characterized by various particle shapes and sizes, rather than using materials with similar characteristics, in order to examine

the degree of particle breakage. It is expected that different soils respond and produce different values of particle breakage regarding their different particle textures and physical properties. The four tested materials, Toyoura sand, JCA sand, Takasegawa sand, and Inagi sand, used in the consolidated drained triaxial compression test and minimum and maximum density test, as well as water absorption test of fine aggregates, were arranged based on the results of sieving analysis.

3.2.1 Toyoura Sand

Toyouura sand, which was Japanese standard sand, is a clean uniform sand with angular to a subangular quartz-rich particle shape. The density (ρ_s) of Toyoura sand was 2.656 g/cm^3 and the water absorption of 0.258%. The maximum (ρ_{dmax}) and minimum (ρ_{dmin}) dry densities were 1.645 g/cm^3 and 1.335 g/cm^3 , respectively. Figure 3.2-1 indicates that the grain size distribution of Toyoura sand, which is relatively narrow (from $106 \mu\text{m}$ to $300 \mu\text{m}$), is different from those of other materials.

3.2.2 JCA Sand

Newly Japan Cement Association (JCA) sand, which is standard sand composed of quartz with silica content, is used for cement testing. The particles of JCA sand are round and smooth. Moreover, JCA sand has a density of 2.652 g/cm^3 and the water absorption is 0.448%. The maximum (ρ_{dmax}) and minimum (ρ_{dmin}) dry densities were 1.779 g/cm^3 and 1.529 g/cm^3 , respectively. In addition to Toyoura sand, JCA sand has a very wide range of grain size from several microns to over 2 mm (Figure 3.2-1). Since the membranes of specimens were easy to break when JCA sand were used in the experiments, puncturing of the membranes during high pressure tests on the JCA sand was prevented by restricting the grain size distribution. Thus, soil particles larger than $850 \mu\text{m}$ (equivalent to a No. 20 sieve) were discarded by dry sieving.

3.2.3 Takasegawa Sand

Takasegawa sand was obtained by sieving and collecting particles of disastrously occurring talus cone deposit at Fudosawa, a branch of the Takase River in Nagano Prefecture in Japan, which consisted of debris with a wide range of sizes. Slope failures along Fudosawa area created and supplied a huge amount of debris into the Takase reservoir (Huang et al., 2012). Talus cone deposits reworked by debris flows in Fudosawa area characterized by granite. The geology of the study area and its vicinity comprises primarily Tertiary Period to mid-Cretaceous granite and intrusive igneous

rocks, such as andesite and sedimentary rocks from the Quaternary Period. Granite with hard, tough and less fractured characteristics occupies the largest part of this study area. In the talus cone slope, however, it appears that granite has experienced the severely weathering processes and hydrothermal alternation. The heat source for hydrothermal alternation is inferred to be related with the intrusion of igneous rocks. Some insight into the reason for this was indicated by INOUE (2000) that andesite mostly occurred as dikes of various widths and was intruded along fault zones leading to the granite severely fractured and contains several intersecting faults associated with shale.

Takasegawa sand comprises primarily quartz and feldspar of angular to subangular shape with $\rho_s = 2.652 \text{ g/cm}^3$ and the water absorption of 0.714%. Nevertheless, due to the angularity of Takasegawa sand, the membranes of specimens were easy to break in the experiments. Puncturing of the membranes during high pressure tests on the coarse soil was prevented by restricting the grain size distribution. Thus, the grain size distribution curve was designed so as to generate higher confining pressures on specimens, which were passed through a No. 40 sieve (450 μm) and retained by a No. 140 sieve (106 μm).

3.2.4 Inagi Sand

Inagi sand is well-graded sand and contains a large amount of fines. For Inagi sand, $\rho_s = 2.691 \text{ g/cm}^3$, the water absorption = 3.010%, $\rho_{dmax} = 1.487 \text{ g/cm}^3$, and $\rho_{dmin} = 1.183 \text{ g/cm}^3$. Inagi sand particles are slightly weathered due to having been located above the ground water level during and after the last glacial age after having been deposited under water during the Pleistocene Era (Kawabe et al., 2011). The shapes of the particles are angular to subangular.

In order to make the experimental condition consistency, consolidated drained triaxial compression test, minimum and maximum density test of soils and water absorption test of fine aggregates were performed on sands graded in the range of 300 μm to 106 μm for Toyoura sand, 850 μm to 106 μm for JCA sand, 2,000 μm to 106 μm for Inagi sand, and 850 μm to 106 μm for Takasegawa sand. The physical properties of the tested materials are listed in Table 3.2-1, the designed grain size distribution curves are shown in Figure 3.2-1 and the microscope photographs of Toyoura sand, JCA sand, Takasegawa sand and Inagi sand are shown in Figure 3.2-2 to Figure 3.2-5, respectively.

Table 3.2-1 Physical properties of tested sands

Materials	Density, ρ_s (g/cm ³)	ρ_{dmax} (g/cm ³)	ρ_{dmin} (g/cm ³)	D ₅₀ (designed) (mm)	Circularity ($4\pi \times \frac{Area}{Perimeter^2}$)	Water Absorption (%)
Toyoura Sand	2.656	1.645	1.335	0.207	0.754	0.279
JCA sand	2.652	1.779	1.529	0.424	0.827	0.421
Takasegawa Sand	2.652	1.637	1.373	0.354	0.434	0.714
Inagi Sand	2.691	1.487	1.183	0.432	0.556	4.707

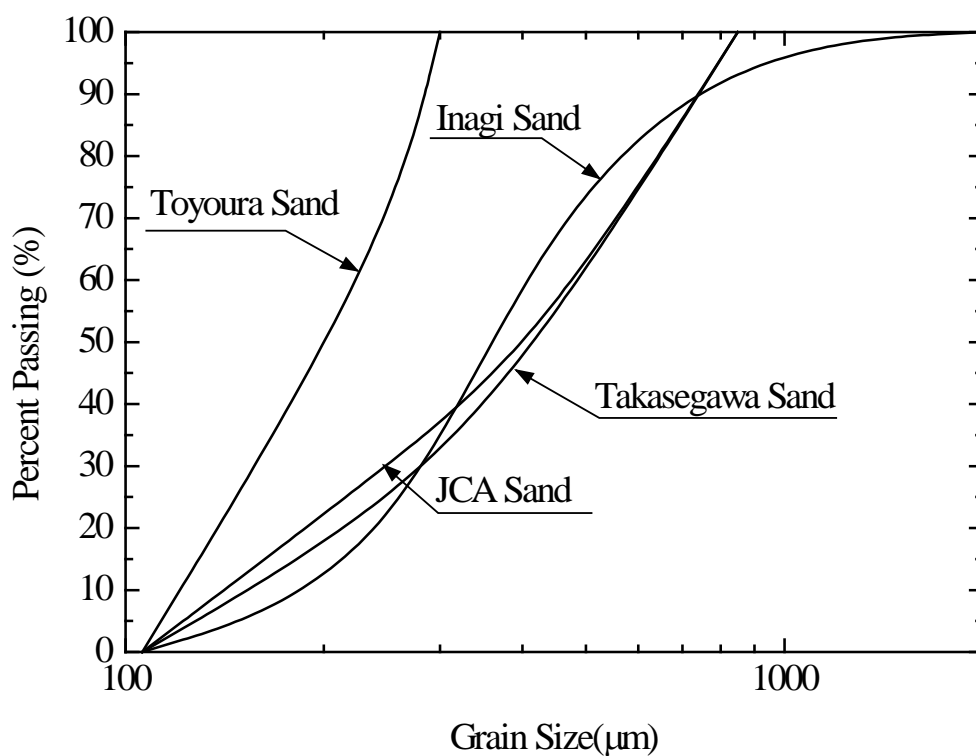


Figure 3.2-1 Grain size distribution curves of tested soils



Figure 3.2-2 Microscope photographs of tested materials - Toyoura Sand



Figure 3.2-3 Microscope photographs of tested materials - JCA Sand



Figure 3.2-4 Microscope photographs of tested materials - Takasegawa sand



Figure 3.2-5 Microscope photographs of tested materials - Inagi Sand

3.3 Laboratory Test Procedures

Laboratory tests are a recognized and growing activity worldwide to assess mechanical properties. They are usually conducted on small specimens that are assumed to be representative of the actual in-situ strength and stiffness. In this study, to study separately the particle breakage, a series of CD triaxial tests (JGS 0524-2009), grain size distribution (JGS 0131-2009), test method for minimum and maximum densities of sands (JGS 0161-2009) and water absorption (JIS A1109-2006) were conducted on four sand specimens. Details of the test apparatus, sample preparation and testing procedure on CD triaxial tests and the minimum and maximum densities of the sands are described below.

3.3.1 Consolidated Drained Triaxial Compression Tests

Triaxial tests have been very important techniques in investigating the particle breakage in granular materials. The specimens are usually tested as element under isotropic initial stresses and isotropic changes in stress and strain conditions. The requirements for devices needed to perform satisfactory tests are given in the following section.

3.3.1.1 Triaxial Test Apparatus

The high pressure triaxial apparatus used in this study was most identical to that used by JGS 0524-2009 typical triaxial apparatus. The main development was that of a large capacity bellofram cylinder to generate apply cell pressure. The high pressure triaxial tests were conducted using computer controlled stress path apparatus with a cell pressure capacity of 4 MPa at a constant rate of deformation. The triaxial testing system employed for this study is schematically shown in Figure 3.3-1. A photo of the overall view of the triaxial loading system is also shown in Figure 3.3-2. A photo of pressure transducer is shown in Figure 3.3-3.

Schematic Diagram of a High Pressure Triaxial Apparatus

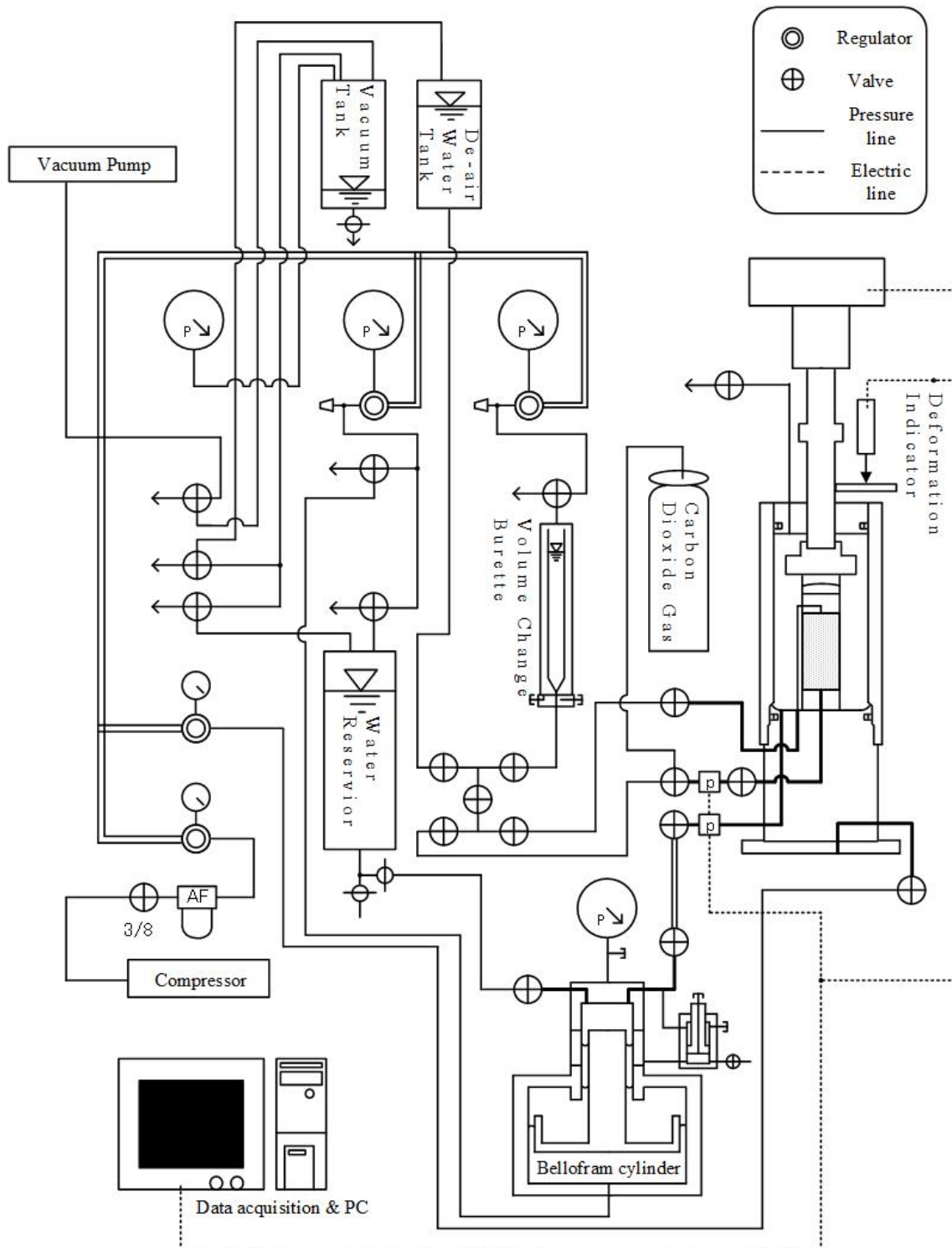


Figure 3.3-1 Schematic diagram of triaxial testing system

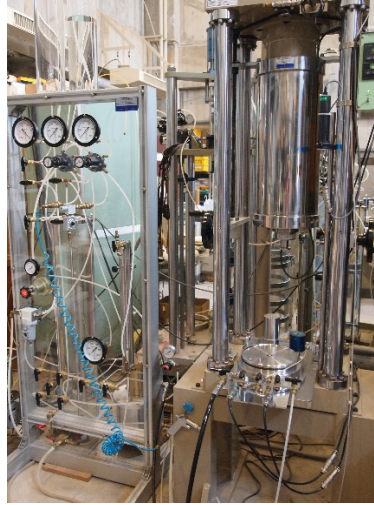


Figure 3.3-2 A photo of the overall view of the triaxial loading system



Figure 3.3-3 A photo of the pressure transducer

1. Axial Loading Device

Triaxial tests are performed using gear-driven loading system by electric motor to provide the rate of axial strain. The maximum capacity of 5MPa loading actuator was used to apply axial force on the specimen. The applied load on the specimen was recorded by individual load cell. The internal submergible load cell positioned above the top platen of the specimen inside the stainless steel cylinder. The strain-amplifier as a feed-back signal used for axial loading has a maximum operational loading capacity of 5 MPa. A photo of axial loading device is also shown in Figure 3.3-4.

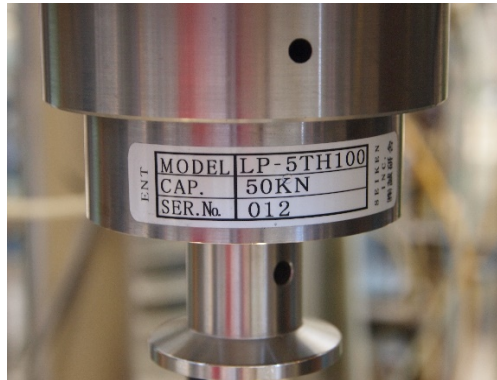


Figure 3.3-4 A photo of the axial loading device

2. Triaxial Compression Chamber

The triaxial compression chamber consists of a top plate and a base plate (Figure 3.3-5) separated by a stainless steel cylinder which is capable to withstand the applied high pressure. The top plate has a vent valve such that air can be forced out of the chamber as it is filled. The base plate has an inlet through which the pressure liquid is supplied to the chamber and at the same time provide connection to the cap to allow saturation and drainage of the specimen during the test procedure.

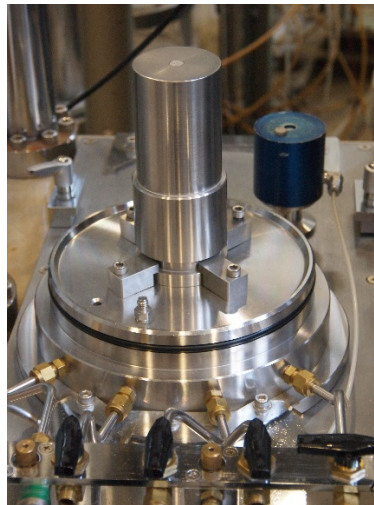


Figure 3.3-5 A photo of a top plate and a base plate

3. Cell Pressure and vacuum systems

When setting up the specimens, a small vacuum was applied to the specimen to allow it to be self-standing during the assembly of the cell until a cell pressure could be applied. A photo of pressure regulator combined with vacuum system and cell pressure system is shown in Figure 3.3-6.

The triaxial cell was mounted on a 300kN loading frame. For high pressure, the

cell pressure was applied by water pressure using bellofram cylinder that can provide pressurized de-aired water into triaxial cell chamber. The valves of pore pressure and axial loads are manual controlled so that special care is needed in controlling the loading systems.

The pore water pressure of the specimen was monitored and controlled by another strain amplifier connected to both top and bottom drainage lines. The role of this strain amplifier was also depending on the testing conditions. Thus, in drained test the strain amplifier was used to control (kept constant) the pore water pressure. The strain amplifier used for cell pressure and pore water pressure has a maximum operational loading capacity of 5 MPa. In order for the cell and back pressures to be measured, two separate pressure transducers were used. One connected to the back pressure line; another one connected to the cell pressure line.

Noted that there was no pore /back pressure system (there would be no build up of pore pressures) used in CD triaxial tests when the material was tested dry.



Figure 3.3-6 A photo of vacuum system combined with cell pressure system

4. Axial Strain and Deformation Indicator

The axial shearing system can be computer-controlled by pulse motor controller so that axial strain can be applied at any rate of deformations. The vertical deformation of the specimen is used to record from the travel of the piston acting on the top of specimen during consolidation. To measure the displacement, the deformation indicator has a range of 50mm capacity which were mounted perpendicular to the specimen. After specimen preparation, the indicator is placed in diametrically opposite location on the top platen of the specimen so that any displacement during consolidation and shearing stage can be monitored. Figure 3.3-7 shows a photo of pulse motor controller and deformation indicator



(a)



(b)

Figure 3.3-7 A photo of (a) pulse motor controller and (b) deformation indicator

3.3.1.2 Sample Preparation

1. Specimen Size

The height to diameter ratio (H/D) was 2, which was equal to that recommended in the JGS 0524-2009 and ASTM D7181-11. The individual height and diameter of the specimen is measured to be nearest less than 2% using a vernier caliper. A minimum of four height measurements and at least three diameter measurements at the quarter points of the height is made to determine the average height and diameter of the specimen.

2. Pluviation Method

The specimens were prepared according to the dry weight of the reconstituted materials into the desired proportions of medium dense and loose state materials using the dry air pluviation method. In the dry air pluviation method, the key factors are the opening of the nozzle, the flow rate, and the drop height of the sand particles. The dry sand was poured into a funnel with its tip controlling the 10-cm drop height. The funnel was continuously moved upward with the surface of the deposit to maintain a constant drop height.

3. Mounting Specimen

After filling the membrane with materials, the membrane was sealed to the top cap using two rubber O-rings. A low-level vacuum of approximately 20 kPa was applied in order to maintain the specimen shape and reduce the disturbances when removing the split mold. After removing the mold, I measured the specimen dimensions with a caliper

and weighed the remaining soil. The cylindrical specimens were 50 mm in diameter and 100 mm in height ($H/D = 2$) as expected. Using the above procedure, I computed the initial void ratio of the sample and then assembled the loading cell and filled the cell chamber with distilled water. Figure 3.3-8 shows photos of sample preparation.

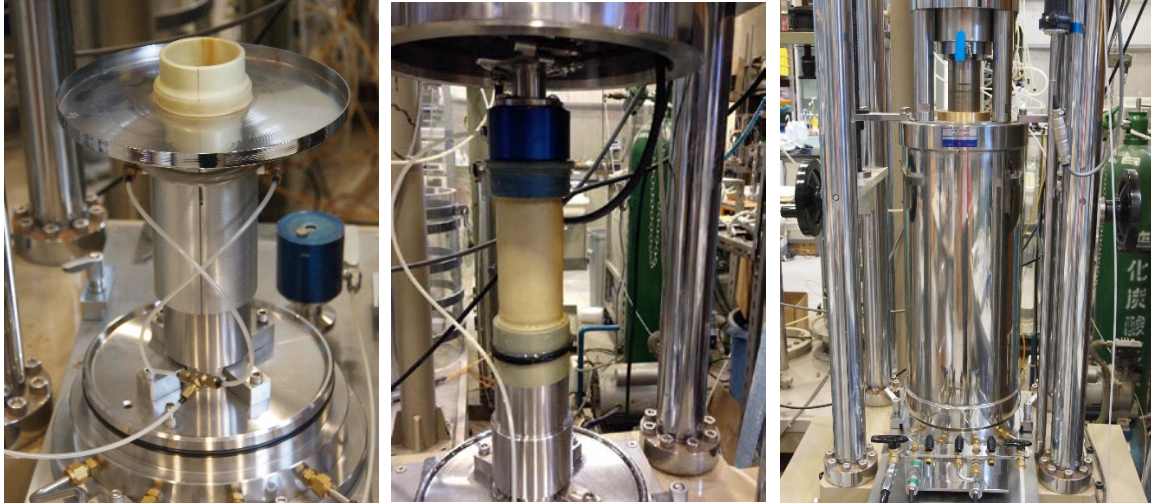


Figure 3.3-8 photos of sample preparation

3.3.1.3 Consolidation

Before the final shearing stage, the specimens had to be gradually taken to the required effective stress condition. Multiple CD triaxial tests (JGS 0524-2009) on four sands were conducted at initial confining pressures ranging from 1 to 4 MPa. With the specimen drainage valves opened hold the back pressure constant, the isotropic stress was applied by increasing both cell pressure and the axial pressure in small increments and allowed the specimens to reach desired confining pressure in a drained state. The specimen was consolidated under a prescribed confining pressure for one hour to several hours, depending on the soil type and the initial dry density.

In this study, most of the techniques and measurement requirements described for CD triaxial tests in accordance with the JGS 0524-2009 test method can be used in carrying out consolidation and shearing tests. Since reconstituted specimens were prepared using dry sand during the test procedure, the saturation phrase of the test procedure was not applied to the specimens in the present study. Within the CD triaxial tests process, the sand remained under the dry condition. Since obtaining the volume change using this experimental apparatus is difficult when testing dry sands, I restricted our discussion on the measurement of volume change and the final void ratio of dry sands.

3.3.1.3 Shearing

Once the desired stress condition have been achieved at various confining pressures, the strain-controlled shearing stage was performed at a shear rate of 1 mm/min until target axial strains (0%, 5%, 10%, 15%, 20% and 40%) were reached. During shearing, the chamber pressure was kept constant while advancing the axial load piston downward against the specimen cap using controlled axial deformation as the loading criterion. Specimen drainage is permitted during shearing (drained test). The pore pressure, axial load, and deformation were recorded using a built-in data acquisition system. Figure 3.3-9 shows a photo of side of the specimen after CD triaxial test.

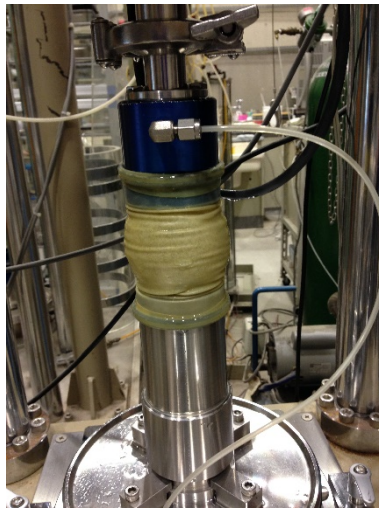


Figure 3.3-9 A photo of side of the specimen after CD triaxial test

After the CD triaxial test, the sands were collected and the grain size distribution after shearing was determined. I conducted the Test method for particle size distribution of soils (JGS 0131-2009) by hand to each of the specimens and continued sieving until not more than 1 mass% of the residue on a sieve passes through the sieve during one minute of sieving. Meanwhile, I also collected materials to perform microscopic photographs after CD triaxial test.

3.3.2 Minimum and Maximum Density Tests

In this study, I adopted relative density test in strict accordance with the JGS procedures for determining maximum density and minimum density, and observed slight increments of water content limits to evaluate the influence of maximum density and minimum density on four types of sands as well as associated changes in material characteristics and grain size distribution. The test methods for determining the soil

particle densities and the minimum and maximum densities of the sands conformed to JGS 0111-2009 and JGS 0161-2009, respectively. The requirements for devices needed to perform satisfactory tests are given in the following section.

3.3.2.1 Test Apparatus

The assembly of the apparatus is shown in Figure 3.3-10. Individual components and accessories are as follows:

1. Mold assembly

A cylindrical metal mold has an inner diameter of 60mm and depth 40mm. A collar used to initially place and then to remove the collar upon completion of densification. It has an inner diameter of 60 mm and depth 23 mm.

2. Funnel

A funnel constructed of smooth paper. The overall funnel length is about 280mm and the narrow stem is about 12mm.

3. Wood Hammer and Straight knife

A wood hammer with a face diameter approximately 30mm in diameter. A single edge stainless steel straight knife 20 cm or more in length.



Figure 3.3-10 A photo of the assembly of the apparatus for the minimum and maximum densities of the sands

3.3.2.2 Sample Preparation

I dried the sands in an oven at a temperature of 110 ± 5 °C for 24 hours. Following the specimen preparation, we introduced slight amounts of moisture to obtain loose and dense specimens that would exhibit minimum density and maximum density.

In this slightly moisture deposition method, I added estimated amounts of water to the oven-dried sands. I thoroughly mixed the sands with proper amounts of water to control the water content and distribute the particles as evenly as possible. Since the percentage of water content depends on material characteristics, the initial water content of the sands was determined in order to evaluate how variations in minimum density and maximum density relate to low water content of sands. In order to minimize segregation of particle sizes, I mixed the specimens carefully to provide as uniform a distribution of particle sizes as possible.

3.3.2.3 Test Procedure

1. Minimum Density Procedure

The minimum and maximum densities of soils were determined in accordance with JGS 0161:2009, which is quite similar to the widely used ASTM, British standard methods, and Eurocode. In this method, I obtained minimum density with 0% water content by pouring the sand into a funnel, allowing it to slide out the end of the tube, and then overfilling the mold above the top in a spiral motion. After placing the sands in the mold, I trimmed the excess sand level with the rim of the mold. The weight of the known volume of sand was then measured and used to determine minimum density.

By varying target water content, I were able to select a moisture that produced very loose specimens. Add sufficient water to the oven dried soil, mix the oven-dried soil to provide an even distribution of particle sizes with as little segregation as possible. Finally, I filled the mold with wet soil by funnel and trimmed the excess sand level with the rim of the mold. The weight of the known volume of sand was then measured and used to determine minimum density at target water content.

I repeated the procedure for each sand type, and recorded scatter plots of minimum density versus low water content for each sand.

2. Maximum Density Procedure

The maximum density tests (ρ_{dmax}) were performed by assembling an extension collar onto the mold and then slowly pouring the sand into the mold in a 10-layer deposition. During and just after filling each layer of sand into mold, I tapped the sides of the mold equally with a hammer to get a uniform deposition rate. I tapped each layer a sufficient number of times (100 blows) to produce the maximum density. After successively tapping layers of sand into the mold, I removed the collar, and then scraped

the sand level with the rim of the mold using a straight knife. Finally, the weight of the known volume of sand was measured and used to determine maximum density. By varying the water content, I were able to select a moisture that produced very dense specimens. Add sufficient water to the oven dried soil, mix the oven-dried soil to provide an even distribution of particle sizes with as little segregation as possible. I repeated the procedure for each sand type, and recorded the maximum densities and low water content for each sand.

The relative density is calculated using minimum and maximum density data directly as follows:

$$D_r = \frac{\left(\frac{1}{\rho_{dmin}} - \frac{1}{\rho_d}\right)}{\left(\frac{1}{\rho_{dmin}} - \frac{1}{\rho_{dmax}}\right)} \times 100(\%) \quad (3.1)$$

where,

D_r = relative density (dimensionless)

ρ_{dmax} = maximum dry density (g/cm^3)

ρ_{dmin} = minimum dry density (g/cm^3)

ρ_d = measured dry density of the sample (g/cm^3)



(a)



(b)

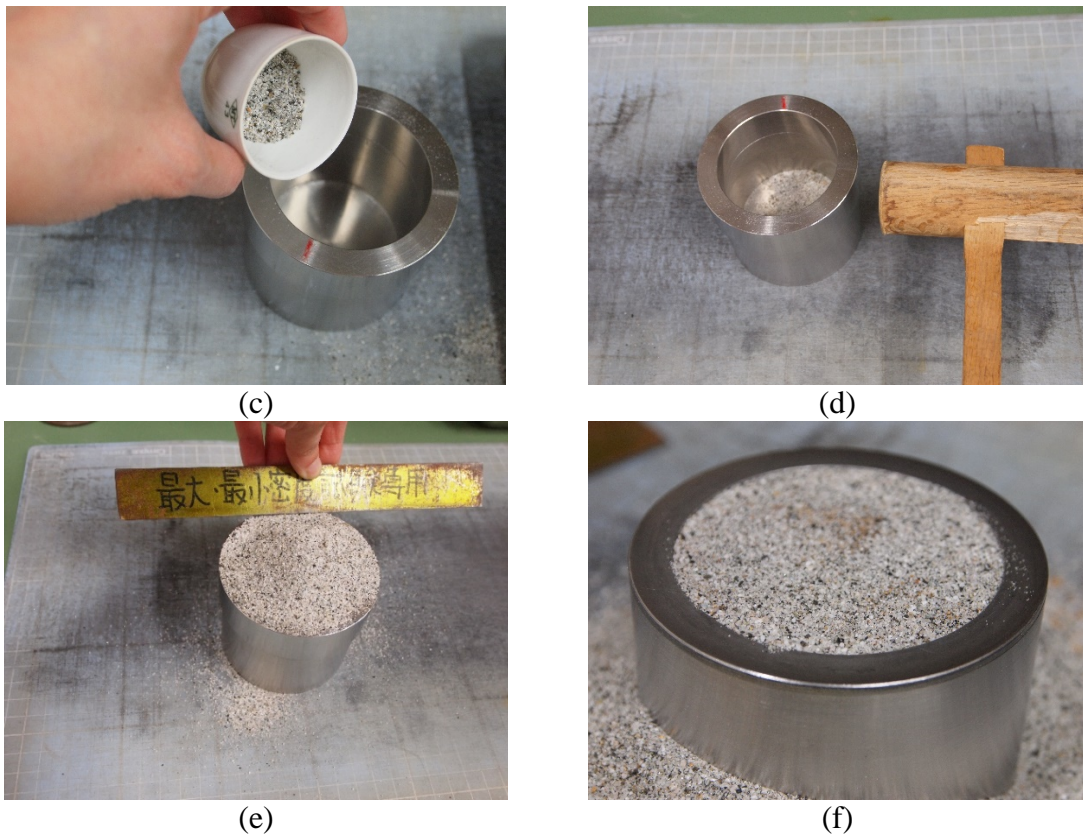


Figure 3.3-11 Photos of low water content on maximum density (a) drop target water content to material (b) mix the oven-dried soil thoroughly to provide an even distribution of particle sizes (c) pour material to mold (d) tamp the mold (e) trim excessive material by straight knife (f) remove the collar and then scraped the sand level

3.2.2.4 Potential Sources of errors

1. The primary factors controlling the minimum and maximum densities of sandy materials are mechanical properties, relative humidity, temperature, grain size distribution, suction, and human manipulation.
2. The laboratory tests that were used to develop criteria for estimating minimum and maximum densities do not take all the necessary factors into consideration. This study showed that controlling relative humidity is critical in preserving sandy materials because unacceptable levels of moisture can significantly affect test results. For example, when materials are taken out of the drying oven, the rapid temperature and relative humidity changes they experience may cause condensation to form on them. In such a case, either high or low relative humidity can provide enough moisture to decrease the materials' relative densities. Materials can readily absorb or release moisture due to fluctuations in relative humidity. This may lead to desiccation and embrittlement of some materials. Thus, we suggest that it is essential

to systematically measure, record, and control relative humidity in order to maintain stable conditions.

3.3.3 Water absorption of fine aggregates

In this study, I adopted water absorption in strict accordance with the JIS procedures for water absorption of fine aggregates, and observed the change in the mass of an aggregate material due to water absorbed in the pore spaces within the particles, compared to the dry condition. The test methods for determining the water absorption of fine aggregates the sands conformed to JIS A1109-2006. Grain size distribution were selected to correspond to designed grain size distribution as shown in Figure 3-2.1. Fine aggregates generally consist of natural sand or crushed stone with most particles smaller than 5 mm. In the research, the grain size distributions of tested sands fall into the range of 2mm-0.106mm. Therefore, in the study, particle size effect on water absorption test is negligible. The requirements for devices needed to perform satisfactory tests at given in the following section.

3.3.3.1 Test Apparatus

The assembly of the apparatus is shown in Figure 3.3-12. Individual components and accessories is as follows:

1. Mold

A metal mold is in the form of a frustum of a cone with dimensions as follows: 40 ± 3 mm inside diameter at the top, 90 ± 3 mm inside diameter at the bottom, and 75 ± 3 mm in height, with the metal having a minimum thickness of 4 mm.

2. Tamper

A metal tamper weighing 304 ± 15 g and have a flat circular tamping face 25 ± 3 mm in diameter.

3. Dryer

The dryer shall have an exhaust slot and shall be capable of maintain a temperature of $105 \pm 5^\circ\text{C}$.

4. Container

A flask or suitable container into which the fine aggregate test sample can be

readily introduced and in which a volumetric flask is satisfactory for a 500 ml test sample of most fine aggregates.



Figure 3.3-12 A photo of The assembly of the apparatus for water absorption of fine aggregates

3.3.3.2 Sample Preparation

I obtained approximately one kilogram of materials and then submerged materials with water for a 24-hour saturation period at a temperature of $20 \pm 5^{\circ}\text{C}$. After the 24-hour soaked condition, I spread the materials on a flat non-absorbent surface exposed to a gently moving current of warm air, and stirred frequently to secure uniform drying condition.

3.3.3.3 Test Procedure

The procedure of water absorption of fine aggregates should be performed as follows:

1. Make and record all weight determinations to 0.1gram.
2. Placed partially materials gently in the mold by filling until additional materials above the top of the mold. Moreover, I tamped the materials into the mold with 25 drops of the tamper to fall freely under gravitational attraction on each drop and then finally, lifted the mold vertically as shown in Figure 3.3-13.
3. Continued drying with constant stirring and make tests at frequent intervals until the tamped material slumps upon the removal of the mold. This indicates that material has reached a surface-dry condition.
4. Prepared materials as described in Section 3.3.3.2, and filled with additional water to materials and mix thoroughly. Cover the top surface of the filled specimen and set aside for 30 minutes.

5. Determine total weight of the container, specimen, and water.

6. Repeat the procedure from 1 to 5 or each of specimens.



(a)



(b)



(c)

Figure 3.3-13 Photos of water absorption of fine aggregates (a) placed materials in the mold (b) tamped the materials into the mold with 25 drops of the tamper (c) lifted the mold vertically

3.3.4 Micro Experimentation

Generally, the micro experimentation is mainly focused on particles size, shape, mineralogy and relative arrangement. Particle shape, relative arrangements and mineralogy are very important criteria for the development of particle breakage for sand. In this study, microscope is used to obtain image of sand and sand-fine mixes. They are discussed in details in coming sections.

3.3.4.1 General Remarks

The digital microscope is used extensively from chemistry to civil engineering development with the primary application being solid-state analysis. The application range from simple images of particle substance to illustrate particle size and shape of particles. In various field, it was the prime tool for examining the particle properties and characteristics.

A digital microscope named KEYENCE VHX-2000 at Department of Civil Engineering in Tokyo Metropolitan University was used for microscopy. A compound microscope has objectives to incorporate observation, image capture, and measurement capabilities and present them in a convenient fashion to the observers by viewing on a PC via USB, a light source to illuminate the sample, a high magnification zoom lens to concentrate the light in a small region of specimens, a stage (360 degree observation) to hold the specimens, a stand to hold all the components and allow for fine and coarse focusing, a camera to capture images of specimens. In this study, it was used to get photographs for tested materials before and after CD triaxial tests. Figure 3.3-14 is photos of KEYENCE VHX-2000 microscope and accessories.

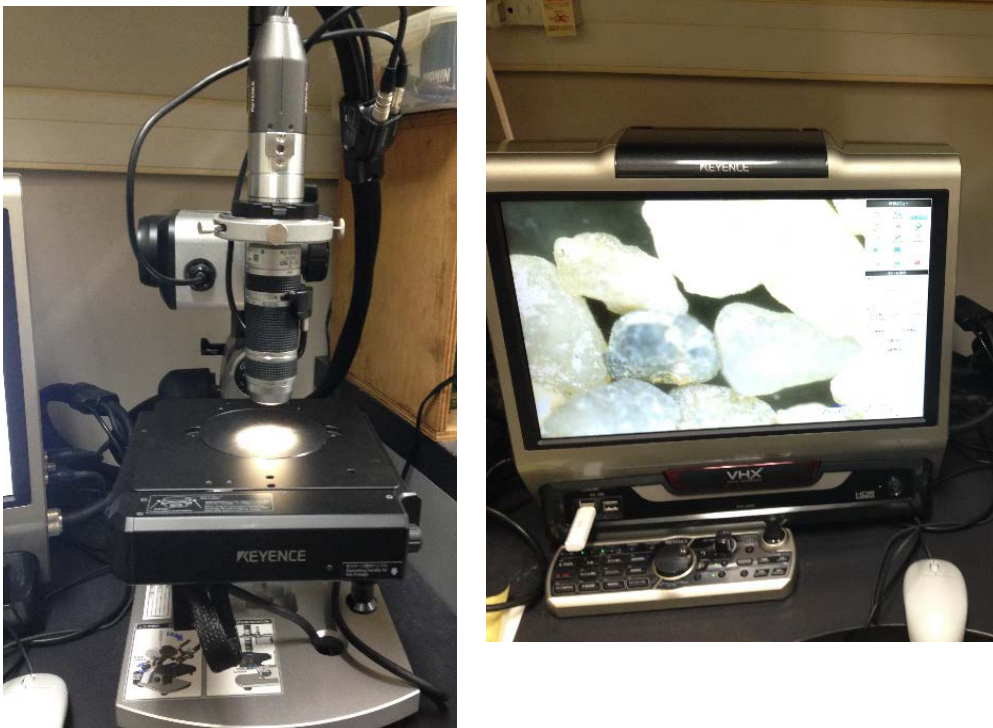


Figure 3.3-14 photos of KEYENCE VHX-2000 microscope

3.3.4.2 Microscopic photographs

Microscope photographs of sands were taken both before and after shearing. Figures 3.3-15, 3.3-16, 3.3-17, and 3.3-18 show microscope photographs of Toyoura sand, JCA sand, Takasegawa sand, and Inagi sand, respectively. In the figures, the left-hand column shows photographs of the sands retained on each sieve before shearing, and the right-hand column shows photographs of the sands retained on each sieve after shearing.

The sieved Toyoura sand before shearing is angular to subangular in shape, as shown in Figures 3.3-15 (a) and 3.3-15 (b). Figures 3.3-15 (c) and 3.3-15 (d) show photographs of the sieved Toyoura sand retained in 250 μm and 106 μm sieves after being sheared under a stress of 4 MPa and a strain of 20%. After shearing, the coarse particles of Toyoura sand were appeared to remained angular-subangular shape. For finer particles, those were considered to be produced from coarse particles with flaws or defects after shearing in the CD triaxial test (Figure 3.3-15 (f)). However, comparing the coarse particles in these photographs, it is impossible to identify the dominant mode of particle breakage.

Microscope photographs of JCA sand (Figure 3.3-16 (a)) revealed that the sieved JCA sand is composed of round-subround particles with grooves. After shearing, JCA particles ($D=75\mu\text{m} - 106\mu\text{m}$) produced by crushing are developed from coarse particle of angular shape (Figure 3.3-16 (g)), Similarity, because JCA sand was very much less compressible and suspected that the fine particles were developed by abrasion of coarse particle, with plate-like shape (Figure 3.3-16 (h)). However, comparing the coarse particles in these photographs, it is impossible to identify the dominant mode of particle breakage for coarser particles after shearing.

Figure 3.3-17 (a) shows that the particle shape and textures of sieved Takasegawa sand before shearing has an angular outline and medium relief of the particle surface. The surface textures of these particles may indicate that Takasegawa sand has a glacial history. As shown in Figures 3.3-17 (d), 3.3-17 (e), and 3.3-17 (f), the shear-induced breakage produced a considerable amount of fine particles, which were often attached to coarser particles. These fine particles produced by shearing are considerably aggregated-like or block-like (Figure 3.3-17 (h)).

After careful washing, the sieved Inagi sand (Figure 3.3-18 (a)) before shearing contained angular to subangular particles, with few fine particles attached to coarser

particles. As shown in Figures 3.3-18 (e), 3.3-18 (f), 3.3-18 (g), and 3.3-18 (h), the coarser particles ($D > 75 \mu\text{m}$) were clothed by fine particle interaction after shearing. A comparison of coarse particles in Figure 3.3-18 (b) and Figure 3.3-18 (I), visually, before shearing, the grain morphology and textures of Inagi sand were with angular outline and medium relief of the grain surface and textures resulting from mechanical and chemical process including fractures. After shearing, the shape of the particles became round and smooth, even glossy and reflective.

The photograph in Figure 3.3-18 (j) shows that the fine particles produced by shearing are generally aggregate-like or block-like.

In this section, the microscopic photographs of the four types of sand do not provide supportive evidence for distinguishing the dominant mode of particle breakage during shearing, (i.e., particle splitting, abrasion, sharp particle corners, and shearing-off asperities) or precisely identifying detailed changes in particle shape after shearing.

3.3.4.3 Potential Sources of errors

It is not appropriate to judge the dominant mode of particle breakage or the change in particle shape after shearing using microscope photographs. The process of particle breakage involves numerous parameters that must be taken into consideration, e.g., material characteristics, time, stress, strain level, and trajectories, inferring that the mode of breakage and particle shape can be expected to vary greatly.

3.4 Summary

CD triaxial test, minimum and maximum density of sands and water absorption of fine aggregates were established and they were equipped with adequate instruments to provide sufficient accuracy of measured quantities such as stress, strain, grain size distribution, minimum and maximum densities, etc. Special effort was given to sample preparation to ensure uniformity of the specimens. Four types of sands were used as tested materials for study particle breakage behavior. The angularity of particle might have significant effect of stress-strain behavior and particle breakage phenomena. Thus, micro-experiments was done with digital microscope to study their shape factor and their relative arrangement in sands. For more detail of test results, they are discussed in Chapter 4.







Before Triaxial Test	After Triaxial Test
	
(a) Toyoura Sand : $D > 250\mu\text{m}$	(c) Toyoura Sand : $D > 250\mu\text{m}$
	
(b) Toyoura Sand : $106\mu\text{m} - 250\mu\text{m}$	(d) Toyoura Sand : $106\mu\text{m} - 250\mu\text{m}$
	
	(e) Toyoura Sand : $75\mu\text{m} - 106\mu\text{m}$
	
	(f) Toyoura Sand : $D < 75\mu\text{m}$

Figure 3.3-15 Microscope photographs of Toyoura sand before and after CD tests








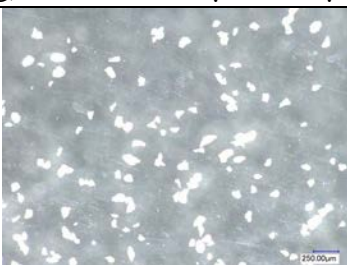
Before Triaxial Test	After Triaxial Test
	
(a) JCA Sand : $D > 425\mu\text{m}$	(d) JCA Sand : $D > 425\mu\text{m}$
	
(b) JCA Sand : $250\mu\text{m} - 425\mu\text{m}$	(e) JCA Sand : $250\mu\text{m} - 425\mu\text{m}$
	
(c) JCA Sand : $106\mu\text{m} - 250\mu\text{m}$	(f) JCA Sand : $106\mu\text{m} - 250\mu\text{m}$
	
	(g) JCA Sand : $75\mu\text{m} - 106\mu\text{m}$
	
	(h) JCA Sand : $D < 75\mu\text{m}$

Figure 3.3-16 Microscope photographs of JCA sand before and after CD tests









Before Triaxial Test	After Triaxial Test
	
(a) Takasegawa Sand : $D > 425\mu\text{m}$	(d) Takasegawa Sand : $D > 425\mu\text{m}$
	
(b) Takasegawa Sand: $250\mu\text{m} - 425\mu\text{m}$	(e) Takasegawa Sand: $250\mu\text{m} - 425\mu\text{m}$
	
(c) Takasegawa Sand: $106\mu\text{m} - 250\mu\text{m}$	(f) Takasegawa Sand: $106\mu\text{m} - 250\mu\text{m}$
	
	(g) Takasegawa Sand: $75\mu\text{m} - 106\mu\text{m}$
	
	(h) Takasegawa Sand: $D < 75\mu\text{m}$

Figure 3.3-17 Microscope photographs of Takasegawa sand before and after CD tests








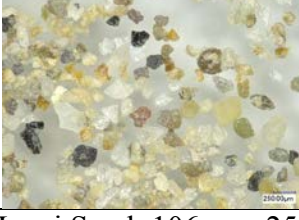
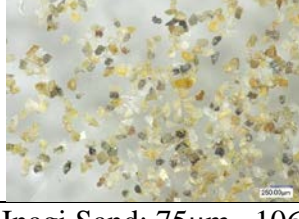

Before Triaxial Test	After Triaxial Test
	
(a) Inagi Sand: $D > 850\mu\text{m}$	(e) Inagi Sand: $D > 850\mu\text{m}$
	
(b) Inagi Sand : $425\mu\text{m} - 850\mu\text{m}$	(f) Inagi Sand : $425\mu\text{m} - 850\mu\text{m}$
	
(c) Inagi Sand : $425\mu\text{m} - 850\mu\text{m}$	(g) Inagi Sand: $250\mu\text{m} - 425\mu\text{m}$
	
(d) Inagi Sand: $106\mu\text{m} - 250\mu\text{m}$	(h) Inagi Sand: $106\mu\text{m} - 250\mu\text{m}$
	
	(i) Inagi Sand: $75\mu\text{m} - 106\mu\text{m}$
	
	(j) Inagi Sand: $D < 75\mu\text{m}$

Figure 3.3-18 Microscope photographs of Inagi sand before and after CD tests

CHAPTER 4 EXPERIMENTAL RESULT ANALYSIS

4.1 General Remarks

In this study, a total of 129 CD triaxial tests, 83 minimum density tests and 68 maximum density tests were conducted on the soils from four sands. Soil specimen were prepared at different particle shape, different grain size distribution, consolidated at different confining pressure and sheared at different axial strain. All the test results are summarized in section 4.2.2.1.

4.2 Drained Behavior of Materials

The drained behavior of sands under stress-strain conditions were used to investigate particle breakage development. Specimen in the triaxial cell is isotopically consolidated and sheared in compression with drainage at a constant rate of axial strain deformation. During shearing, the drainage valve is opened; this results are no buildup of pore pressures.

4.2.1 Stress-Strain Response

In the test program, the development of particle breakage was examined for four sands by performing a series of experiments using CD triaxial compression tests to investigate the stress-strain response of soils.

The deviator stress-axial strain relations obtained in CD triaxial tests for specimens of Toyoura sand, JCA sand, Inagi sand, and Takasegawa sand at confining pressures between 1 and 4 MPa are shown in Figures 4.2-1 through 4.2-4. The results of the CD triaxial tests on specimens are expressed in terms of the deviator stress-strain relation. Taking σ_1' and σ_3' as the maximum and minimum effective principal stresses the triaxial specimen is subjected to, then the deviator stress, $q = \sigma_1' - \sigma_3'$. The axial strain is denoted as ϵ_a .

Figures 4.2-1 through 4.2-4 indicate that the stress gradually increased with strain and then decreased from the maximum value to an approximately constant value with increasing axial strain. Figures 4.2-1 and 4.2-2 reveal that, under the drained condition, the stress-strain response ($q-\epsilon_a$) for JCA sand was able to sustain a high deviator stress and a relatively small strain may be sufficient in order to reach a constant stress. In

addition to JCA sand, the stress-strain response of Toyoura sand has a higher deviator stress and reached a steady state after reaching a low axial strain. Furthermore, the stress-strain curve of Inagi sand displayed a slight drop after reaching a peak state, where the peak shear strain is relatively high at 30%, as compared to 20% for Takasegawa sand.

Figure 4.2-3 indicates that under a confining pressure of 2 MPa, for JCA sand, a stiffer initial response occurred at a low shearing strain and then decreased after reaching a peak before gradually approaching a constant stress value. Similar behaviors have been observed in Takasegawa and Inagi sands, whereby the stress-strain responses gradually deformed and continued to deform at relatively larger strains. Moreover, as shown in Figure 4.2-4, the deviator stress built up gradually and reached a constant value at a large axial strain for Inagi sand, whereas for JCA sand, the deviator stress reached a peak value and then decreased at relatively low axial strain to a constant value comparable to that for Inagi sand. When an Inagi sand is sheared, the stress increases with strain more gradually as compare to the JCA sand and the maximum deviator stress finally approaches a value very close to the ultimate stress value obtained for the JCA sand.

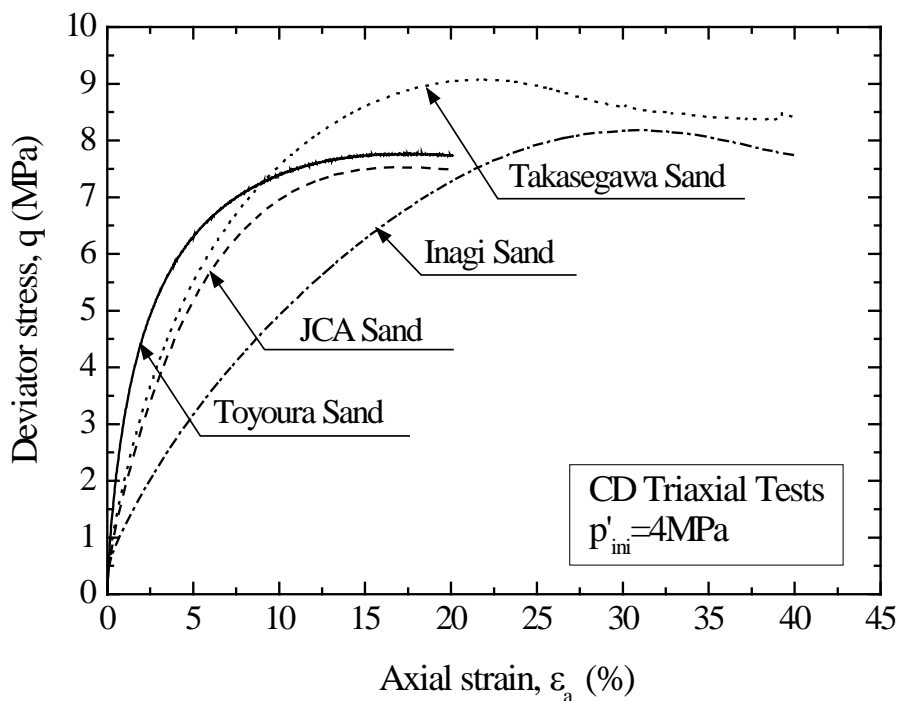


Figure 4.2-1 Stress-strain curves at 4 MPa confining pressure

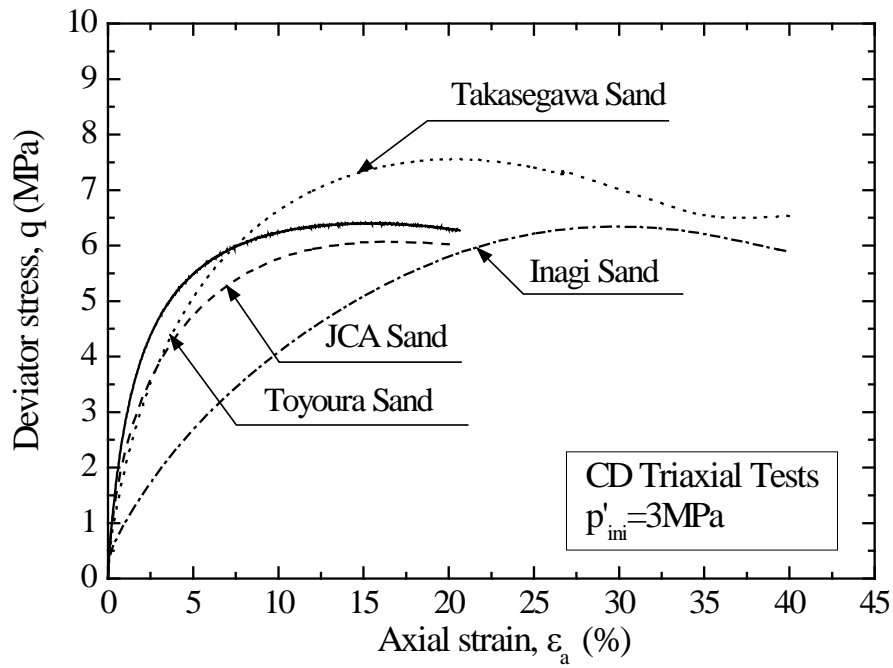


Figure 4.2-2 Stress-strain curves at 3MPa confining pressure

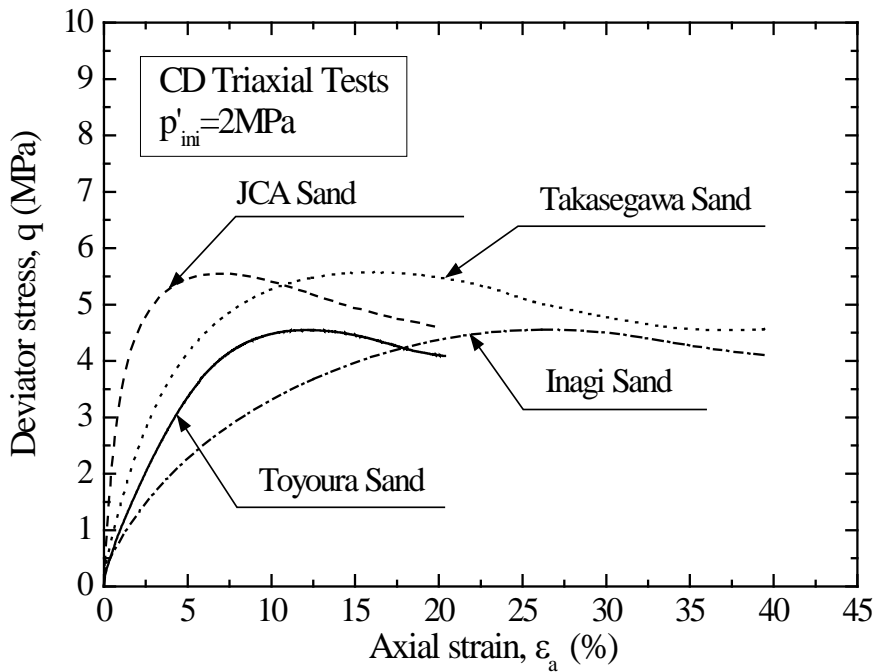


Figure 4.2-3 Stress-strain curves at 2 MPa confining pressure

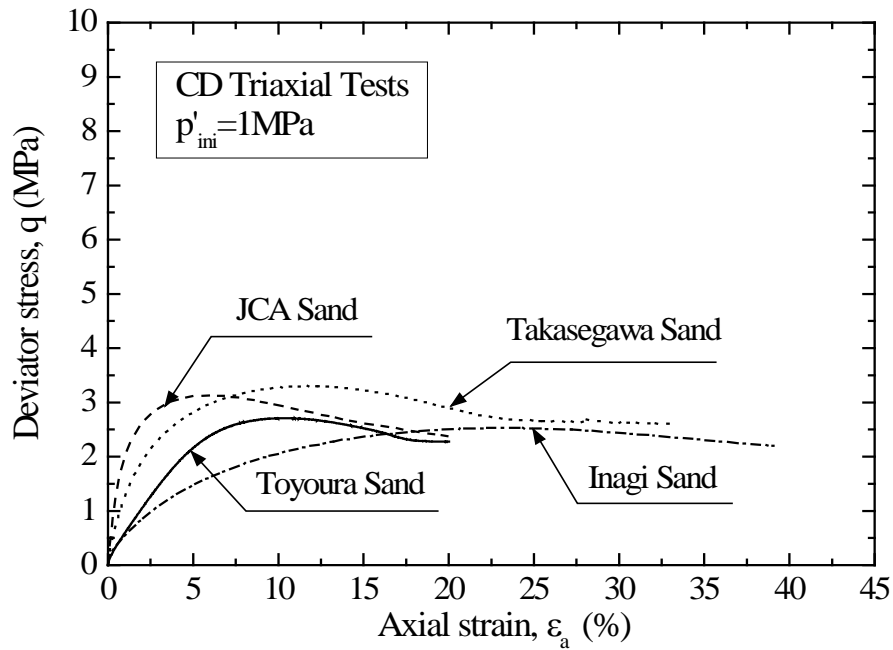


Figure 4.2-4 Stress-strain curves at 1 MPa confining pressure

Figure 4.2-5 to Figure 4.2-8 show the variation of deviator stress with confining pressure for four types of sands tested under different strain levels. For comparison, a clear distinction between the stiff (hard) and weak (brittle) sands can be observed in Figures 4.2-5 through 4.2-8. The results indicate that the maximum deviator stress of either stiff or weak particles increases with increasing initial confining pressure. Under the same initial confining pressure, stiff particles have higher deviator stress than brittle particles.

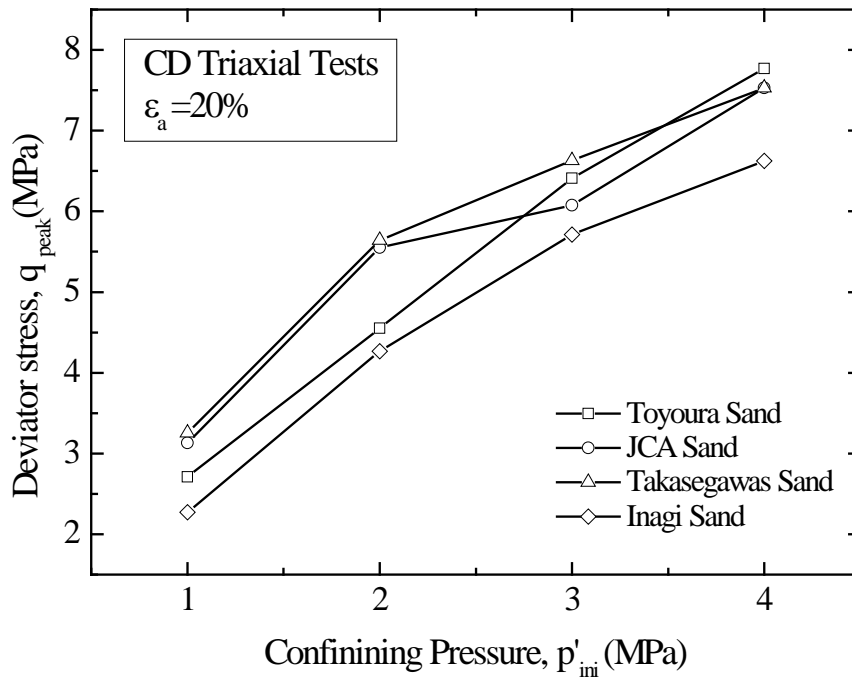


Figure 4.2-5 Variation of deviator stress with confining pressure for various sands at 20% axial strain

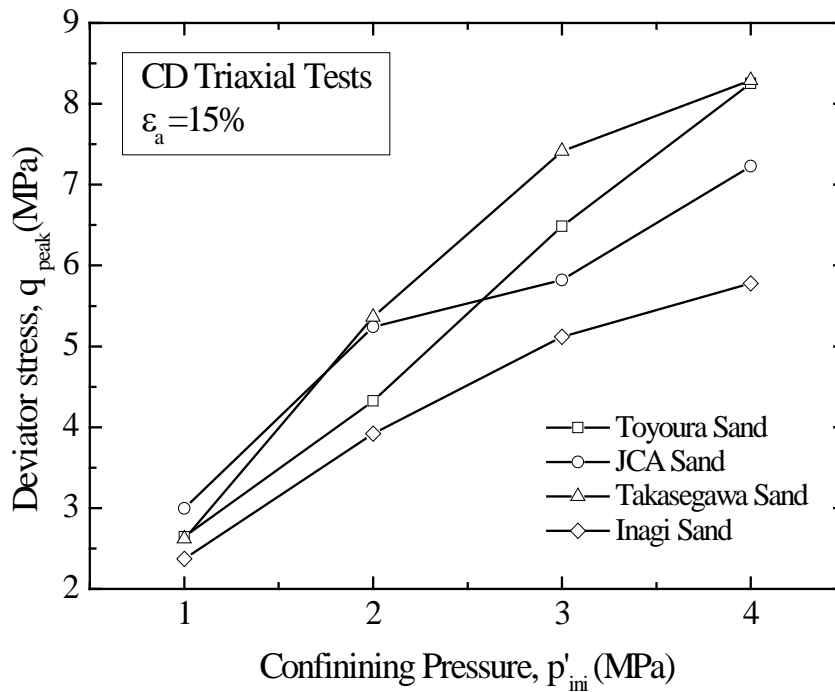


Figure 4.2-6 Variation of deviator stress with confining pressure for various sands at 15% axial strain

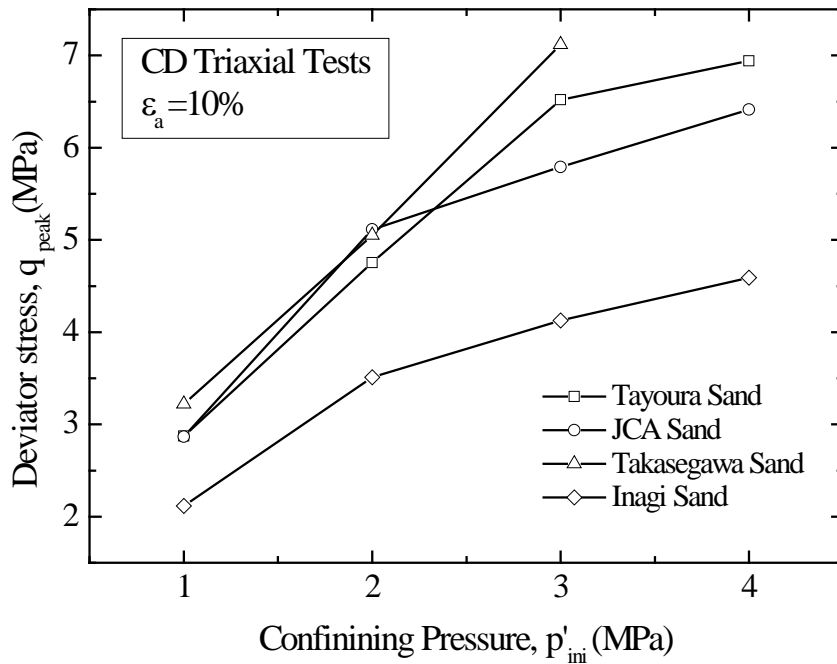


Figure 4.2-7 Variation of deviator stress with confining pressure for various sands at 10% axial strain

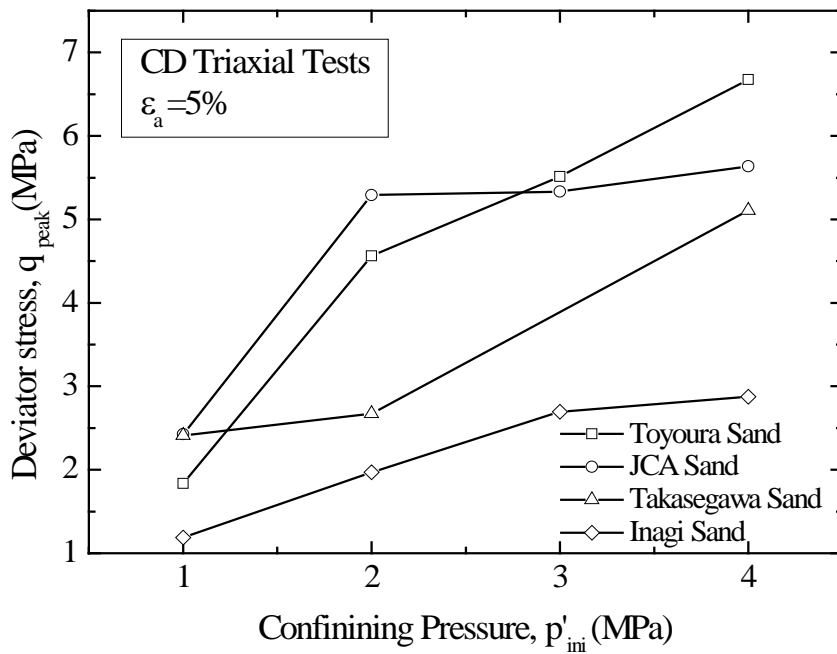


Figure 4.2-8 Variation of deviator stress with confining pressure for various sands at 5% axial strain

4.2.2 Investigation of Grain size distribution

Due to the stress concentrations, the applied stresses were sufficient to cause particle surface abrasion, sharp particle corners and edges, or split particles. Therefore, it is important to note that the stresses applied in the present study were sufficient to cover a wide range of stresses required for simulating the breakage behavior of materials. Prior to the start of the CD triaxial tests, the Test Method for Particle Size Distribution of Soils was conducted in accordance with JGS 0131-2009, and the grain size distributions at this stage were used to check the alternation of the grain size distribution of the particle breakage after the CD triaxial tests. The amount of particle breakage that developed under different shearing matrices for angular and rounded materials was determined by grain size distribution curves. Therefore, in order to investigate whether particle breakage occurred during shearing, sieve analyses were conducted after the tests. The experimental results of the grain size distribution for each of the sands described above are summarized in 4.2.2.1. Figures 4.2-9 through Figures 4.2-12 show the evolution of the grain size distribution curves with increasing confining pressure from 1 to 4 MPa under an axial strain of 20% for the four types of sand plotted on a semi-logarithmic scale. Figure 4.2-13 to Figure 4.2-16 present the evolution of the grain size distribution curves with increasing various axial strain levels at confining pressure of 4MPa.

Figures 4.2-9 through Figures 4.2-12 show that an increase in particle breakage after tests shifted the grain size distribution curve to a finer fraction. That is because some of the particles contained in the specimen undergo fragmentation, the final curve moves toward left of the plot (Marsal, 1985). The grain size distribution curve before the CD triaxial test is plotted for reference. The test results indicate that the grain size distribution curves obtained after each test depend on the characteristics of the granular materials and the testing conditions. Comparisons of JCA sand and Takasegawa sand (Figure 4.2-10 and Figure 4.2-11) with the grain size distributions from test that reached 20% axial strain, in JCA sand, the development of breakage with increased confining pressure did not occur significantly, with the before and after test grain size distribution curves remaining close together. Yet, it can be seen in Figure 4.2-11 that as the confining pressure increased, there was an increase in the difference between before and after test grain size distribution curves on Takasegawa sand. This difference in behavior was clearly revealed that Takasegawa sand is more brittle than JCA sand.

The evolutions of grain size distribution at 4 MPa confining pressure under various

axial strains for the four types of sand were plotted in Figures 4.2-13 through Figures 4.2-16. In Figure 4.2-14, the development of breakage on JCA sand with increased axial strain did not occur significantly, with the grain size distribution curves before and after test remaining close together. Yet, in Figure 4.2-15, it was clear to see that the difference of grain size distribution curves between before and after test was significantly greater for the Takasegawa sand. Note that the grain size distribution at 40 % axial strain shifted a lot further than 20 % axial strain; while the grain size distribution after consolidation stage was not so significant. It meant that with larger axial strain, it accelerated the occurrence of particle breakage. This changes was also observed on Toyoura sand and Inagi sand. The results show that as the axial strain increased there was an increase in difference between grain size distribution curves before and after test on Toyoura sand and Inagi sand (Figure 4.2-13 and Figure 4.2-16). Toyoura sand had significant change after consolidation stage, and then tended to stabilize with increasing axial strain, either did Inagi sand. Based on these four sands, it was concluded that an increase in axial strain caused more breakage; while the magnitude of particle breakage depends on particle characteristics.

When compared to the sands which was only performed on consolidation stage ($\epsilon_a=0\%$), the effect of isotropic compression of specimens at different strain levels is also referred from Figure 4.2-13 to Figure 4.2-16. In the case of Toyoura sand, the original curve has approximate 67 % finer than 250 μm . After consolidation at 4MPa, enough particles had broken down so that grading shifted to 87% finer than 250 μm , which produced about 15 % breakage after test. In the case of JCA sand, the original curve has approximate 50 % finer than 250 μm . After consolidation, the change of grain size distribution from before (50%) to after (51%) test was very small. In the case of Takasegawa sand, the original curve has approximate 49 % finer than 250 μm . It was approximately 51% finer than 250 μm after test. Lastly, the original curve has approximate 12 percent finer than 250 μm for Inagi sand. After consolidation at 4MPa, Inagi sand shifted to 43% finer than 250 μm after test which produced about 29 % breakage. This behavior illustrated that JCA sand and Takasegawa sand were no obvious difference in breakage behavior after consolidation; while Toyoura sand and Inagi sand produced more breakage after consolidation.

From the tests at 4 MPa confining pressure (Figure 4.2-13 through Figures 4.2-16), the grading curves are different for each stress levels, so that not only does the amount of particle breakage increases with stress level, but also particle breakage tend to increases with strain level.

A reduction in particle sizes produced by shear-induced grain crushing was observed in relation to the original grain size distribution. Experimental results showed that the change of GSD was evident from left shifted in the curves. This implied that grain size distributions consistently revealed specimens at the end of the shear stage that were characterized by a fines content larger than that of natural samples.

Consequently, from the positions of the different grain size distribution curves in the figures, it is clear that Inagi sand to be the most brittle material, followed by Toyoura and Takasegawa sands. Whereas, the grain size distribution for JCA sand shows that the smallest amount of particle breakage occurred for the stiff particles.

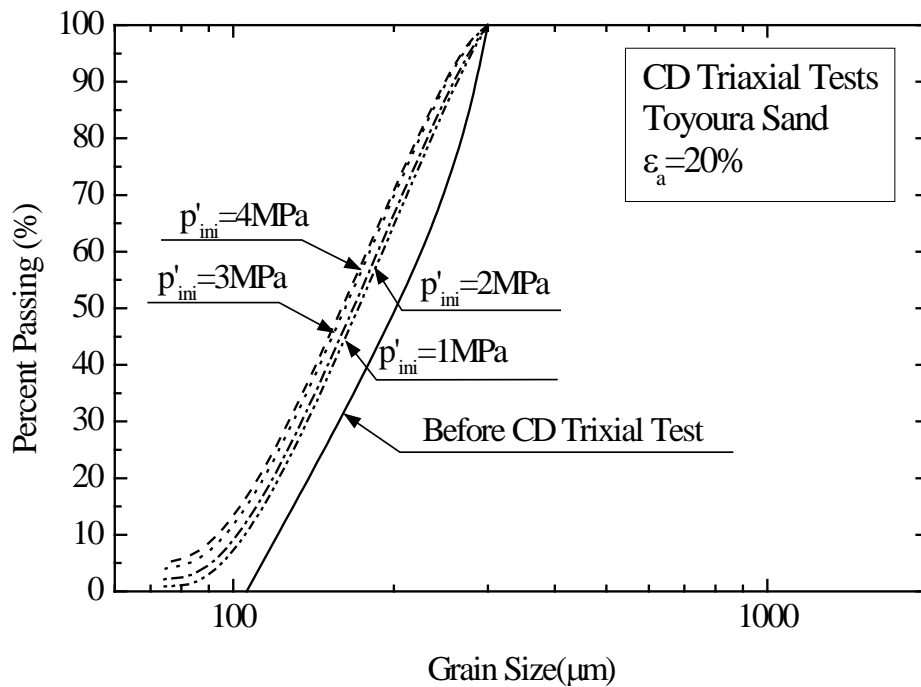


Figure 4.2-9 Grain size distribution curves of Toyoura sand under a confining pressure of 1MPa to 4 MPa o at 20% axial strain-before and after CD triaxial tests

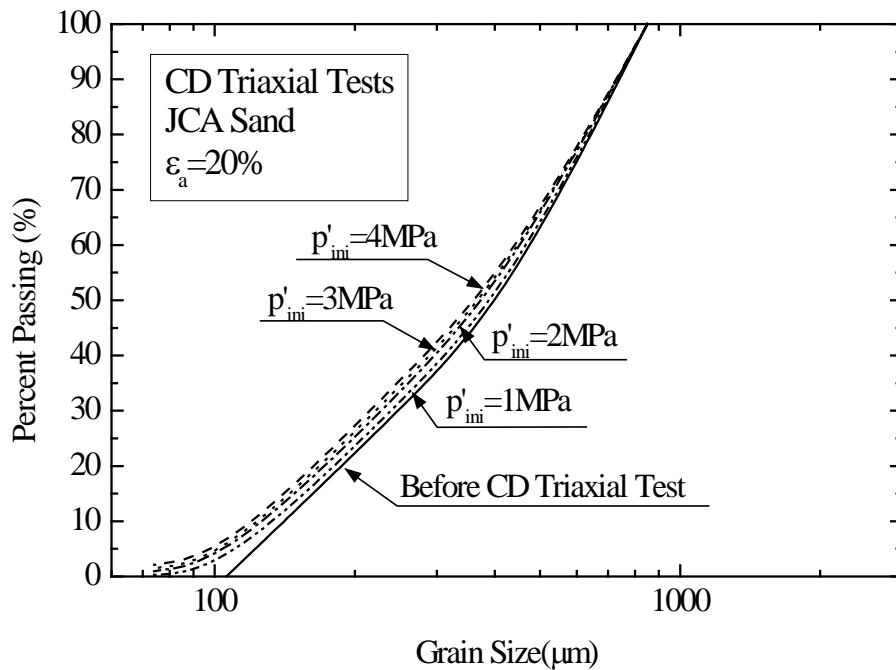


Figure 4.2-10 Grain size distribution curves of JCA sand under a confining pressure of 1MPa to 4 MPa at 20% axial strain-before and after CD triaxial tests

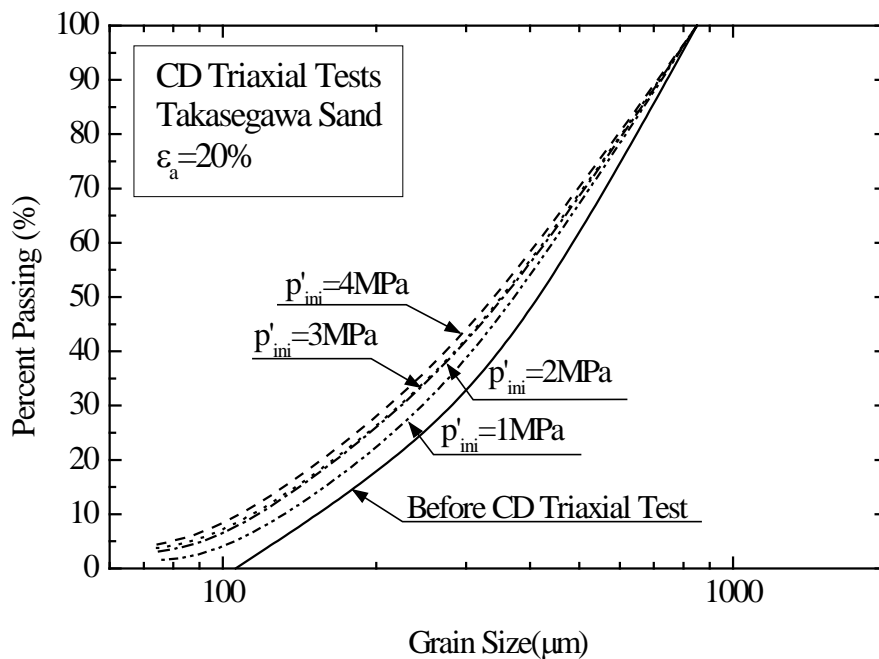


Figure 4.2-11 Grain size distribution curves of Takasegawa sand under a confining pressure of 1MPa to 4 MPa at 20% axial strain-before and after CD triaxial tests

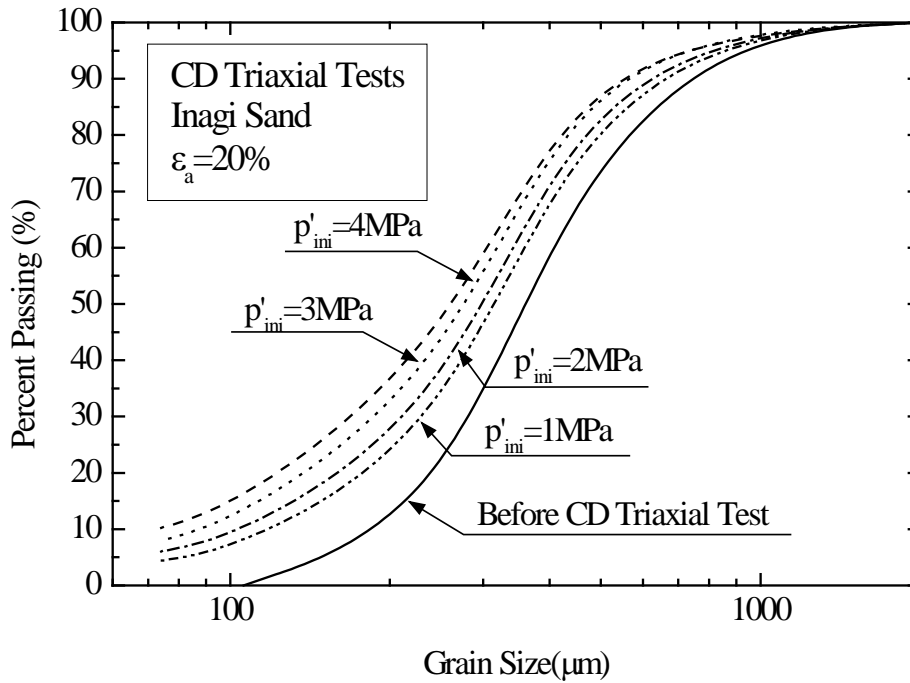


Figure 4.2-12 Grain size distribution curves of Inagi sand under a confining pressure of 1MPa to 4 MPa at 20% axial strain-before and after CD triaxial tests

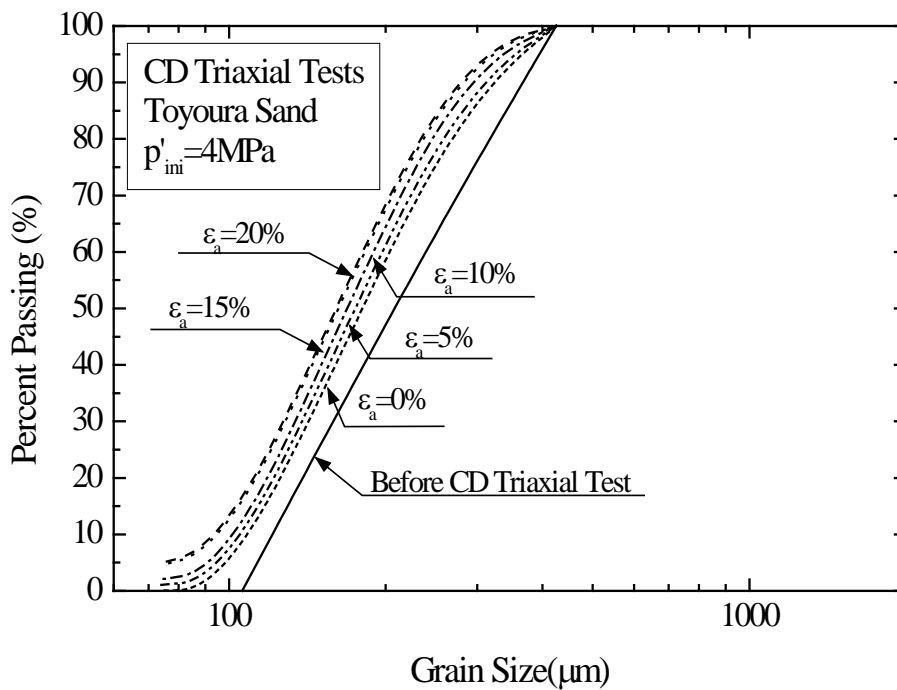


Figure 4.2-13 Grain size distribution curves of Toyoura sand under 4MPa confining pressure at various axial strains-before and after CD triaxial tests

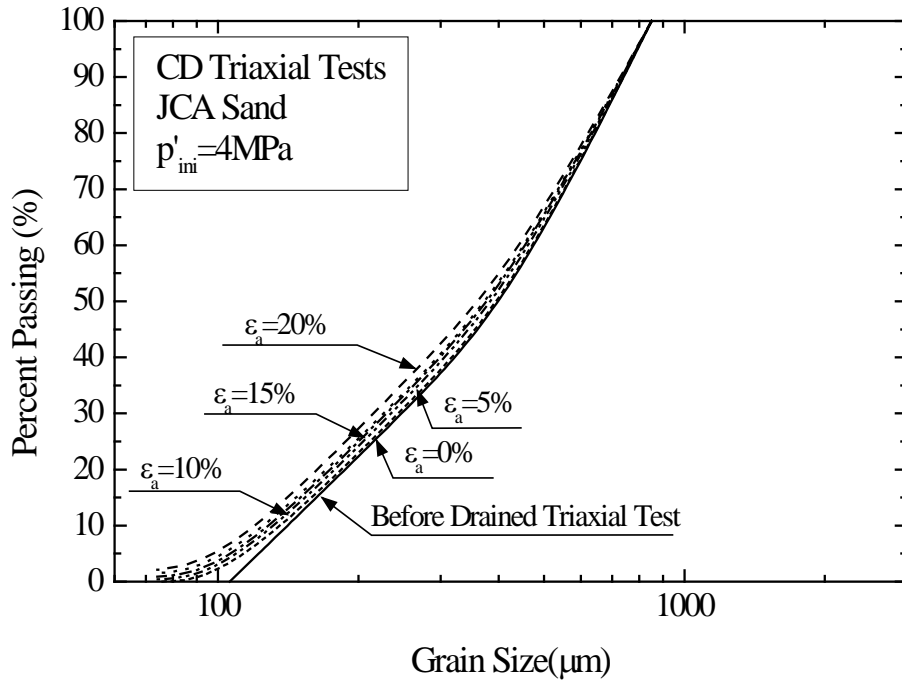


Figure 4.2-14 Grain size distribution curves of JCA sand under 4MPa confining pressure at various axial strains-before and after CD triaxial tests

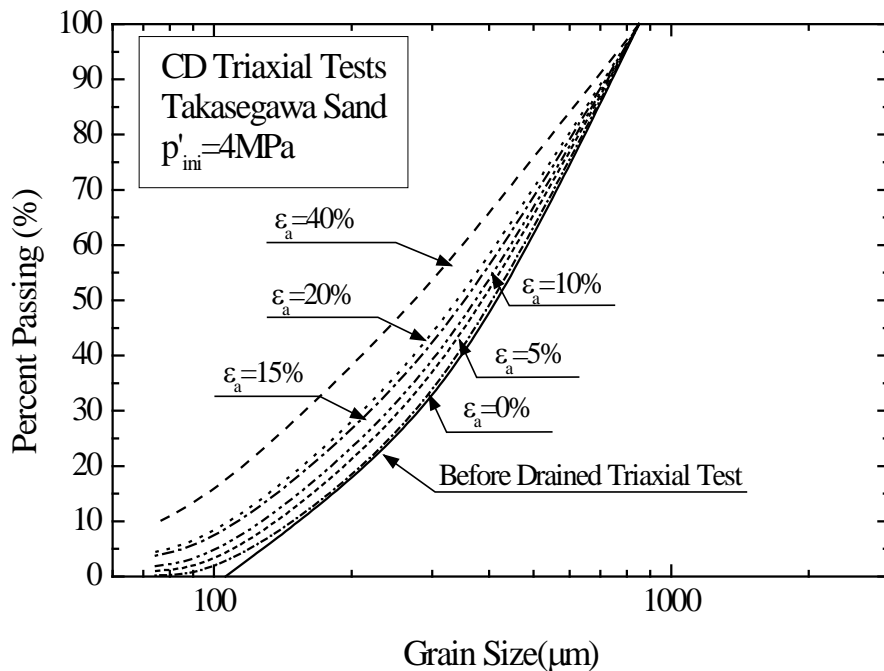


Figure 4.2-15 Grain size distribution curves of Takasegawa sand under 4MPa confining pressure at various axial strains-before and after CD triaxial tests

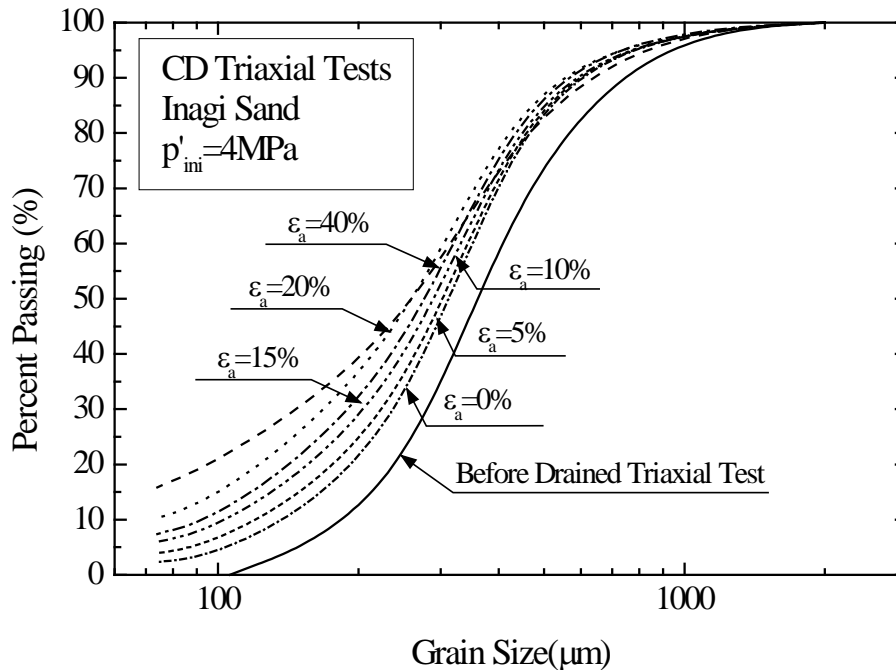


Figure 4.2-16 Grain size distribution curves of Inagi sand under 4MPa confining pressure at various axial strains-before and after CD triaxial tests

4.2.3 Investigation of Particle Breakage

As mentioned in literature review (Chapter 2), several researchers have proposed empirical methods to quantify the magnitude of particle breakage using changes in particle size distribution curves. In this section, different types of breakage index was dependent on visual observation and required a measure of judgement.

A direct comparison of the difference in particle breakage observed for four types of soil at under various stress and strain levels is investigated by visual examination. Visual examination of sheared specimens after triaxial testing revealed that the greatest amount of particle breakage was observed in Inagi sand, followed by Takasegawa sand, Toyoura sand, and JCA sand. This indicates that Ingai sand was crushed and compressed so much that the level of particle breakage was exceed those of the three other sands. In order to examine quantitatively the amount of particle breakage, I discussed the degree of particle breakage in terms of increment of fines content (ΔF_c), Marsal's, Hardin's, Lee & Farhoomand's (D_{15}), and D_{50} breakage indices. Details of the experimental results and quantification of particle breakage are described below.

4.2.3.1 Increment of fines content

Quantifying particle breakage by increment of fines content after testing is the change between the fines content of the sheared specimen and the original specimen (Nakata et al., 1998). The amount of particle breakage which developed under different stress and strain levels for four types of soil is illustrated by increment of fines content shown on Figure 4.2-17 and Figure 4.2-18. As known in Figure 4.2-19 and Figure 4.2-20, these data indicated that Inagi sand produced more fine particles than Takasegawa sand, Toyoura sand, and JCA sand.

Based on the test results, particles of Inagi sand are very brittle and fragile not only because it is porous but also because it is angular in shape; it is the combination of these two factors that makes the particle highly crushable. It is postulated that axial strain measured during the test is the result of both stress concentrations of the specimen and particle breakage. Good agreement between the visual examination results and the corresponding tendency for the increment of fines content (Figure 4.2-19 and Figure 4.2-20) is evident, indicating that the particle breakage of Inagi sand was proportional to the stress and strain input and that particle breakage may not have ceased even after the degree of particle breakage reached steady state.

In addition, a direct comparison of the difference in breakage observed for angular soils, i.e. Toyoura sand and Takasegawa sand, and rounded soil, i.e. JCA sand, at different strain conditions is shown in Figure 4.2-13 to Figure 4.2-16 as well. In all cases much more breakage was observed for the angular soils than for the rounded soil under the same stress and strain conditions.

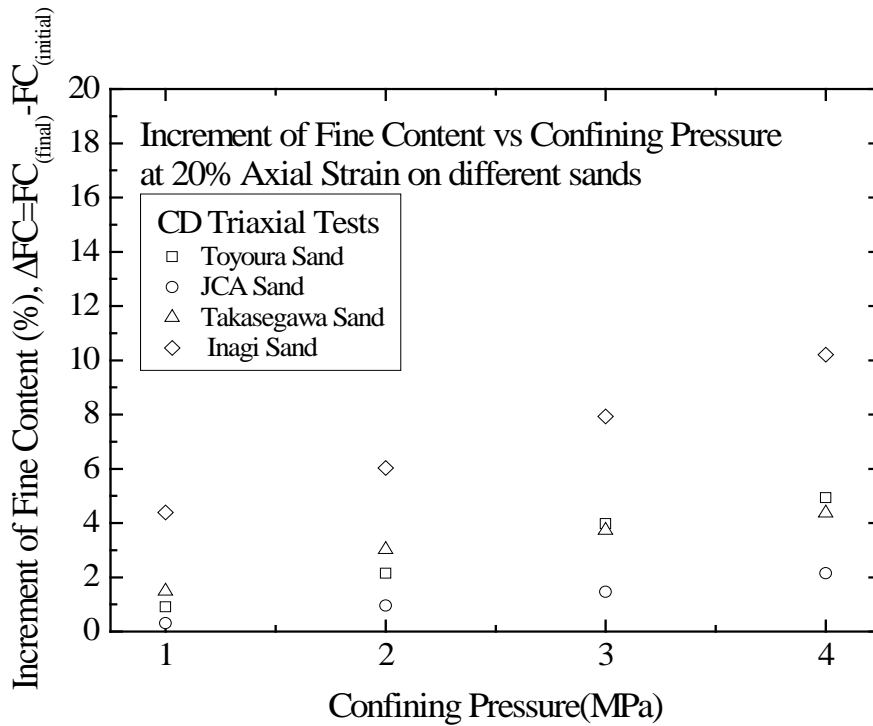


Figure 4.2-17 Increment of fines content versus confining pressure at an axial strain of 20%

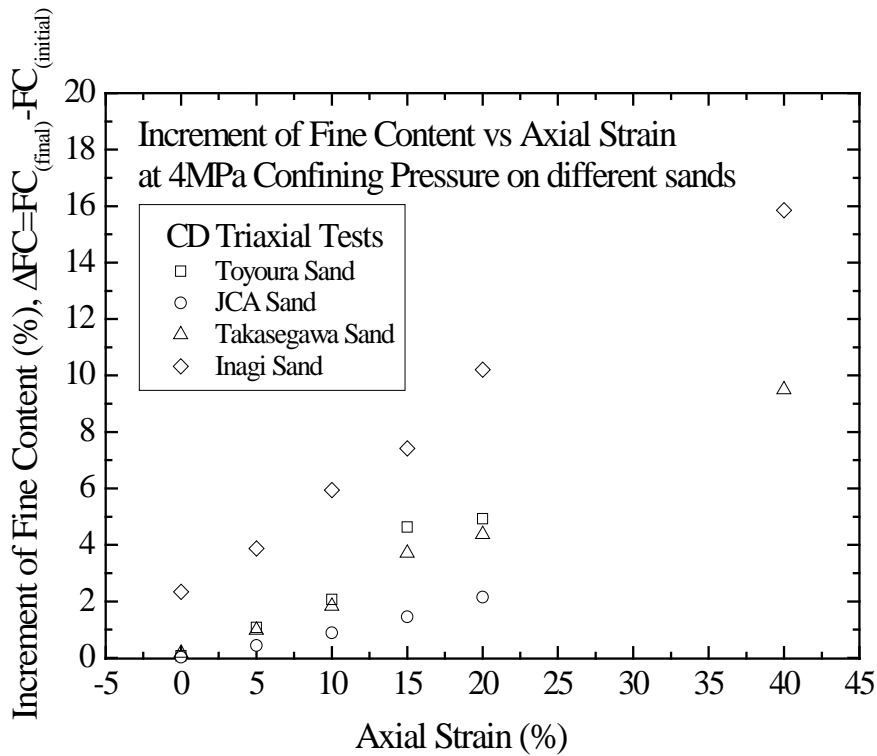


Figure 4.2-18 Increment of fines content versus axial strain at a confining pressure of 4 MPa

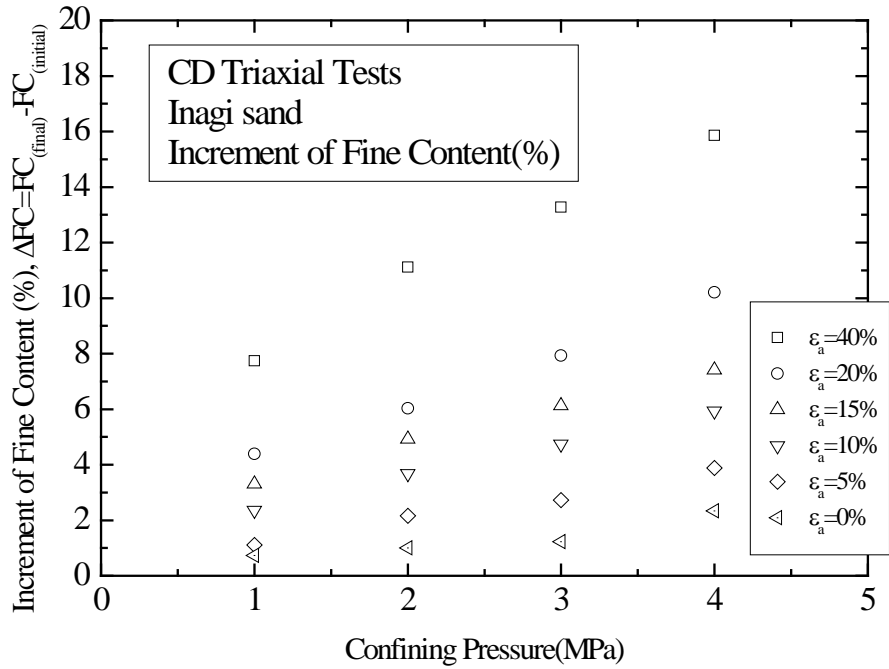


Figure 4.2-19 Increment of fines content versus confining pressure for Inagi sand

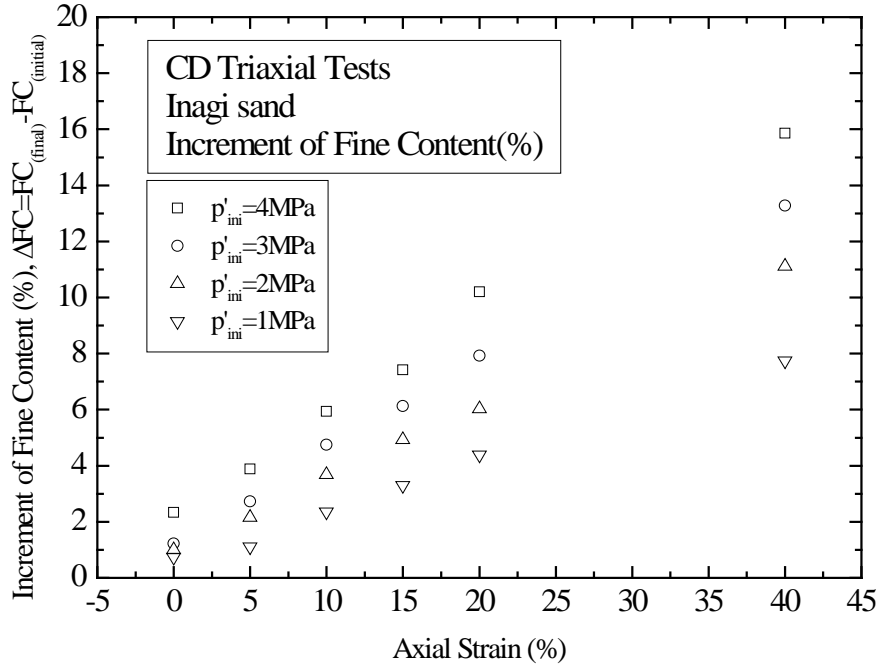


Figure 4.2-20 Increment of fines content versus axial strain for Inagi sand

4.2.3.2 Marsal's Breakage Index (B_g)

Marsal's (1967) breakage index is calculated from the changes in the amount of materials retained on each sieve size before and after tests. The percentage of particles retained in each sieve is determined at both stage. Due to the particle breakage, the percentage of the particles retained in large size sieves will decrease and the percentage of particles retained in small size sieves will increase (Aghaei -Araei et al, 2010). The sum of the decreases will be equal to the sum of increase in the percentage retained (Marsal,1967; Hardin, 1985; Aghaei -Araei et al, 2010). All sieve sizes are theoretically included in the computation of this breakage index (Lade et al, 1996). Comparisons of Marsal's breakage index after CD triaxial tests for four types of sand under 1 to 4MPa at various axial strains are shown in Figure 4.2-21 and Figure 4.2-22.

As shown in Figure 4.2-21, based on the Marsal's breakage index, for the same confining pressure at 20% of axial strain Toyoura sand suffered the most particle breakage, the magnitude of particle breakage for Inagi sand is followed by Toyoura sand, Takasegawa sand exhibited a moderate amount of particle breakage, while JCA sand exhibited the least particle breakage. Figure 4.2-22 presents the Marsal's breakage index against axial strain. As illustrated in this figure, increasing axial strain also increased particle breakage for four soils.

The degree of particle breakage for Toyoura sand at an axial strain of 20 % is greater than that for Inagi sand (Figure 4.2-21) because of following reason. This may be because the grain size distribution of Toyoura sand falls into the narrow sieve interval, it tends to be greatest amount of particles retained on one or two sieve size interval a grain size of 300 to 250 μm in this case, to be used in calculation the degree of particle breakage. Contrarily, because the grain size distribution curve of other three materials is wide-range, it tends to be very little materials left for comparison on the original sieves.

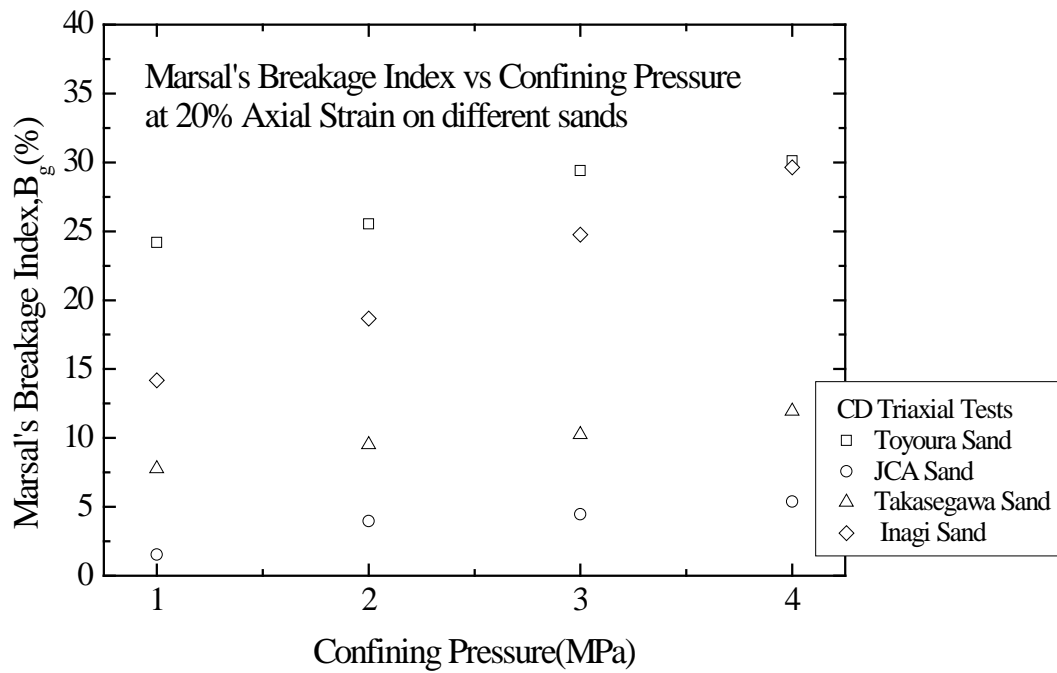


Figure 4.2-21 Marsal's breakage index versus confining pressure at an axial strain of 20%

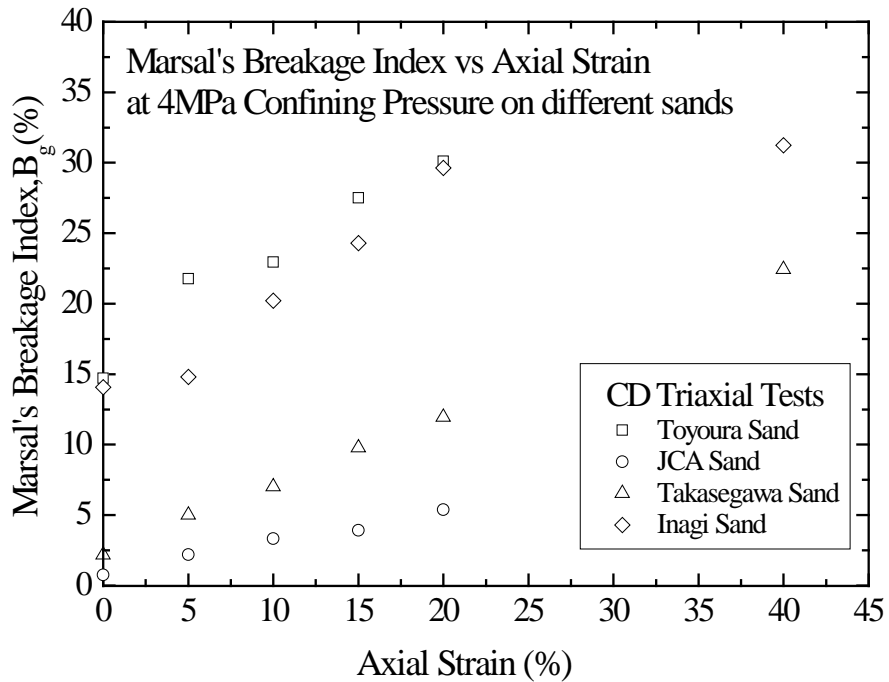


Figure 4.2-22 Marsal's breakage index versus axial strain at a confining pressure of 4 MPa

4.2.3.3 Hardin's Breakage Index (B_r)

Previous chapter has already introduce the Hardin's method to quantify the magnitude of particle breakage using entire grain size distribution. Hardin (1985) reported that B_r is proportional to B_{p0} for soil with the same mineralogy, particle shape, void ratio, stress state, and loading-induced path. Hence, Hardin (1985) suggested a relative particle breakage index as B_r/B_{p0} . The data of Hardin's particle breakage index for four types of sand are plotted corresponding to confining pressure and axial strain shown on Figure 4.2-23 and Figure 4.2-24.

In Figure 4.2-23, for the same confining pressure at 20 % of axial strain Inagi sand suffered the most particle breakage, Toyoura sand and Takasegawa sand exhibited a moderate amount of particle breakage, while JCA sand exhibited the least particle breakage. It is expected that JCA sand exhibited low values of particle breakage index because of the following two reasons.

1. JCA sand has a wider grain size distribution compared with the more uniformly graded Toyoura sand and thus, the particles were supported by neighboring particle better (Mandl et al., 1977; Hardin, 1985; Gerolymos and Gazetas, 2007; Sadrekarimi and Olson 2008).
2. The predominant material of JCA sand is stiff and rounded quartz. Therefore, some of particle may have deformed slightly and created a cushioning effect rather than breaking during drained shear.

Although Inagi sand has slightly broader grading in comparison to JCA sand (see Figure 3.2-1), Inagi sand suffered a larger amount of particle breakage, in particular during drained shear (Figure 4.2-24). This was likely because of its stiffness contrast and slightly weaker particle mineralogy compared with mineralogy of JCA sand.

Increasing axial strain also increased particle breakage of Inagi sand. Specimen HTC194 was sheared to an axial strain of 40% and was damage more severely ($B_r = 0.252$) than specimen HTC 171 that was sheared to 20% axial strain ($B_r = 0.231$). This implies that as axial strain to a very large axial strain, the rate of particle breakage increases and grain size distribution approaches linear relationship.

Since all sieve sizes are involved in the area calculation, this method is thought to be relatively stable and reliable. However, Hardin ignored particle breakage on silt-clay size particles because the larger stresses required to crush silt-clay particles.

Furthermore, this method was determined by calculating the area between the grain size distribution curve and particles greater than a constant 74 μm , any small errors or inaccurate in the determination individual grain size distribution are attenuated in the calculation of particle breakage (Lade et al. 1996). Thus, the estimation using Hardin's method became ambiguous and was not sensitive to finer fraction. In this method, if necessary, I would suggest to adjust the definition of b_{p0} to include silt- and clay size particles to account for the large percentage of fines produces during shear.

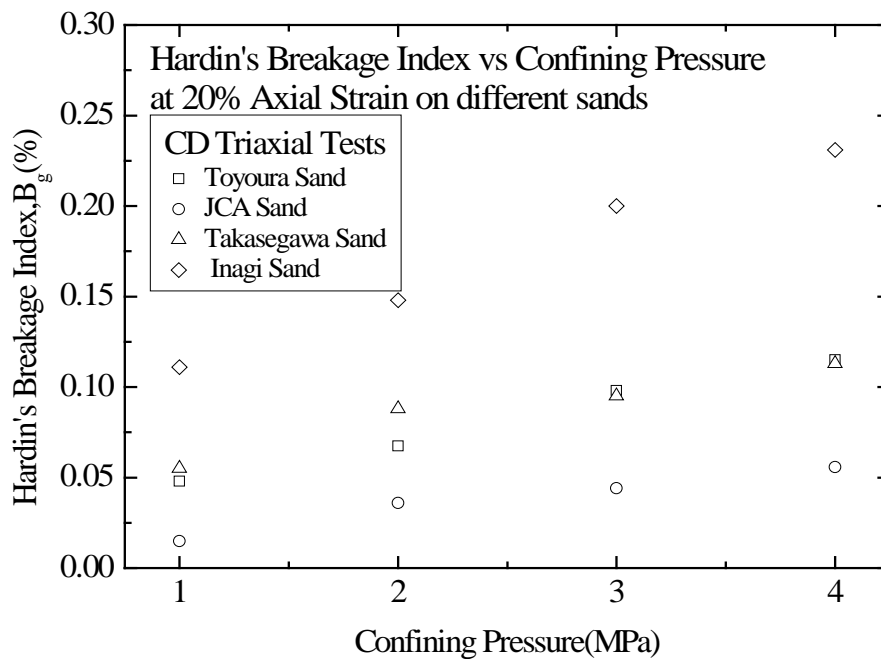


Figure 4.2-23 Hardin's breakage index versus confining pressure at an axial strain of 20%

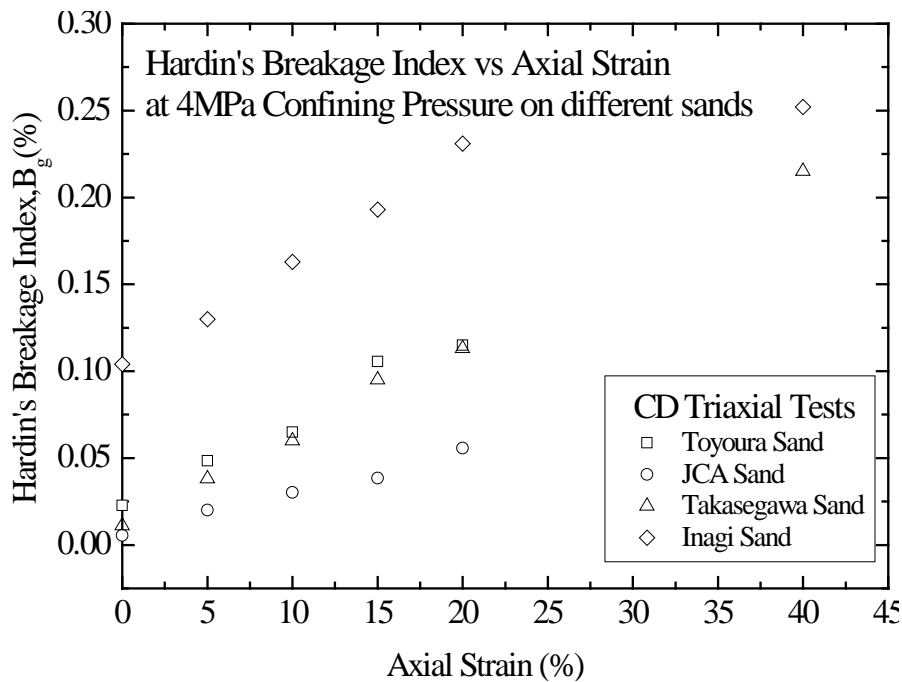


Figure 4.2-24 Hardin's breakage index versus axial strain at a confining pressure of 4 MPa

4.2.3.4 Lee & Farhoomand's Breakage Index (D_{15})

In this section, the results of investigation on the particle breakage phenomenon in four types of sand with Lee and Farhoomand's breakage index is studied. The relation for Lee and Farhoomand's breakage index has been presented in Table 4.2-1.

As proposed by Lee and Farhoomad (1967), D_{15} 's breakage index evaluated the particle breakage based on the horizontal distance between particle size distribution curves at 15% finer (Hardin, 1985) before and after tests. The original application of this method was to investigate particle breakage, when studying materials to be used in the filter of an earth dam. They investigated the effect of particle breakage on compressibility in terms of grain size, grain shape, grain size distribution and stress level, as well as K_0 ratio; and as D_{15} is an important parameter in designing earth dam's filters (Ghanbari et al., 2008).

Figures 4.2-25 through 4.2-26 illustrated that when Inagi sand subjected to high confining pressure, the D_{15} grain size after shearing became very small, whereas the D_{15} grain size of Toyoura sand and JCA sand remained unchanged or was rarely crushed. This indicates that the particle diameter at 15% in the cumulative distribution of Inagi sand and Takasegawa sand, for example, produced more breakage than round to subround particles, e.g., Toyoura and JCA sands.

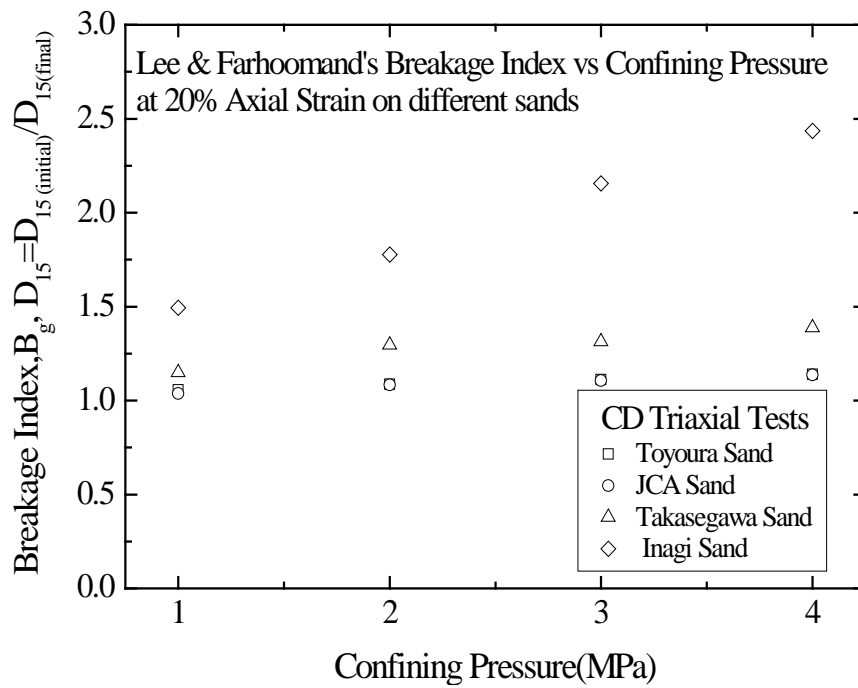


Figure 4.2-25 D_{15} 's breakage index versus confining pressure at an axial strain of 20%

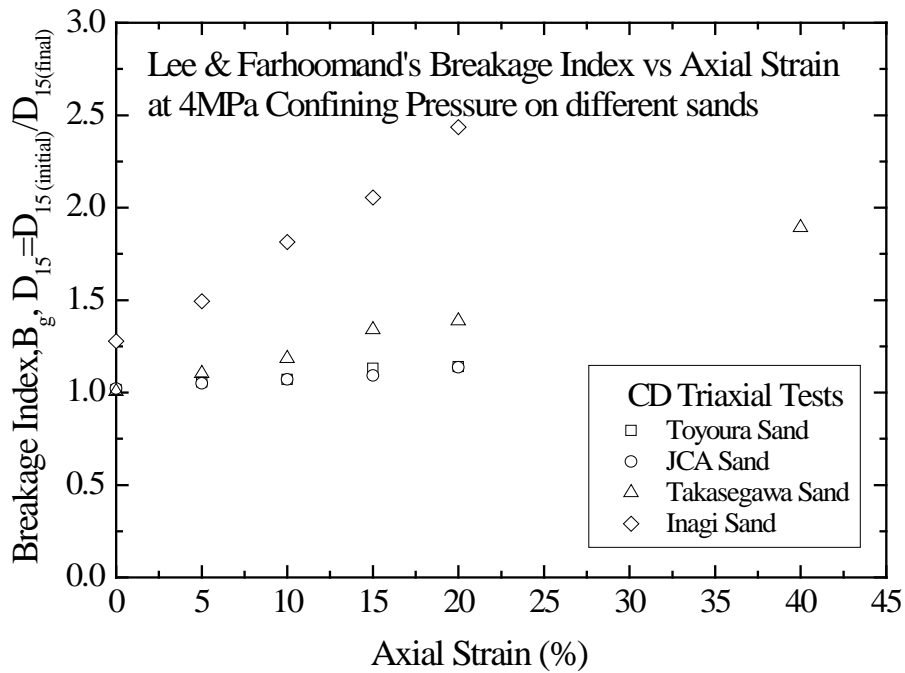


Figure 4.2-26 D_{15} 's breakage index versus axial strain at a confining pressure of 4 MPa

4.2.3.5 D_{50} breakage index

In this section, the results of investigation on particle breakage phenomenon in four types of soil with the average grain size ratio is studied. The experimental results for the average particle size ratio has been presented in Table 4.2-1. According to this study, the particle breakage index of materials is defined as the horizontal distance between the two curves of before and after tests which as the ratio of D_{50} of materials before tests to the D_{50} of materials after conducting the tests (Ghanbari et al., 2008).

D_{50} 's breakage index is based only on one grain size. The scatter of results (Figures 4.2-27 and 4.2-28) indicates that particle breakage occurred during the shearing stage of testing, and the D_{50} grain size of Toyoura sand changed significantly based on the evidence of particle breakage. This may be because particle breakage was more significant in specimens with more uniformly graded particles than well-graded particles (Nakata et al. 2001), the particle diameter at 50% in the cumulative distribution of Toyoura sand produced more breakage than those of the three other sands.

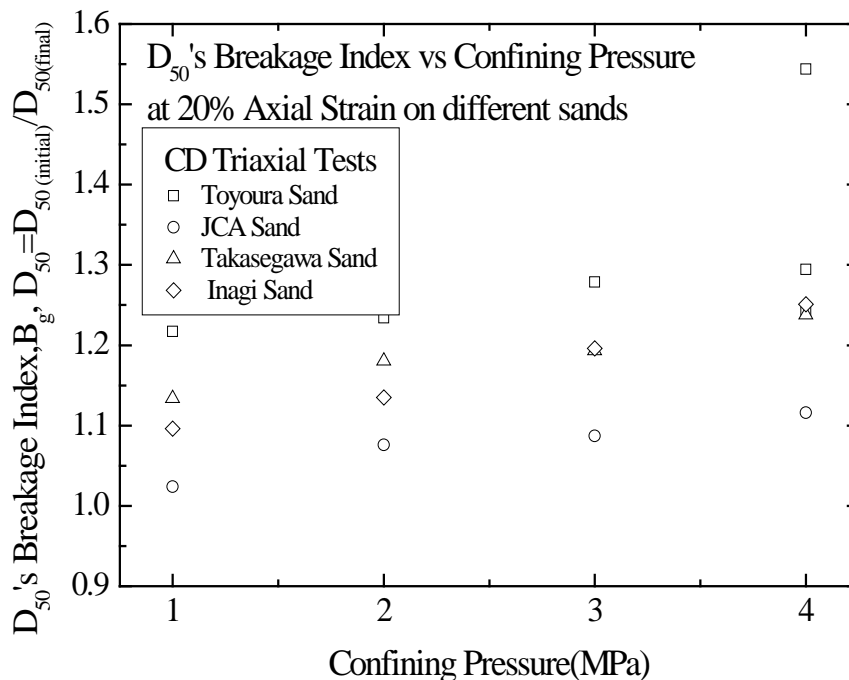


Figure 4.2-27 D_{50} 's breakage index versus confining pressure at an axial strain of 20%

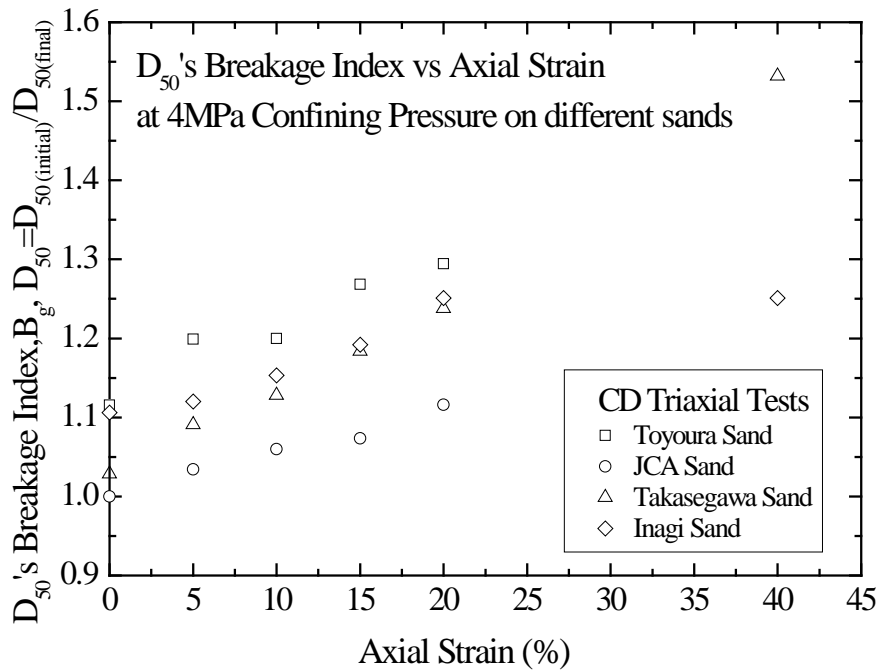


Figure 4.2-28 D_{50} 's breakage index versus confining pressure at axial strain at a confining pressure of 4 MPa

4.2.3.6 Summary

In this section, I conducted CD triaxial tests on four types of sands with different characteristics in order to induce particle breakage. The grain size distributions of specimens before and after stress were reported. I collected the experimental results and adopted methods of particle breakage to examine the particle breakage index. The experimental results for the grain size distribution on each of the sands described above are summarized in Table 4.2-1, while the experimental results for the particle breakage index is listed in Table 4.2-2. Note that this researched focused on grain size distribution, and the particle breakage were used only to supplement the test findings. Analysis of the test results revealed the following conclusions.

1. It is not appropriate to judge the dominant mode of particle breakage or the change in particle shape after shearing using microscope photographs. The process of particle breakage involves numerous parameters that must be taken into consideration, e.g., material characteristics, time, stress, strain level, and trajectories, inferring that the mode of breakage and particle shape can be expected to vary greatly.
2. The CD triaxial test results indicated that the maximum deviator stress of either stiff or weak particles increases with increasing initial confining pressure. Under the same axial strain, stiff particles have a higher deviator stress than brittle particles.

3. A comparison of the grain size distribution of four types of sand revealed Inagi sand to be the most brittle material, followed by Toyoura sand, Takasegawa sand, and JCA sand.
4. In the present study, I adopted Marsal's breakage index, Hardin's breakage index, Lee and Farhoomad's breakage Index, D_{50} , and the increment of fines content (ΔF_c) to examine the degree of particle breakage. Each empirical method provided inconsistent results compared with the evolution of grain size distribution and the increment of fines content (ΔF_c). Having compared the various methods, the particle breakage proposed by Marsal indicates that when the grain size distribution curve of materials falls into narrow range, it tends to be greatest amount of particles retained on one or two sieve size interval to be used in calculation the degree of particle breakage. Contrarily, when the grain size distribution curve of materials is wide-range, it tends to be very little materials left for comparison on the original sieves.
5. Hardin's breakage index was determined by calculating the area between the grain size distribution curve and particles greater than a constant $74\mu\text{m}$. However, Hardin's breakage index ignores silt-size particles in calculation. Therefore, the application of Hardin's breakage index to materials that contain or induce a large amount of finer particles after shearing would not be appropriate.
6. Both Lee and Farhoomad's breakage index and D_{50} 's breakage index were used to measure criteria related to particle size scale. Quantifying particle breakage should prevent inaccurate estimation of both the numerator and denominator of the equation. Any errors in judgment of the denominator of the equation have a greater impact on particle breakage estimation because errors in the denominator can amplify the particle breakage index.
7. I examined the degree of particle breakage in terms of Marsal's, Hardin's, Lee & Farhoomand's, D_{50} 's breakage indices, and increment of fines content (ΔF_c). It can be concluded that the magnitude of particle breakage of sands during shear deformation has linear relationship with confining stress and axial strain level.

Table 4.2-1 Summary of test results on four types of sand (1/6)

Materials	Test ID	Initial Void Ratio e_{ini}	Confining Pressure P'_{ini} (MPa)	Axial Strain $\epsilon_a(\%)$	Grain Size Distribution after CD Triaxial Test					Particle Breakage				
					Percent Passing (%)					Marsal	Hardin	D ₁₅	D ₅₀	ΔFC
					850 μ m	425 μ m	250 μ m	106 μ m	75 μ m					
Toyoura Sand	HTC250	0.820	4	20	—	—	94.11	8.73	4.93	30.105	0.115	1.140	1.294	4.930
	HTC084	0.775	4	15	—	—	93.13	7.98	4.63	27.515	0.106	1.130	1.268	4.634
	HTC107	0.788	4	10	—	—	90.17	3.92	2.07	22.961	0.065	1.071	1.200	2.071
	HTC257	0.789	4	5	—	—	85.76	2.16	1.07	21.759	0.048	1.057	1.199	1.069
	HTC074	0.803	4	0	—	—	82.40	0.23	0.07	14.703	0.023	1.016	1.115	0.073
	HTC253	0.797	3	20	—	—	93.40	6.74	3.98	29.402	0.098	1.111	1.279	3.978
	HTC088	0.790	3	15	—	—	88.53	5.04	2.90	23.594	0.075	1.083	1.222	2.898
	HTC108	0.740	3	10	—	—	87.33	3.08	1.61	21.302	0.056	1.066	1.190	1.605
	HTC258	0.795	3	5	—	—	88.36	1.45	0.71	24.363	0.067	1.056	1.213	0.708
	HTC078	0.765	3	0	—	—	83.24	0.18	0.04	14.421	0.022	1.016	1.077	0.041
	HTC082	0.775	2	20	—	—	89.60	3.77	2.14	25.522	0.067	1.087	1.234	2.142
	HTC092	0.737	2	15	—	—	86.99	1.41	0.73	23.346	0.045	1.056	1.211	0.726
	HTC259	0.802	2	10	—	—	80.97	1.88	0.99	16.972	0.039	1.040	1.159	0.991
	HTC255	0.774	2	5	—	—	85.75	1.00	0.46	21.750	0.039	1.040	1.192	0.459
	HTC256	0.787	2	0	—	—	77.39	0.09	0.02	13.393	0.020	1.016	1.116	0.017
	HTC094	0.784	1	20	—	—	87.49	1.66	0.91	24.197	0.048	1.057	1.217	0.914
HTC098	0.756	1	15	—	—	87.80	1.13	0.59	23.501	0.043	1.048	1.200	0.587	

Table 4.2-2 Summary of test results on four types of sand (2/6)

Materials	Test ID	Initial Void Ratio e_{ini}	Confining Pressure P'_{ini} (MPa)	Axial Strain $\epsilon_a(\%)$	Grain Size Distribution after CD Triaxial Test					Particle Breakage				
					Percent Passing (%)					Marsal	Hardin	D_{15}	D_{50}	ΔFC
					850 μ m	425 μ m	250 μ m	106 μ m	75 μ m					
Toyoura Sand	HTC254	0.785	1	10	—	—	84.99	0.98	0.43	20.991	0.038	1.040	1.185	0.432
	HTC114	0.773	1	5	—	—	84.92	0.22	0.09	14.710	0.023	1.012	1.112	0.086
	HTC165	0.775	1	0	—	—	78.45	0.11	0.00	9.884	0.015	1.000	1.080	0.003
JCA Sand	HTC178	0.605	4	20	—	55.39	35.38	3.99	2.15	5.390	0.0557	1.136	1.116	2.146
	HTC184	0.607	4	15	—	53.93	33.19	2.93	1.45	3.926	0.0385	1.092	1.073	1.452
	HTC185	0.640	4	10	—	53.33	32.87	1.98	0.88	3.325	0.0302	1.071	1.060	0.883
	HTC186	0.637	4	5	—	52.20	32.05	1.28	0.44	2.198	0.0200	1.050	1.034	0.440
	HTC187	0.606	4	0	—	50.54	30.76	0.33	0.02	0.761	0.0055	1.021	1.002	0.020
	HTC179	0.603	3	20	—	54.47	34.19	3.11	1.46	4.469	0.0440	1.106	1.087	1.463
	HTC180	0.621	3	15	—	53.02	32.53	2.20	1.01	3.022	0.0294	1.064	1.055	1.006
	HTC181	0.595	3	10	—	51.78	31.60	1.91	0.56	2.093	0.0203	1.050	1.029	0.559
	HTC182	0.638	3	5	—	51.61	31.16	1.00	0.33	1.606	0.0140	1.031	1.024	0.331
	HTC183	0.585	3	0	—	50.50	30.34	0.31	0.01	0.503	0.0041	1.012	1.005	0.013
	HTC225	0.518	2	20	—	53.97	32.91	2.70	0.95	3.966	0.0359	1.084	1.076	0.950
	HTC226	0.524	2	15	—	50.80	31.42	2.11	0.70	2.112	0.0174	1.057	1.014	0.695
	HTC227	0.523	2	10	—	50.20	31.39	1.64	0.44	1.643	0.0126	1.044	1.000	0.438
HTC228	0.515	2	5	—	48.80	30.62	1.39	0.20	2.584	0.0039	1.031	0.977	0.199	

Table 4.2-3 Summary of test results on four types of sand (3/6)

Materials	Test ID	Initial Void Ratio e_{ini}	Confining Pressure P'_{ini} (MPa)	Axial Strain $\epsilon_a(\%)$	Grain Size Distribution after CD Triaxial Test					Particle Breakage				
					Percent Passing (%)					Marsal	Hardin	D_{15}	D_{50}	ΔFC
					850 μ m	425 μ m	250 μ m	106 μ m	75 μ m					
JCA Sand	HTC229	0.517	2	0	—	47.57	29.78	0.81	0.00	3.239	-0.0057	1.018	0.955	0.003
	HTC221	0.533	1	20	—	51.54	31.26	1.21	0.31	1.542	0.0149	1.037	1.024	0.311
	HTC222	0.537	1	15	—	50.71	30.35	1.23	0.21	1.583	0.0093	1.025	1.012	0.211
	HTC223	0.542	1	10	—	50.65	30.09	1.08	0.13	1.632	0.0076	1.025	1.010	0.128
	HTC224	0.569	1	5	—	49.48	29.36	0.86	0.05	1.507	0.0003	1.000	1.000	0.052
	HTC230	0.530	1	0	—	47.21	29.29	0.72	0.003	3.510	-0.0087	1.000	0.951	0.003
Takasegawa Sand	HTC206	0.685	4	40	—	68.30	45.43	16.10	9.49	22.427	0.215	1.892	1.532	9.495
	HTC207	0.696	4	20	—	60.94	34.17	7.67	4.37	11.940	0.113	1.388	1.238	4.370
	HTC208	0.729	4	15	—	58.51	32.78	6.59	3.71	9.780	0.095	1.340	1.184	3.713
	HTC212	0.685	4	10	—	56.02	29.09	3.74	1.82	7.018	0.060	1.184	1.128	1.825
	HTC211	0.704	4	5	—	53.99	26.73	1.99	0.98	4.994	0.038	1.103	1.091	0.985
	HTC210	0.669	4	0	—	51.01	23.37	0.54	0.17	2.170	0.011	1.005	1.029	0.169
	HTC202	0.630	3	40	—	66.74	42.07	14.23	8.95	19.074	0.191	1.771	1.430	8.951
	HTC203	0.638	3	20	—	59.24	32.29	6.28	3.73	10.236	0.095	1.313	1.193	3.728
	HTC204	0.599	3	10	—	55.09	28.29	3.18	1.79	6.091	0.083	1.270	1.174	3.046
	HTC201	0.633	3	15	—	58.23	31.31	5.17	3.05	9.232	0.053	1.170	1.105	1.791
HTC200	0.605	3	5	—	51.89	24.52	1.39	0.70	2.885	0.021	1.049	1.043	0.700	

Table 4.2-4 Summary of test results on four types of sand (4/6)

Materials	Test ID	Initial Void Ratio e_{ini}	Confining Pressure P'_{ini} (MPa)	Axial Strain $\epsilon_a(\%)$	Grain Size Distribution after CD Triaxial Test					Particle Breakage				
					Percent Passing (%)					Marsal	Hardin	D_{15}	D_{50}	ΔFC
					850 μ m	425 μ m	250 μ m	106 μ m	75 μ m					
Takasegawa Sand	HTC205	0.652	3	0	—	50.32	23.39	0.31	0.10	1.317	0.007	1.000	1.026	0.103
	HTC199	0.632	2	40	—	62.41	36.76	9.15	5.50	13.757	0.133	1.485	1.286	5.503
	HTC214	0.666	2	20	—	58.52	32.22	5.53	3.02	9.516	0.088	1.295	1.180	3.015
	HTC196	0.598	2	15	—	57.56	30.80	4.52	2.67	8.555	0.075	1.237	1.155	2.674
	HTC197	0.580	2	10	—	53.36	26.74	2.02	1.08	4.362	0.036	1.109	1.072	1.083
	HTC198	0.634	2	5	—	50.20	23.08	0.69	0.32	1.810	0.008	1.000	1.019	0.319
	HTC213	0.688	2	0	—	50.73	23.67	0.43	0.04	1.728	0.010	1.010	1.029	0.036
	HTC215	0.691	1	40	—	59.16	32.08	5.60	3.30	10.156	0.090	1.287	1.193	3.302
	HTC216	0.703	1	20	—	56.77	27.89	2.81	1.49	7.769	0.055	1.149	1.134	1.488
	HTC217	0.670	1	15	—	52.43	25.33	1.42	0.77	3.426	0.026	1.060	1.056	0.766
	HTC218	0.680	1	10	—	51.06	24.95	1.46	0.71	2.058	0.020	1.060	1.029	0.709
	HTC219	0.683	1	5	—	50.21	23.80	0.63	0.24	1.207	0.010	1.027	1.019	0.238
HTC220	0.653	1	0	—	49.25	22.76	0.18	0.01	0.673	0.001	1.005	1.000	0.006	
Inagi Sand	HTC194	1.075	4	40	98.26	80.47	43.23	21.36	15.86	31.229	0.252	3.757	1.251	15.855
	HTC171	1.109	4	20	98.13	87.51	41.63	14.62	10.21	29.634	0.231	2.435	1.251	10.206
	HTC172	1.098	4	15	98.65	86.57	36.30	10.81	7.41	24.305	0.193	2.055	1.192	7.414
	HTC173	1.099	4	10	98.26	85.18	32.22	8.77	5.94	20.218	0.163	1.814	1.153	5.939

Table 4.2-5 Summary of test results on four types of sand (5/6)

Materials	Test ID	Initial Void Ratio e_{ini}	Confining Pressure P'_{ini} (MPa)	Axial Strain ϵ_a (%)	Grain Size Distribution after CD Triaxial Test					Particle Breakage				
					Percent Passing (%)					Marsal	Hardin	D_{15}	D_{50}	ΔFC
					850 μ m	425 μ m	250 μ m	106 μ m	75 μ m					
Inagi Sand	HTC174	1.128	4	5	98.34	84.63	26.81	6.06	3.88	14.812	0.130	1.494	1.120	3.879
	HTC175	1.114	4	0	98.39	84.07	22.85	3.68	2.33	14.070	0.104	1.277	1.099	2.335
	HTC191	1.046	3	40	97.88	78.05	38.51	18.32	13.27	26.637	0.210	3.023	1.176	13.274
	HTC149	1.093	3	20	98.46	86.71	36.74	11.96	7.93	24.744	0.200	2.156	1.196	7.927
	HTC151	1.077	3	15	98.14	84.00	32.70	8.93	6.12	20.704	0.161	1.839	1.157	6.123
	HTC154	1.082	3	10	98.44	83.02	28.76	6.98	4.75	16.765	0.136	1.594	1.131	4.749
	HTC163	1.051	3	5	97.91	73.96	21.23	4.25	2.73	9.323	0.064	1.246	1.050	2.730
	HTC157	1.028	3	0	98.14	79.47	19.73	2.17	1.22	9.467	0.069	1.174	1.073	1.223
	HTC192	1.045	2	40	98.23	76.00	34.94	15.32	11.11	22.939	0.176	2.529	1.131	11.113
	HTC144	1.061	2	20	98.20	82.07	30.67	8.86	6.02	18.674	0.148	1.777	1.135	6.025
	HTC145	1.058	2	15	98.10	78.09	27.49	7.22	4.92	15.487	0.115	1.575	1.099	4.922
	HTC146	1.032	2	10	98.39	82.81	26.48	5.64	3.69	14.481	0.121	1.461	1.113	3.686
	HTC147	1.111	2	5	98.35	78.86	22.31	3.48	2.16	10.313	0.082	1.264	1.079	2.158
	HTC148	1.032	2	0	98.45	80.80	18.58	1.67	1.00	10.798	0.069	1.139	1.073	1.000
	HTC193	1.049	1	40	98.04	74.53	28.75	10.76	7.74	16.746	0.126	1.865	1.086	7.745
	HTC141	1.051	1	20	98.07	78.84	26.19	6.83	4.38	14.191	0.111	1.494	1.096	4.384
HTC139	1.079	1	15	98.45	81.72	23.53	5.10	3.30	11.725	0.106	1.328	1.093	3.298	

Table 4.2-6 Summary of test results on four types of sand (6/6)

Materials	Test ID	Initial Void Ratio e_{ini}	Confining Pressure P'_{ini} (MPa)	Axial Strain ϵ_a (%)	Grain Size Distribution after CD Triaxial Test					Particle Breakage				
					Percent Passing (%)					Marsal	Hardin	D_{15}	D_{50}	ΔFC
					850 μ m	425 μ m	250 μ m	106 μ m	75 μ m					
Inagi Sand	HTC140	1.053	1	10	98.47	80.78	21.82	3.70	2.36	10.784	0.090	1.252	1.086	2.357
	HTC142	1.075	1	5	98.21	78.42	17.41	1.92	1.12	8.419	0.057	1.105	1.057	1.115
	HTC143	1.059	1	0	98.31	78.72	16.73	1.21	0.74	8.717	0.053	1.087	1.057	0.737

4.3 Brittleness Degree of Sands

4.3.1 Introduction

In section 4.2, I examined the experimental results of stress-strain relationship and degree of particle breakage corresponding to Marsal, Hardin, Lee & Farhoomands and D_{50} as well as increment of fines content (ΔF_c) on four types of sand. The summaries of those concluded that show that the amount of particle breakage continues to very large strains even when the steady state for four sands was reached at higher stress levels. Also, the degree of particle breakage has linear relationship with stress levels and shear strains during the shearing process. This also implies that the amount of particle breakage at steady state is independent of the path taken to reach it but is depends on the magnitude of stress levels and axial strains.

In this case, it appears reasonable to assume that breakage does not completely cease at higher stress conditions. Thus, the idea of the definition of a parameter brittleness degree (B_d) which represents the particle brittleness of sands came from the previously described fact that the amount of particle breakage had linear relation to confining stress levels and axial strain during the shearing process. However, it's difficult to select a good method and introduced to the new parameter (B_d) for evaluating the amount of particle breakage because of unique requirements and limitation of calculation method.

A number of studies on the effect of fines content (F_c) under the undrained monotonic response of sands have been published in recent years. It has been point out that undrained soil behavior was governed by fines content (F_c) which controlled soil matrix. Therefore, for simplicity, I select increment of fines content (ΔF_c) as a basis to determine of brittleness degree (B_d) value.

When the number of unknown independent variable are negligible, i.e. material characteristics, time, energy and trajectories, the constitutive equation is simply related to the stress and strain variables. Furthermore, one of key problems for this equation is that the dominant mode of particle breakage is very difficult to determine, leading to problems in the determination of amount of particle breakage. In the present study, domain mode of particle breakage is negligible and intuitively assume that the fine particles that developed by breakage are not capable to produce multiple small pieces under stress condition. Finally, particle breakage will not occur if either confining stress or axial strain levels is not present.

4.3.2 Determination of Brittleness degree (B_d) value

A functional relationship $F_c = B_d (\sigma_3', \varepsilon_1)$ is proposed in this section which is able to evaluate the brittleness degree of sands, and yet has a simple form. This idea of this equation came from the previous description which is the amount of fines content (F_c) has linear relationship with stress levels and shear strains during the shearing process. The linear relationship is expressed by an equation as follows:

$$dF_c = B_d \frac{\sigma_3'}{p_a} d\varepsilon_1 \quad (4.1)$$

where σ_3' is the minimum principal stress, ε_1 is the maximum principal strain and $p_a = 100$ kPa is atmosphere pressure. Note that equation (4.1) is applicable to shear process; not applicable to isotropic consolidation.

4.3.2.1 Prediction of brittleness degree (B_d) value

1. Prediction of brittleness degree by increment of fines content (ΔF_c).

The data obtained from the experimental program is used to evaluate the predictive ability of particle breakage indices in terms of increment of fines content (ΔF_c) against $\sigma_3'/p_a \times \varepsilon_1$.

Given a variable i increment of fines content (ΔF_c) and a number of variable $\sigma_3'/p_a \times \varepsilon_1$ that related to increment of fines content (ΔF_c), linear regression analysis is applied to quantify the brittleness degree (B_d) of the relationship between increment of fines content (ΔF_c), confining stress and axial strain.

The brittleness degree (B_d) can be obtained with the regression analysis of the test results. The test data plotted in Figures 4.2-17 and Figure 4.2-18 is rearranged to plot the increment of fines content during the shear process after consolidation versus the values of $\sigma_3'/p_a \times \varepsilon_1$. In Figure 4.3-1, Particle breakage is considered to occur after consolidation which meant the amount of particle breakage was subtracted to origin. Therefore, the straight lines drawn through the data and the slope is reported in the form of the equation that defines the best-fit line.

According to this figure the tested sands in the present study has brittleness degree (B_d) of 0.981% for Inagi sand, brittleness degree (B_d) of 0.981% for Inagi sand, $B_d = 0.629$ % for Takasegawa sand, $B_d = 0.629$ % for Takasegawa sand, $B_d = 0.598$ % for Toyoura sand and $B_d = 0.236$ % for JCA sand.

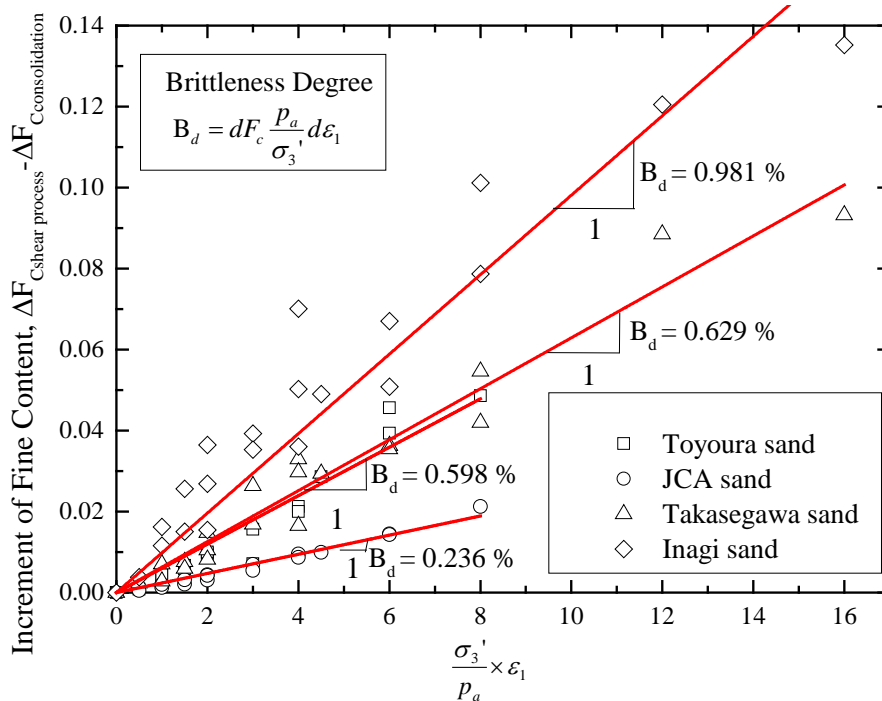


Figure 4.3-1 Increment of fines content and $\sigma_3'/p_a \times \epsilon_1$ relationship

2. Prediction of brittleness degree by various particle breakage indices

The amount of particle breakage which obtained from various particle indices, B_g , (Marsal, Hardin, Lee and Farhoomand and D_{50}) are plotted against $\sigma_3'/p_a \times \epsilon_1$ for reference. The summary of brittleness degree (B_d) for each sands by various particle breakage indices is given in Table 4.3-1.

Same process of detailed analysis as increment of fines content (ΔF_c), given a variable particle breakage indices and a number of variable $\sigma_3' d\epsilon_1/p_a$, linear regression analysis is applied to quantify the brittleness degree (B_d) of the relationship between particle breakage indices, confining stress and axial strain. In Figure 4.3-2 to Figure 4.3-5, using best-fit line to obtained the slope of each sand and straight lines drawn through the data. The slope is reported in the form of the equation that defines the best-fit line. Particle breakage is considered to occur after consolidation which meant the amount of particle breakage was subtracted to origin.

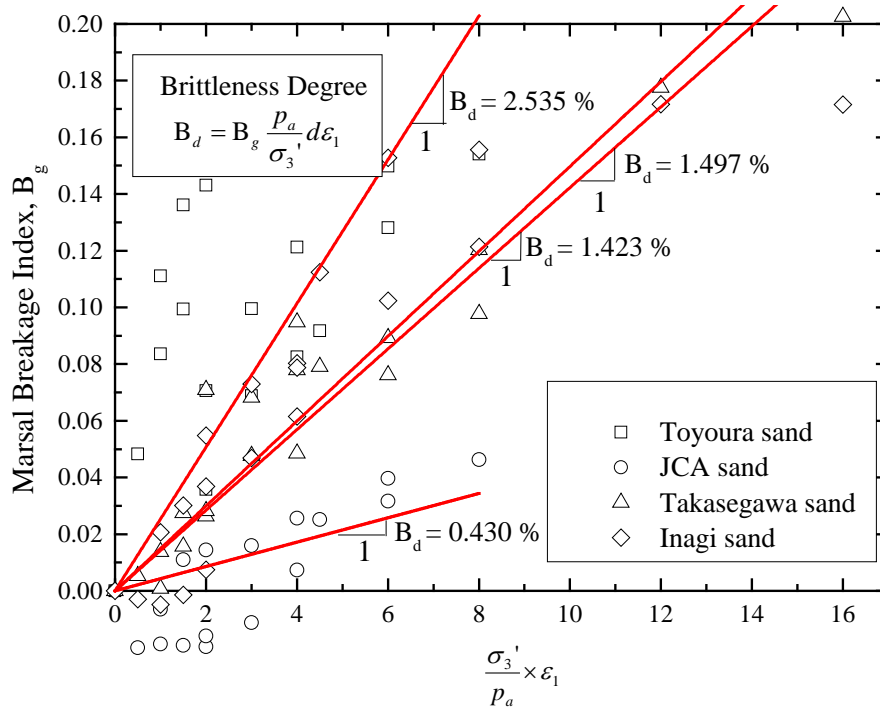


Figure 4.3-2 Marsal's breakage index and $\sigma_3'/p_a \times \epsilon_1$ relationship

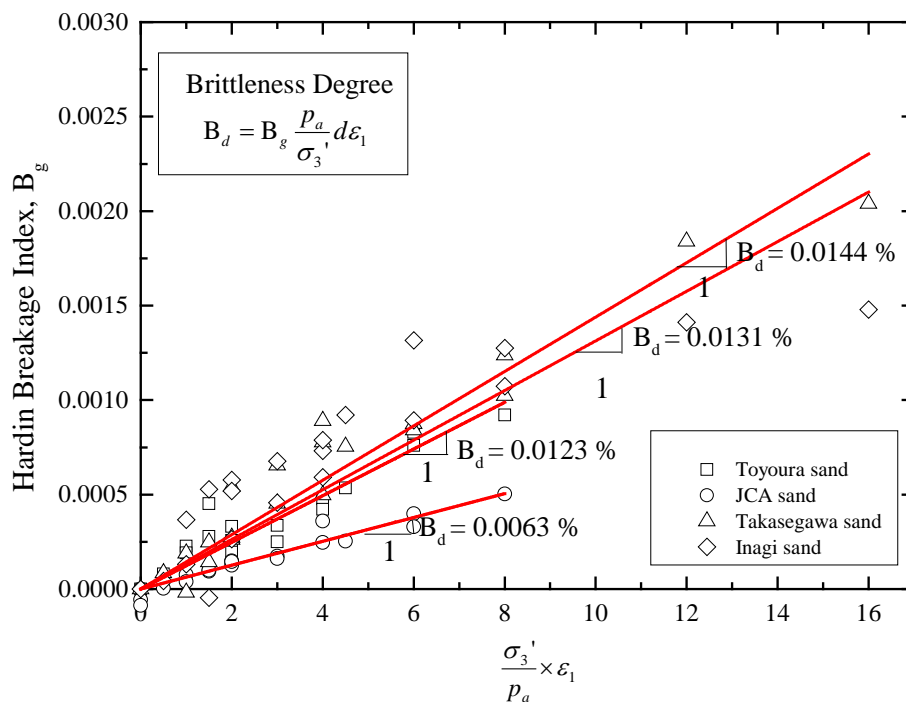


Figure 4.3-3 Hardin's breakage index and $\sigma_3'/p_a \times \epsilon_1$ relationship

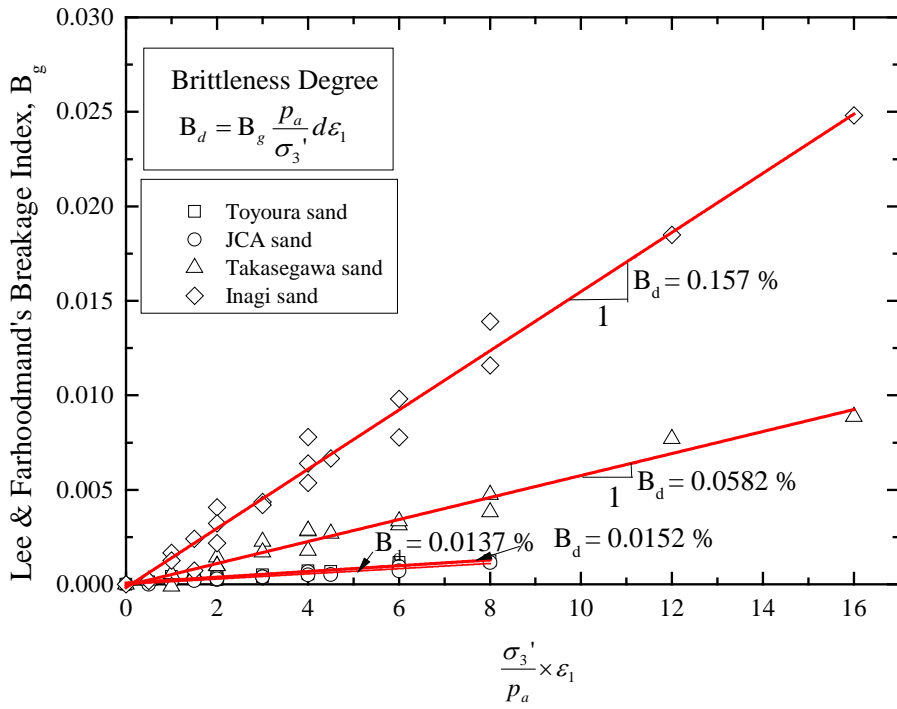


Figure 4.3-4 Lee & Farhoodmand's breakage index and $\sigma_3'/p_a \times \epsilon_1$ relationship

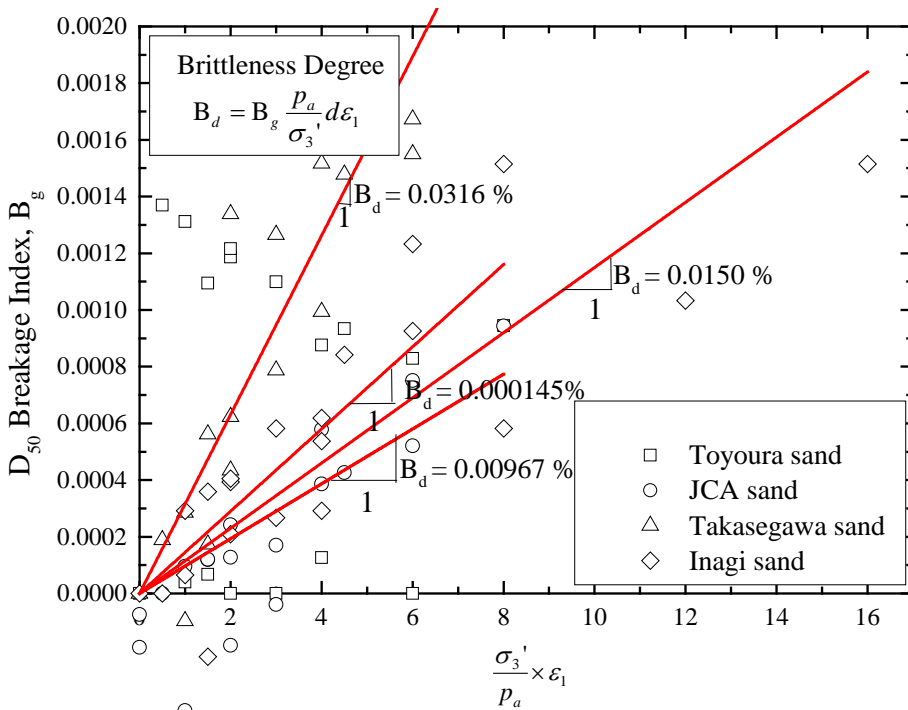


Figure 4.3-5 D_{50} 's breakage index and $\sigma_3'/p_a \times \epsilon_1$ relationship

Table 4.3-1 Summary of brittleness degree for each sands

Material	Brittleness degree(B_d)				
	ΔF_c	Marsal	Hardin	D_{15}	D_{50}
Toyoura sand	0.598%	2.535%	0.0123%	0.0152%	0.0145%
JCA sand	0.236%	0.236%	0.0063%	0.0137%	0.00967%
Takasegawa sand	0.629%	1.423%	0.0144%	0.0582%	0.0316%
Inagi sand	0.981%	1.497%	0.0131%	0.157%	0.0150%

4.3.2.2 Summary

The purpose of this section was to propose a linear equation to assess the amount of particle breakage. The following conclusion can be drawn:

1. A number of studies on the effect of fines content (F_c) under the undrained monotonic response of sands have been published in recent years. It has been point out that undrained soil behavior was governed by fines content (F_c) which controlled soil matrix. Therefore, for simplicity, I select increment of fines content (ΔF_c) as a basis to determine of brittleness degree (B_d) value.
2. I conducted a series of consolidated drained triaxial compression test on sand under a wide range of confining stress and strain levels. I then adopted the fines content as an index to quantify the magnitude of particle breakage. From experimental results, we found that degree of particle breakage has linear relationship with stress levels and axial strains so that a linear equation based on increment of fines content (ΔF_c) and brittleness degree (B_d) associated with stress and strain levels is then proposed as $dF_c = B_d(\sigma_3'/p_a)d\varepsilon_1$.

4.4 Density Evaluation Based on Test Method for Minimum and Maximum densities of sands

It is well known that densities play an important role in defining the strength of soils. Typically, the strength of soil decreases as dry density decreases, being associated with increased water content, as expected. The effects therefore investigated for four types of material by examining the minimum and maximum densities under low water content conditions.

In the author's experiments, determining minimum and maximum densities was not so easy. Laboratory test results were often highly sensitive to variable parameters, i.e. mechanical properties, relative humidity, temperature, grain size distribution, suction, and human manipulation, These resulted in imprecise measurements of minimum and maximum densities.

In this study, I adopted relative density in strict accordance with the JGS procedures for determining minimum and maximum densities, and observed low water content limits to evaluate the influence of minimum and maximum densities on three types of sands as well as associated changes in material characteristics and grain size distribution.

I performed a series of minimum and maximum density tests on four types of sands to investigate the effect of low water content. The test methods for determining the soil particle densities and the minimum and maximum densities of the sands conformed to JGS 0111-2009 and JGS 0161-2009, respectively.

4.4.1 Effect of low water content on Minimum and Maximum Densities

To study the effect of low water content on densities of four types of material, a standard test methods for minimum and maximum densities were carried out. The dry density and relative density of each specimen were determined and plotted versus low water content. The designed grain size distribution curves are referred to Figure 3.2-1.

4.4.1.1 Toyoura sand

These test results demonstrated that the dry density of Toyoura sand decreased with increasing low water content (Figure 4.4-1). As the water content (ω) increased from 0 % to 0.3%, the maximum density of the Toyoura sand remained constant at 1.6 g/cm³, while the minimum density decreased from 1.35 g/cm³ to 1.20 g/cm³.

The relationship between low water content and maximum relative density can also be seen in Figure 4.4-2, where the maximum relative density can be seen to remain constant until the water content reached 0.75%, decreasing thereafter from 100% to 75% as the water content was raised. The minimum relative density of the Toyoura sand initially remained constant until the water content reached 0.1%. As the water content increased from 0.1% to 0.2%, the minimum relative density of the Toyoura sand decreased by 25%, and by 100% as the water content increased from 0.1% to 0.5%. For this sand, the minimum relative density at 0.5% water content was 4 times higher than that at 0.2%. It is clear that adding a small amount of water to the Toyoura sand had a more significant effect on minimum relative density than on maximum relative density.

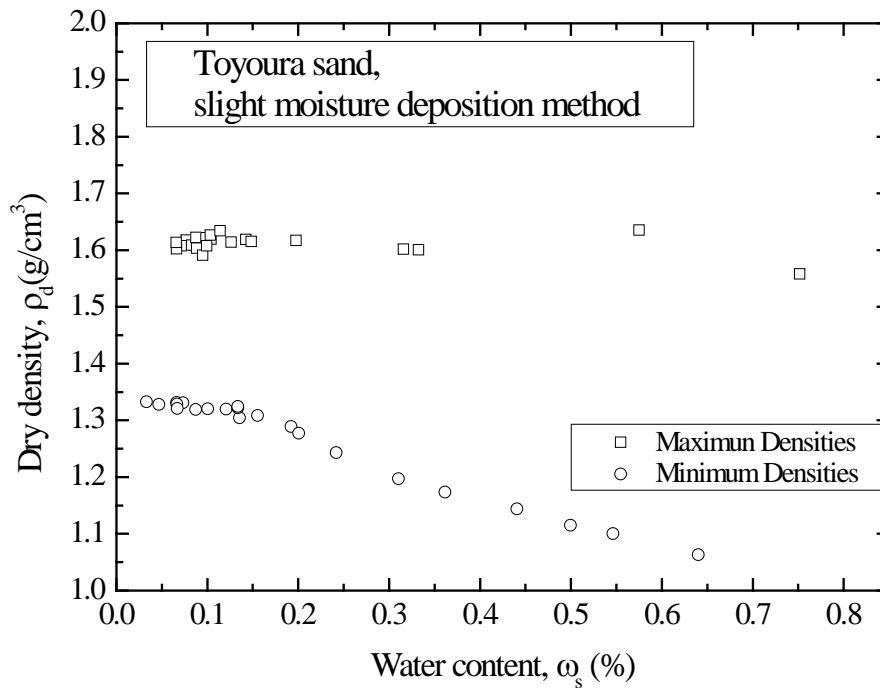


Figure 4.4-1 Dry density versus water content (Toyourea Sand)

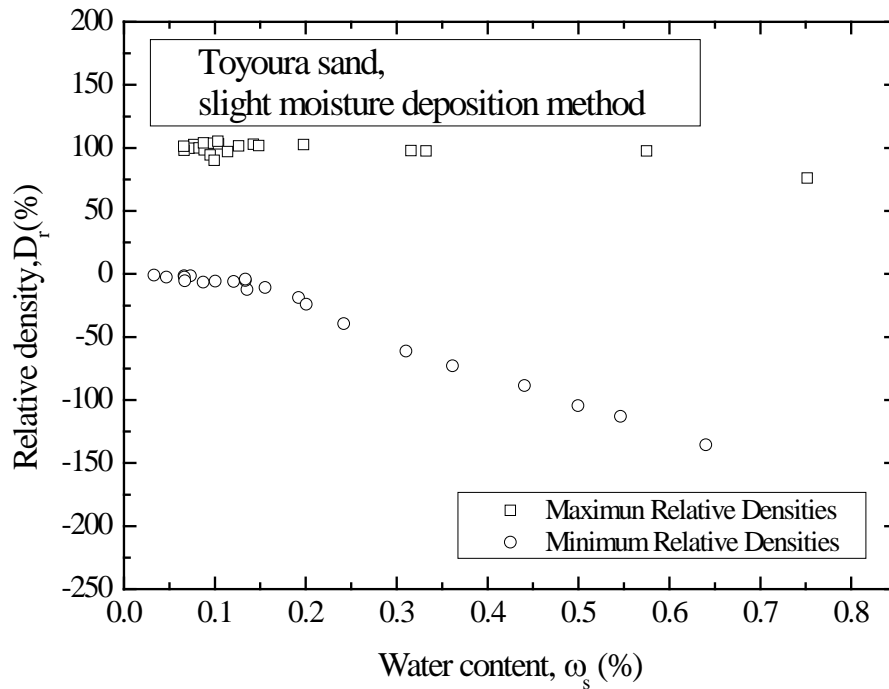


Figure 4.4-2 Relative density versus water content (Toyouira Sand)

4.4.1.2 JCA sand

The results of the minimum and maximum density test on the JCA sand are shown in Figure 4.4-3. It shows that a small amount of water added to JCA sand had more significant effects on minimum density than on maximum density. When the water content increased from 0 % to 0.5 %, the maximum density stayed constant at approximately 1.8 g/cm^3 . The minimum density decreased from 1.5 g/cm^3 to 1.15 g/cm^3 in the same interval.

It is surprising how the addition of water content affects the minimum relative density quite severely. As illustrated in Figure 4.4-4, when the water content rose from 0 % to 0.1 %, the minimum relative density decreased by 50 %; while the maximum relative density was constant at 100 %. Furthermore, when water content increased from 0 % to 0.5 %, the minimum relative density of JCA sand dropped by 200 %; but the maximum relative density was still remained constant at 100 %. For this sand, the change of the minimum relative density at 0.5 % water content was approximately twice higher than that at 0.2 %.

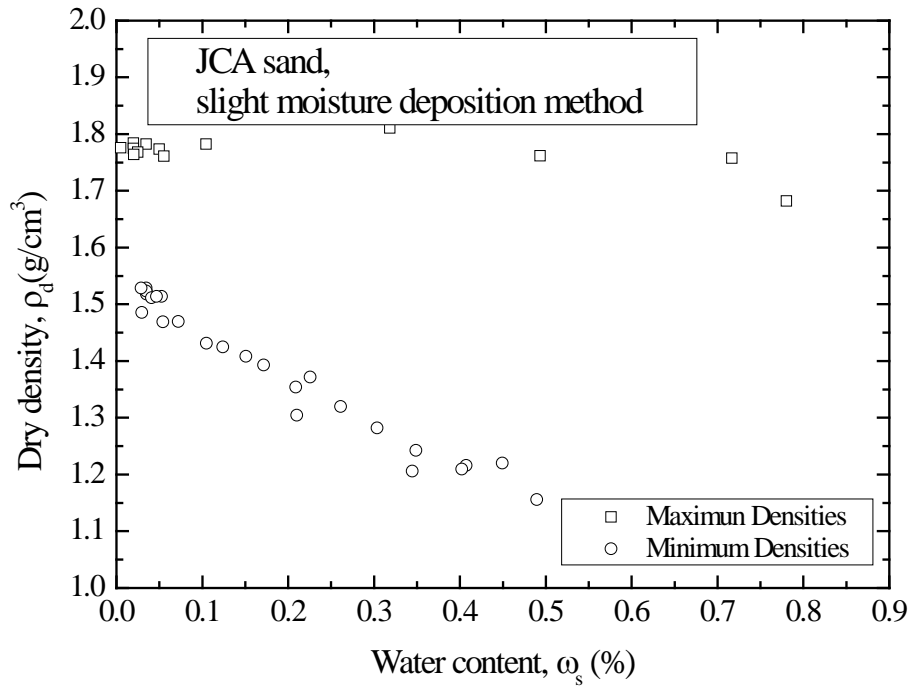


Figure 4.4-3 Dry density versus water content (JCA Sand)

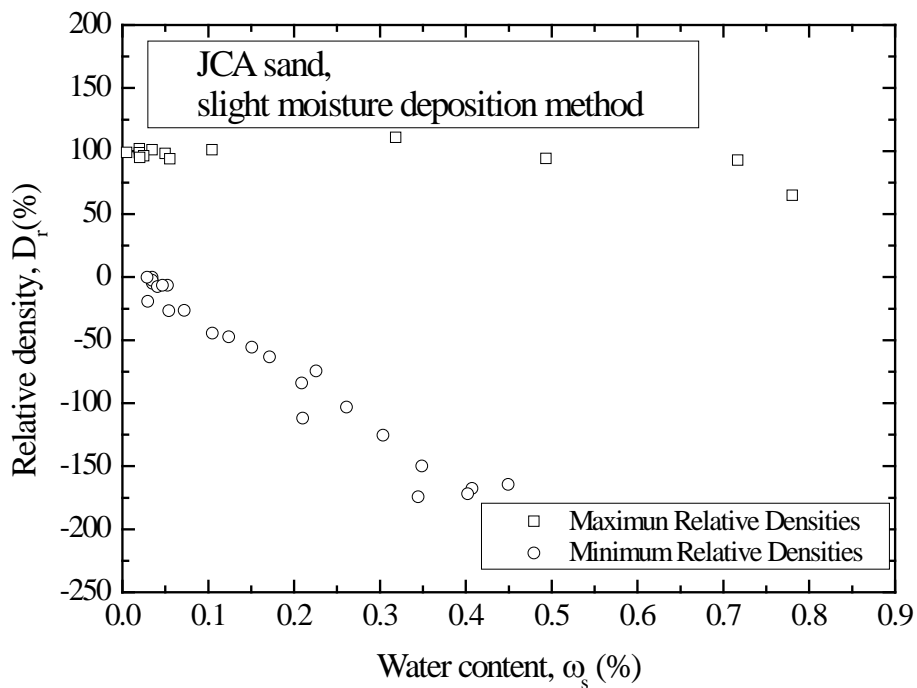


Figure 4.4-4 Relative density versus water content (JCA Sand)

4.4.1.3 JCA sand (250 μm -150 μm)

Similar relative density behavior has been observed in JCA sand in which soil

particles larger than 250 μm and smaller than 150 μm were discarded by dry sieving. The minimum density of this JCA sand (250 μm -150 μm) was strongly influenced by variations in small levels of water content, with minimum density decreasing as water content increased (Figure 4.3-5). As the water content increased from 0.05 % to 0.1 %, the maximum density remained constant at 1.6 g/cm^3 , but the minimum density decreased from 1.4 g/cm^3 to 1.2 g/cm^3 .

Figure 4.4-6 shows that an increase of 0.1 % in the water content of the sieved JCA sand (250 μm -150 μm) leads to a marked reduction in minimum relative density, from 0 % to -150 %. In addition, the maximum relative density gradually decreased with increasing water content. As the water content increased from 0 % to 0.9 %, the maximum relative density decreased approximately by 75 %. As mentioned previously, the relative density is a function not only of density, humidity, and human manipulation, but also of grain size distribution. The sieved JCA sand is more sensitive to small increases in water content than the other materials, and its relative density changes significantly with small changes in water content.

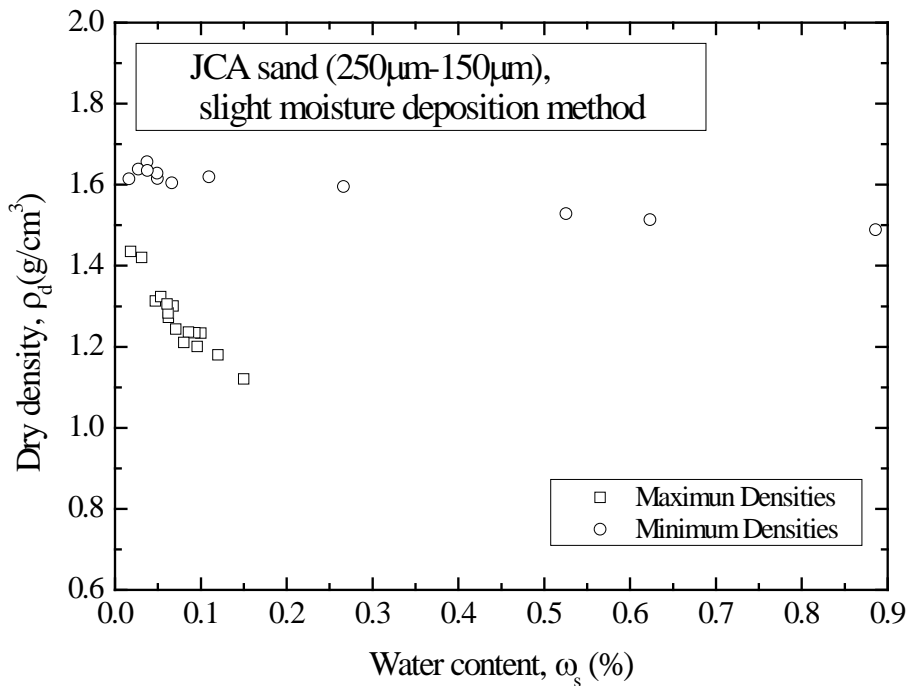


Figure 4.4-5 Dry density versus water content (JCA Sand, 250 μm -150 μm)

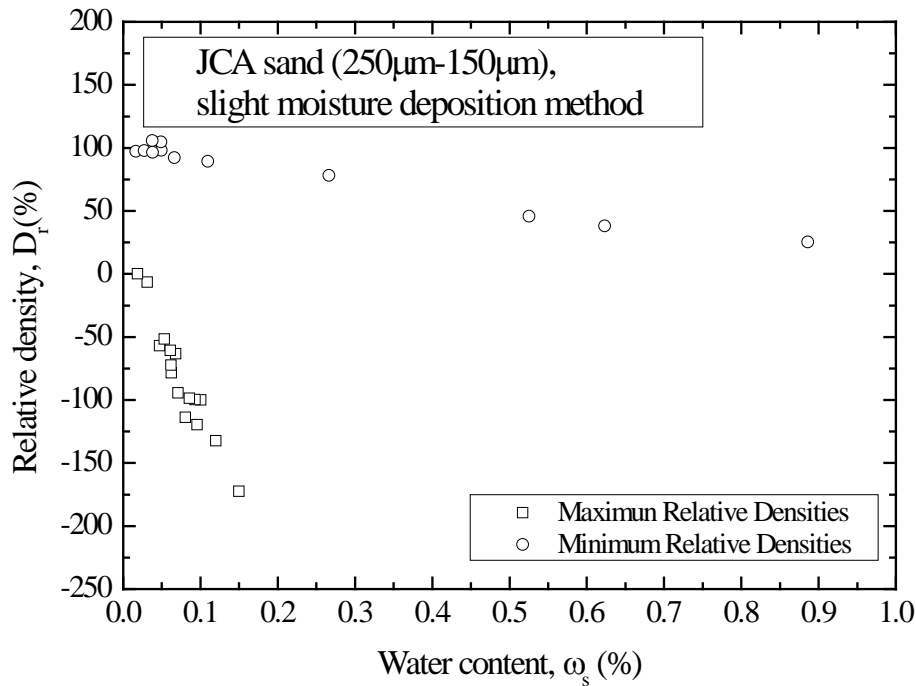


Figure 4.4-6 Relative density versus water content (JCA Sand, 250 μm -150 μm)

4.4.1.4 Takasegawa sand

These test results demonstrated that the dry density of Takasegawa sand decreased with increasing water content (Figure 4.4-7). As the water content increased from 0 % to 0.5%, the maximum density of the Toyoura sand remained constant at 1.6 g/cm^3 , while the minimum density decreased from 1.36 g/cm^3 to 1.25 g/cm^3 .

Figure 4.4-8 show that the relationship between water content and maximum relative density can also be seen in Figure 4.4-8, where the maximum relative density can be seen to remain constant until the water content reached 0.7 %, decreasing thereafter from 100 % to 75 % as the water content was raised. The minimum relative density of the Takasegawa sand initially remained constant until the water content reached 0.1 %. As the water content increased from 0.1 % to 0.5 %, the minimum relative density of the Takasegawa sand decreased by 50 %, and by 250 % as the water content increased from 0.1 % to 0.5 %. For this sand, the minimum relative density at 1 % water content was five time higher than that at 0.5 %. The influence of water effects on soil particles are as sensitive as JCA sand.

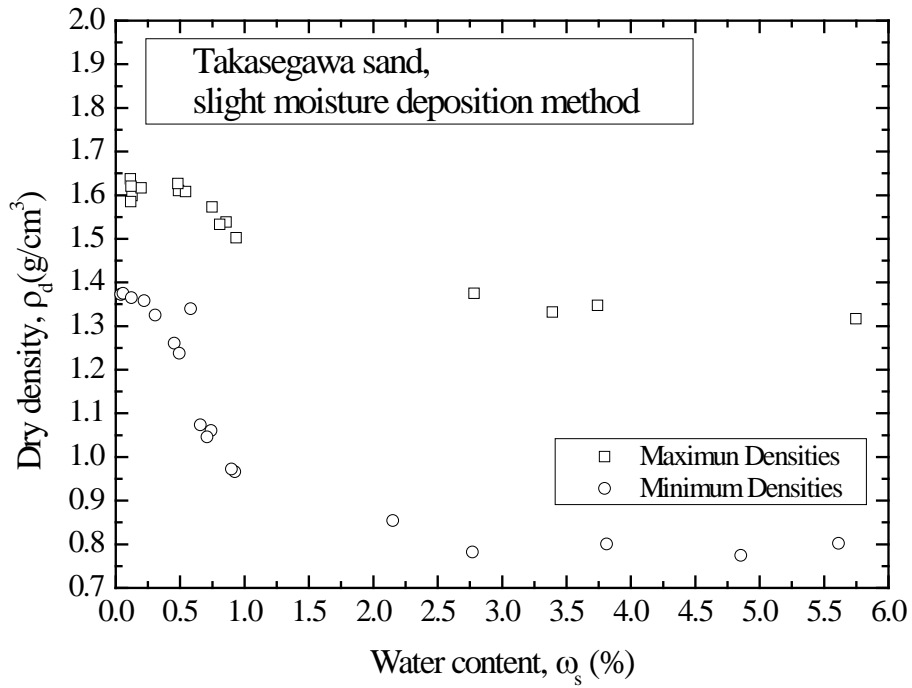


Figure 4.4-7 Dry density versus water content (Takasegawa sand)

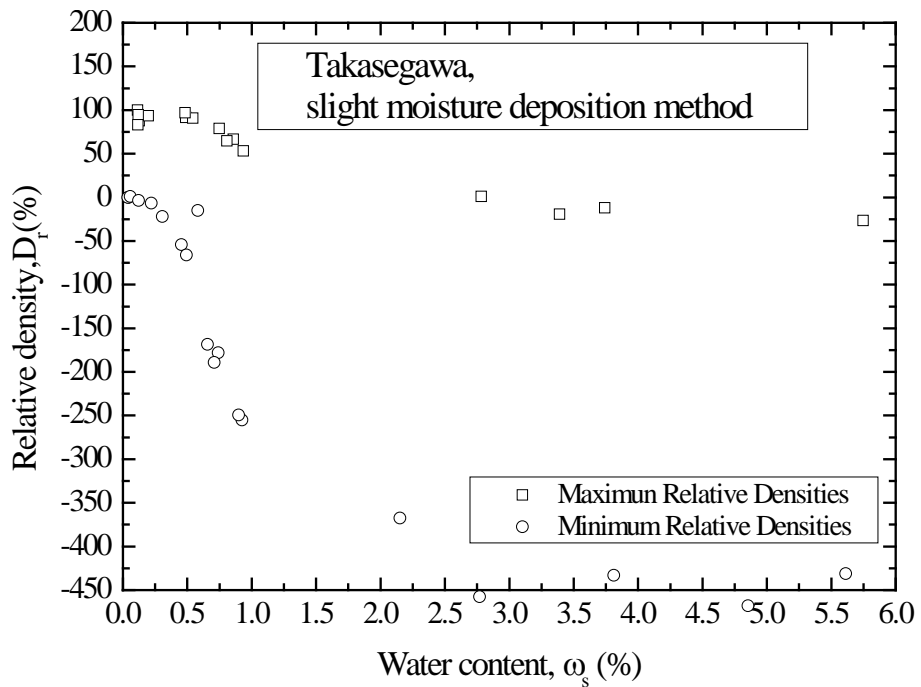


Figure 4.4-8 Relative density versus water content (Takasegawa sand)

4.4.1.5 Inagi sand

In contrast to the Toyoura JCA and Takasegawa sands, Figure 4.4-9 presents the maximum (ρ_{dmax}) and minimum (ρ_{dmin}) densities of the Inagi sand, which is less sensitive to the influence of water content. When the water content increased from 1 % to 5 %, the maximum density decreased from 1.5 g/cm³ to 1.4 g/cm³, while the minimum density decreased from 1.2 g/cm³ to 1.0 g/cm³. Similarly, Figure 4.3-10 shows the relative density-water content relationship for Inagi sand. As the water content for Inagi sand rose from 0 % to 5 % the minimum relative density dropped from 0 % to -75 % and the maximum relative density decreased from 100% to 75 %. For this sand, the change of the minimum relative density at 6.5 % water content was approximately twice higher than that at 5.0 %.

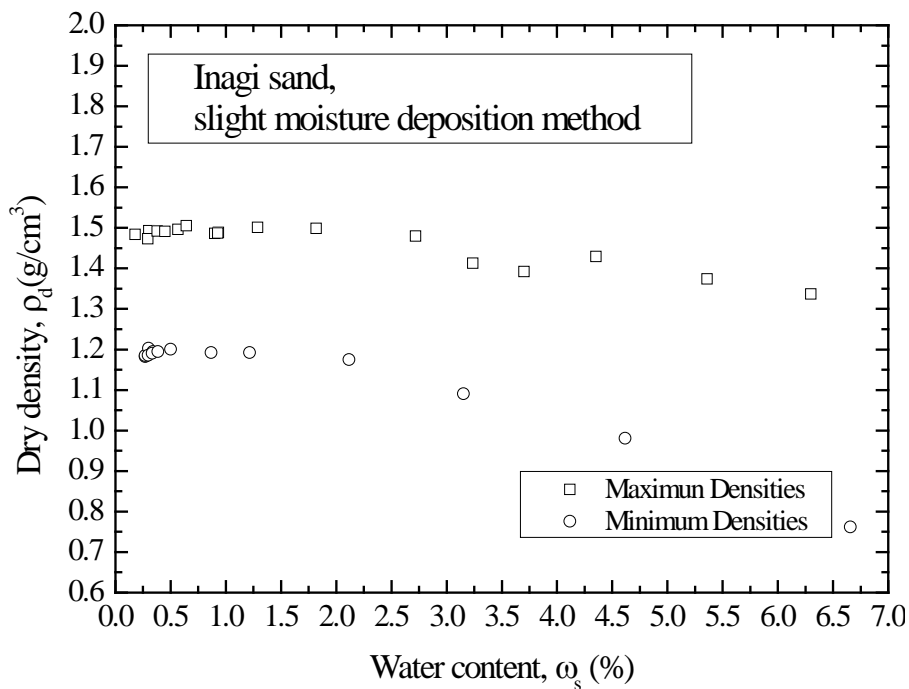


Figure 4.4-9 Dry density versus water content (Inagi sand)

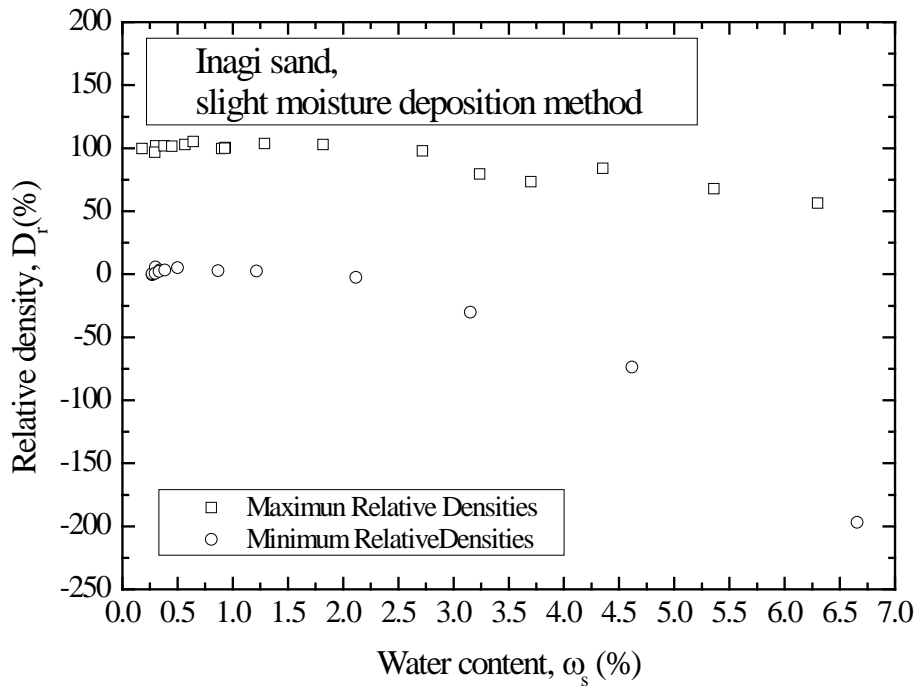


Figure 4.4-10 Relative density versus water content (Inagi sand)

4.4.1.6 Summary of analysis

The minimum and maximum density data have been presented with conventional linear water content (ω). Dry Density-water content relationship has proposed alternatives with a logarithm ω axis for four sands. The principle purpose of the work presented in this section, however, is to observe whether convergence is seen in this relationship or not. With such a wide range of sands that investigated here, for which the experiments process are also likely to be varied, it is also most unlikely that a single set of axes would be optimum for all the sands. A logarithmic water content axis was tried for Figure 4.4-11 to Figure 4.4-14 but the resulting plot gave the relationship that was still not straight but convex upwards rather than concave.

The effect of changing the water content observed here is somewhat in contrast to four types of sand as shown from Figure 4.3-11 to Figure 4.4-14. One particular detailed study compared Toyoura sand, JCA sand, and Takasegawa sand with the same water content. For the same water content increased from 0.1 % to 0.5 % , the maximum density of Toyoura sand, JCA sand, and Takasegawa sand remained constant at 1.6 g/cm³, 1.8 g/cm³, 1.6 g/cm³ and 1.4 g/cm³, respectively; while the minimum density of Toyoura sand decreased from 1.35 g/cm³ to 1.10 g/cm³, the minimum density of JCA sand decreased from 1.45 g/cm³ to 1.10 g/cm³, and the minimum density of Takasegawa

sand decreased from 1.4 g/cm^3 to 1.25 g/cm^3 . Finally, the minimum density of Inagi sand stayed constant at 1.2 g/cm^3 .

Similar comparison on relative density behavior has been observed on four sands. As illustrated in Figure 4.4-13, when the water content increased from 0.1 % to 0.5 %, the maximum relative density of Toyoura sand, JCA sand, Takasegawa sand and Inagi sand stayed constant at approximately at 100%. However, as small amount of water added to four sands, they had more significant effects on minimum density than on maximum density. As illustrated in Figure 4.4-14, when the water content rose from 0.1 % to 0.5 %, the minimum relative density of the Toyoura sand, JCA sand, and Takasegawa sand decreased by 100 %, 200 %, and 50 %, respectively. In contrast to the Toyoura sand, JCA sand, and Takasegawa sands, the minimum relative density of the Inagi sand, which is less sensitive to the influence of water content. As the water content for Inagi sand rose from 0.1 % to 0.5 %, the minimum relative density stayed constant at 0 %.

In total four different sands were tested, the results imply that JCA sand is more sensitive to small increases in water content than the other three sands, and its relative density changes significantly with small changes in water content. According to Das (2002), the decrease of dry density with the increase of water content can be attributed to the capillary tension effect. At lower water contents, the capillary tension of the JCA sand in the pore water inhibits the tendency of the soil particles to move around and be densely compacted. On the other hand, I found that the minimum relative density of the Inagi sand reached -50% when 3% water content was added. This can imply that low water content can induce more suction in the Toyoura sand, JCA sands and Takasegawa sand than in Inagi sand, so that small increases in water contents lead to large changes in the densities and relative densities of sandy materials, can either overestimate or underestimate the water content's effect and can yield a relative density varying two- to threefold or more, resulting in incorrectly biased estimates.

As might also be observed from test results, the primary factors controlling the minimum and maximum densities of sands not only are mechanical properties, grain size distribution, suction, and human manipulation, but also relative humidity and temperature. It implies that controlling relative humidity is critical in preserving sands because unacceptable levels of moisture can significantly affect test results. For example, when materials are taken out of the drying oven, the rapid temperature and relative humidity changes they experience may cause condensation to form on them. In such a case, either high or low relative humidity can provide enough moisture to

decrease the materials' relative densities. Sands can readily absorb or release moisture due to fluctuations in relative humidity. This may lead to desiccation and embrittlement of some materials. Thus, I suggest that it is essential to systematically measure, record, and control relative humidity in order to maintain stable conditions.

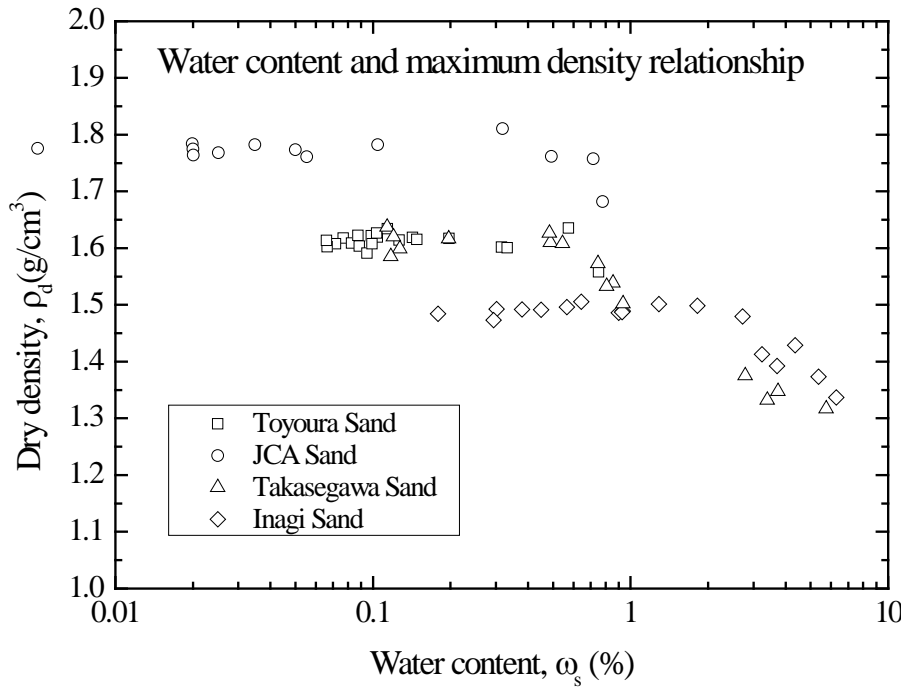


Figure 4.3-11 Water content and maximum density relationship

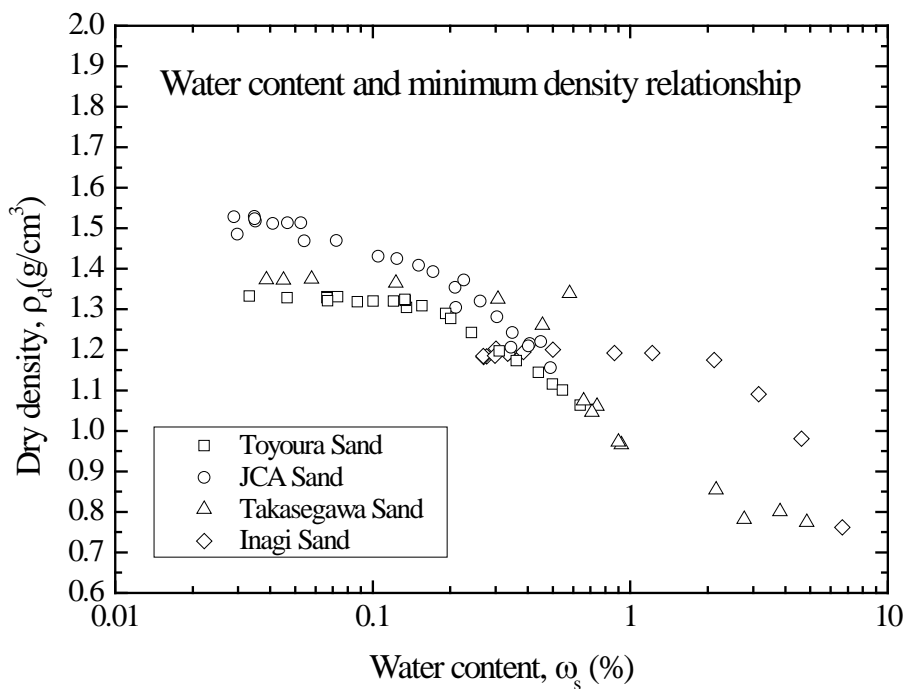


Figure 4.3-12 Water content and minimum density relationship

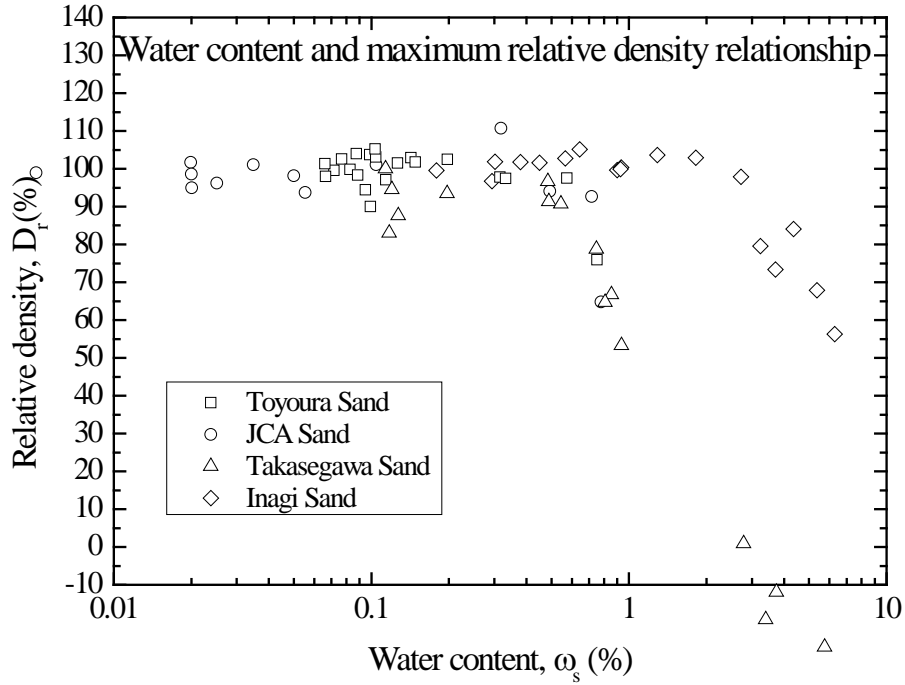


Figure 4.3-13 Water content and maximum relative density relationship

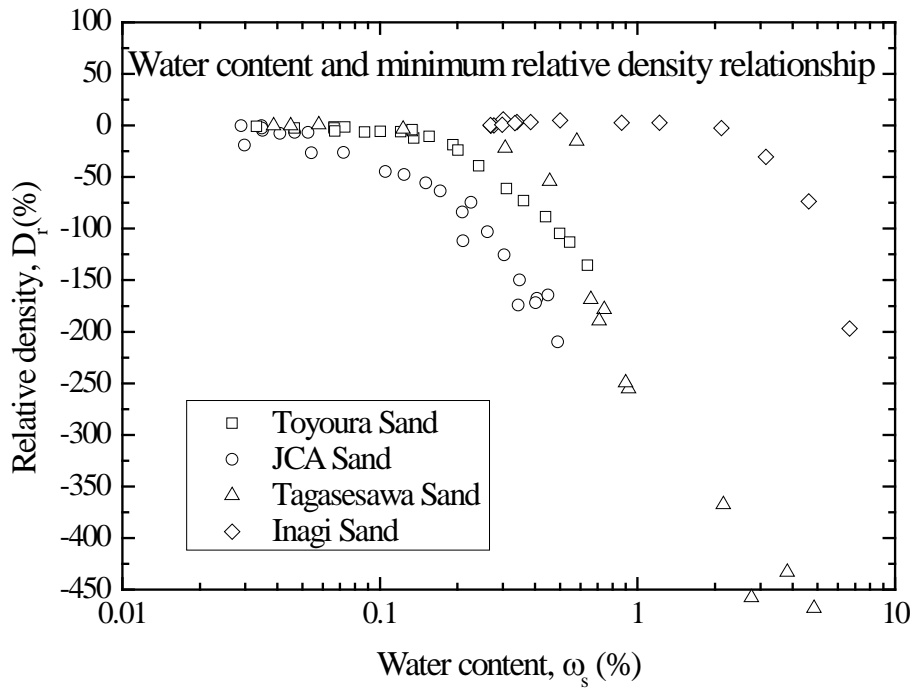


Figure 4.3-14 Water content and minimum relative density relationship

4.5 Water Effects Related to Particle Breakage

In this dissertation, the purpose of this research is looking for a low cost and less time-consuming approaches to evaluate the particle breakage. In order to meet the requirement of purpose, firstly, a series of consolidated drained (CD) triaxial compression tests were performed, analyzed and compared on four types of sands to examine the method of particle breakage indices. Through these process, I can obtain the degree of particle breakage by triaxial test under a given stress and strain levels. Furthermore, I adopted relative density for determining minimum and maximum densities, and observed low water content limits to evaluate the influence of minimum and maximum densities on four types of sands. Water absorption test of sands were also selected to examine the feasibility.

In this section, I presented experimental investigations for water effects on particle breakage phenomena for four types of sand. The analysis of water action on particle breakage is based on previously obtained experiment results including stress-strain response measured by Consolidation drained triaxial compression tests, grain size distribution of original sand prior to shear and after shear, the results of particle breakage indices, and minimum relative density of low water content changes, as well as water absorption with selected materials. In the following sections, I discussed the effect of water content and water absorption on densities of sands. Then, I examined the relationship between water effect and brittleness degree and selected an appropriate method for evaluating the magnitude of particle breakage.

4.5.1 Effect of water content and water absorption on densities of sands

I have already discussed the effect of low water content on minimum and maximum density in previous section. It has been pointed out from the previous summary that Toyoura sand, JCA sand and Takasegawa sand are more sensitive to small increases in water content than the Inagi sand, and their relative density changes significantly with small changes in water content. Therefore, in this section, it is further summarized the phenomena of water absorption on relative densities of soils.

As illustrated Figure 4.4-14, when adding 0.1 % water content to Toyoura sand, the minimum relative density of the Toyoura sand remained constant at 0%; whereas adding additional 0.1 % of water content into Toyoura sand, the minimum relative density of the Toyoura sand tended to have significantly decreased by 25 %. This phenomenon could be explained as Toyoura sand has smooth and slightly porous surface which does

not readily absorb water into its inter-particles. The surface of Toyoura sand initially are dry, but the inter-particle voids are saturated with water. In this condition, no water is present on the surface. As small amount of water introduced to Toyoura sand, once complete saturation, surface absorption would no longer take place and the water remains on the surface. As a consequence, the minimum relative density values of Toyoura sand decreased as the extra water occupied extra volume of voids.

Furthermore, in the case of JCA sand, the data in Figure 4.4-14 clearly show that as the water content rose from 0 % to 0.1 %, the minimum relative density decreased by 50%. Furthermore, when water content increased from 0 % to 0.2 %, the minimum relative density of JCA sand dropped by 100 %. For this sand, the change of the minimum relative density at 0.2 % water content was approximately twice higher than that at 0.1 %. Therefore, the minimum relative density of this JCA sand was strongly influenced by low water content in the same interval. JCA sand has a fine, smooth texture with a poor water-holding capacity. When adding a small amount of water to the JCA sand, no water was able to seep into JCA sand, the water was presented on the surface. As a result, the minimum relative density of JCA sand decreased significantly with increasing low water content.

Moreover, as illustrated in Figure 4.4-14, minimum relative density of Takagase sand is less sensitive than Minimum relative density of Toyoura sand. In this case of, as adding 0.1 % water content to Takasegawa sand, the minimum relative density of the Takasegawa sand stayed constant at 0 %; while adding additional 0.2 % of water content into Takasegawa sand, the minimum relative density tended to decreased by 25%. This phenomenon could be explained as Takasegawa sand has angular and slightly porous surface which does not readily absorb water into its inter-particles. The surface of Takasegawa sand initially are dry, but the inter-particle voids are partially saturated with water. In this condition, no water is present on the surface. As small amount of water introduced to Takasegawa sand, once complete saturation, surface absorption would no longer take place and the water remains on the surface. As a consequence, the minimum relative density values of Takasegawa sand decreased as the extra water occupied extra volume of voids.

Last but not least, by contrast, Inagi sand is a porous material containing rough texture with small portion of fine particles. Porous Particles absorb water from the larger pores easily because it takes less energy to pull water from porous materials than from non porous materials. Table 1 shows the water absorption of Inagi sand is higher than the other two sands, meaning Inagi sand has higher capacity for holding water by

porous particles. Therefore, it is clear that a relationship between water absorption and the volume of pores would be expected.

In Figure 4.4-14, I found that the minimum relative density of Inagi sand can be seen to remain constant until the water content reached 2 %, decreasing thereafter from 0 % to -30 % as the water content was raised from 2 % to 3 %. In this condition, when 2 % water content was added, inter-particle voids of Inagi sand was full of water, but no water is presented on the surface. As the water content for Inagi sand rose from 2 % to 3 %, surface absorption would no longer occur, and then water tended to remain on the surface, resulting in minimum relative density of the inagi sand started to decrease. Thus, for Inagi sand, it is implied that the minimum relative density of Inagi sand is less sensitive to the influence of water content.

In this section, I explained the physical reasons to describe the densities of sands are dependent on water effects. Then, water effects on densities and particle breakage of sand were determined by regression analysis process and it is discussed in details in next subsections.

4.5.2 Determination of minimum dry density- water content relationship

From the available published papers, it was pointed out that the particle breakage is the function of particle density, strength, angularity, grain size distribution, stress level, strain level, anisotropy and water content. In section 4.2, I discussed the effects of grain size distribution, stress level and strain conditions for particle breakage. Furthermore, in section 4.3, I also discussed the effect of water content on dry density. It can be inferred that water content reflects that the particles can be crushed under the water effect, thereby affecting the shear strength. The primary objective of this analysis is to develop a reasonable semi-empirical equation by evaluating the dry density of sand changing with water content.

It has been discussed in previous section, the data points of either minimum dry density of sands or minimum relative density of sands shifted downwards with increase in water content. Minimum dry density of sand is more sensitive to slight increases in water content than corresponding maximum dry density of sand and its minimum relative density changes significantly with small changes in water content. Thus, the data set of minimum relative density is used to examine the sensitivity of low water content.

A total of 83 data of minimum relative density tests were plotted against logarithm low water content as illustrated in Figure 4.4-14. To examine the sensitivity of water content on each sand, sands with D_{rmin} at $\omega_s = 0.5\%$ were used for this purpose and brittleness degree (B_d) obtained from the regression analysis of increment of fines content (ΔF_c) were plotted against corresponding D_{rmin} at $\omega_s = 0.5\%$ of each sand. The obtained data is summary in Table 4.4-1 and presented in Figure 4.4-1.

To further examined the relationship of minimum relative density and low water content. With the data from the minimum density tests, the linear fit between brittleness degree (B_d) and logarithm water content can be presented by the following equation.

$$B_d = a - b \log(\omega_s) \quad (4.2)$$

where ω_s is low water content corresponding to various sands ; a and b are material constants.

The section of appropriate material constants, interception a and slope b , was done by regression analysis process. The key feature of regression analysis was the assumption that each sand has its own trend line and all data points will come to a single trend line corresponding to each sand in brittleness degree (B_d) and low water content (ω_s). In this case, a value of $a = 0.91$ and $b = 0.003$ obtained from linear fit. The process can be repeated for D_{rmin} at any value of ω_s and any linear bars can be achieved by regression analysis.

The process was repeated for 4 other particle breakage indices of sands for reference and hence total 5 results were achieved. Variation of brittleness (B_d) against low water content (ω_s) for various particle breakage indices are presented in Figure 4.5-2 to Figure 4.5-5.

Table 4.5-1 Summary of sands with D_{rmin} at $\omega_s = 0.5\%$

Materials	D_{rmin} at $\omega_s = 0.5\%$	Brittleness Degree (B_d)
Toyoura sand	-105	0.598%
JCA sand	-210	0.236%
Takasegawa sand	-50	0.629%
Inagi sand	0	0.981%

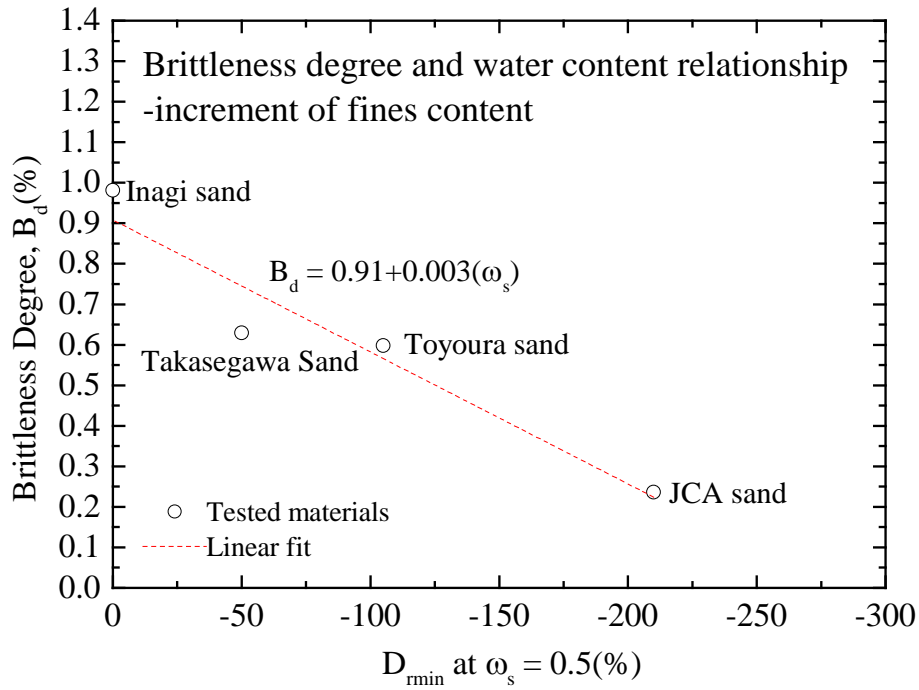


Figure 4.4-1 Minimum relative density and brittleness degree relationship

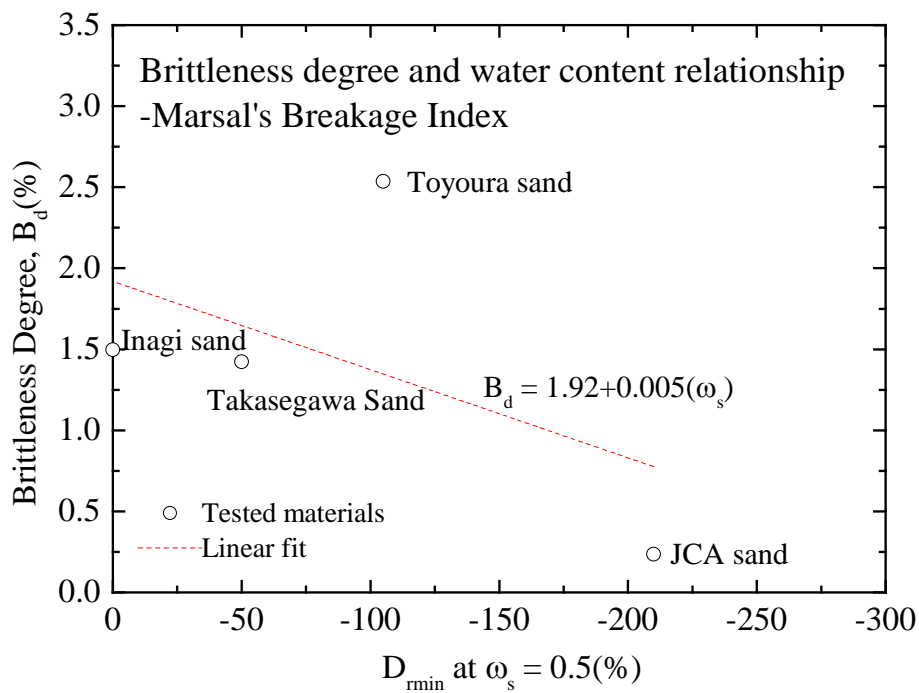


Figure 4.4-2 Brittleness degree and water content relationship – Marsal's breakage index

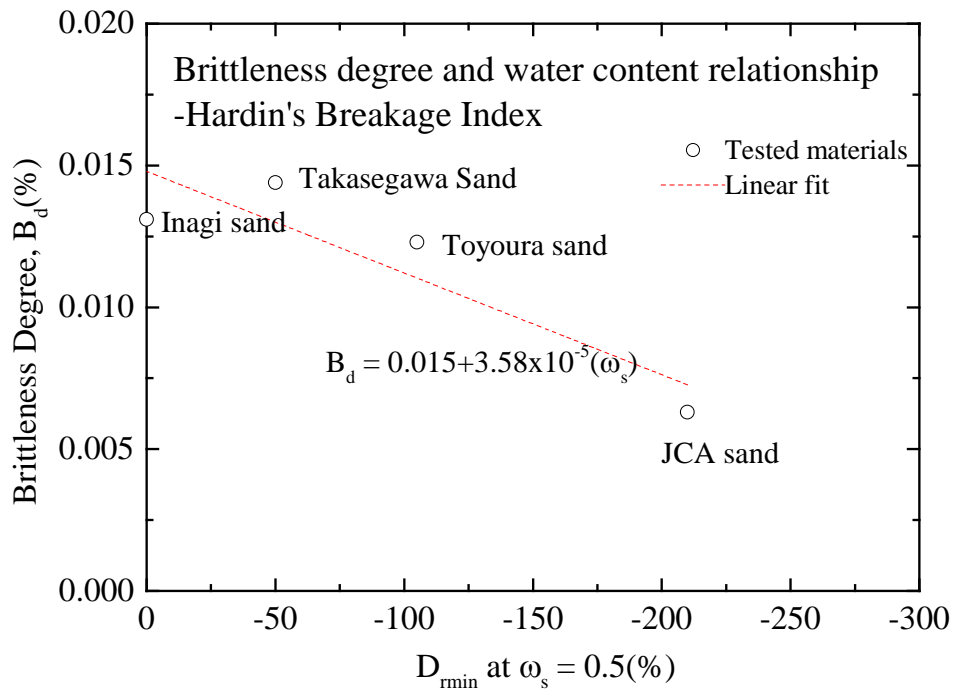


Figure 4.4-3 Brittleness degree and water content relationship – Hardin's breakage index

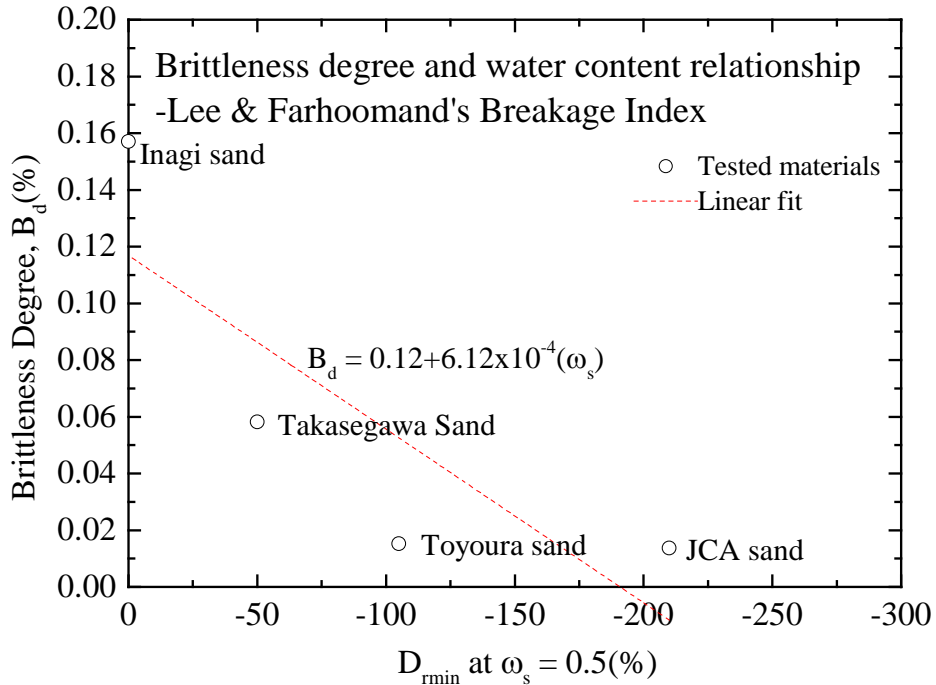


Figure 4.4-4 Brittleness degree and water content relationship – Lee and Farhoomand's breakage index

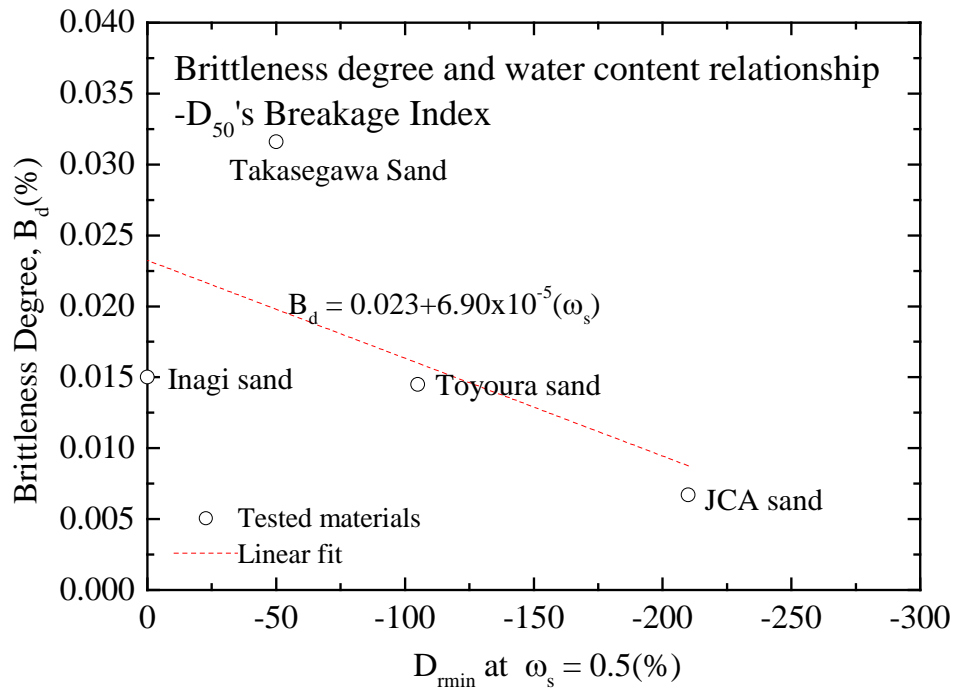


Figure 4.4-5 Brittleness degree and water content relationship – D₅₀'s breakage index

According to experimental results, an increase in low water content resulted in a decrease in minimum dry density as well as a decrease in minimum relative density. Despite the experimental results revealed that the minimum relative density data points is highly dependent on water content, the scatter plot has insufficient data points to perform the regression analysis and to illustrate the relation between brittleness degree and water content. The predictions may be inaccurate and largely influenced by random factors due to lack of data points. Therefore, this method is not appropriate to carried out for assessing the degree of particle breakage.

4.5.3 Determination brittleness degree - water absorption relationship

To investigate the validity of concepts mentioned in section 4.4.1, the relationship between brittleness degree (B_d) of sands corresponding to water absorption (a_p) is studied. Equation (4.1) was used to calculate a B_d value, and then to examine whether a unique relationship can be obtained utilizing the water absorption as parameters to determine a and b values. However, this best-fit line analysis procedure has some serious limitations. It needs large of test data as input and thus, intrinsically it is a very time-consuming process. Moreover, this process may yield reasonable a and b values. To examine the effect of water absorption on each sand, water absorption results were used for this purpose and brittleness degree (B_d) obtained from the regression analysis

of the increment of fines content (ΔF_c) were plotted against corresponding water absorption (a_p) as presented in Figure 4.5-6. The plots showed that the water absorption ability of Inagi sand is more significantly than Toyoura sand and JCA sand, evidencing the higher the water absorption ability, the higher the B_d is.

Then, the linear fit between brittleness degree (B_d) and logarithm water absorption can be presented by the following equation.

$$B_d = a - b \log(a_p) \quad (4.3)$$

where a_p is water absorption corresponding to various sands. Interception a and slope b present the regression analysis from brittleness degree (B_d) and water absorption (a_p). In this case, a value of $a = 0.7$ and $b = 0.45$ obtained from linear fit.

The process was repeated for 4 other particle breakage indices of sands fore reference and hence total 5 results were achieved. Variation of brittleness (B_d) against water absorption (a_p) for various particle breakage index are presented in Figure 4.5-7 to Figure 4.5-10.

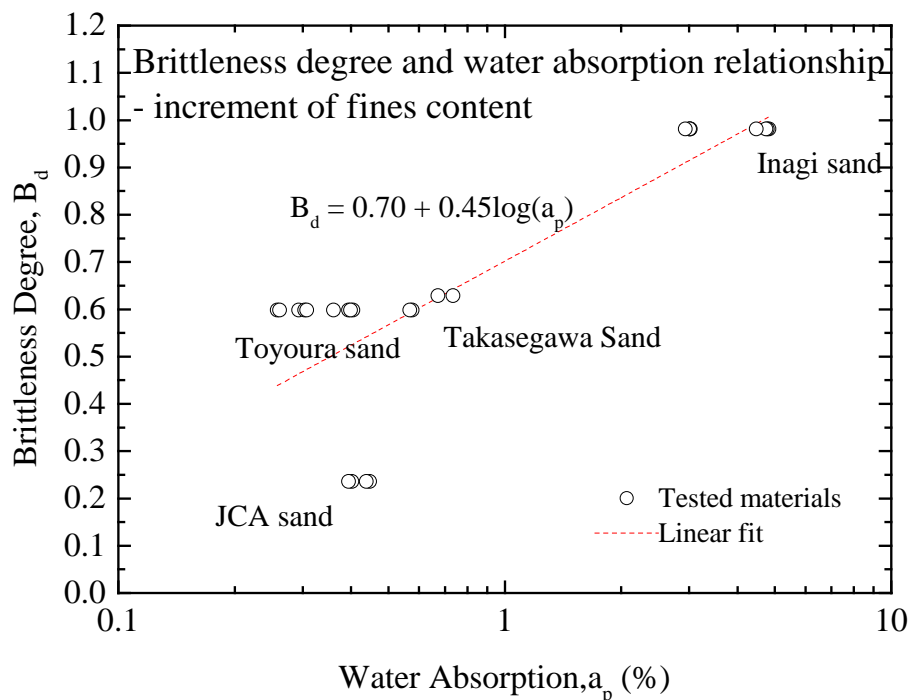


Figure 4.4-6 Brittleness degree and water absorption relationship - increment of fines content

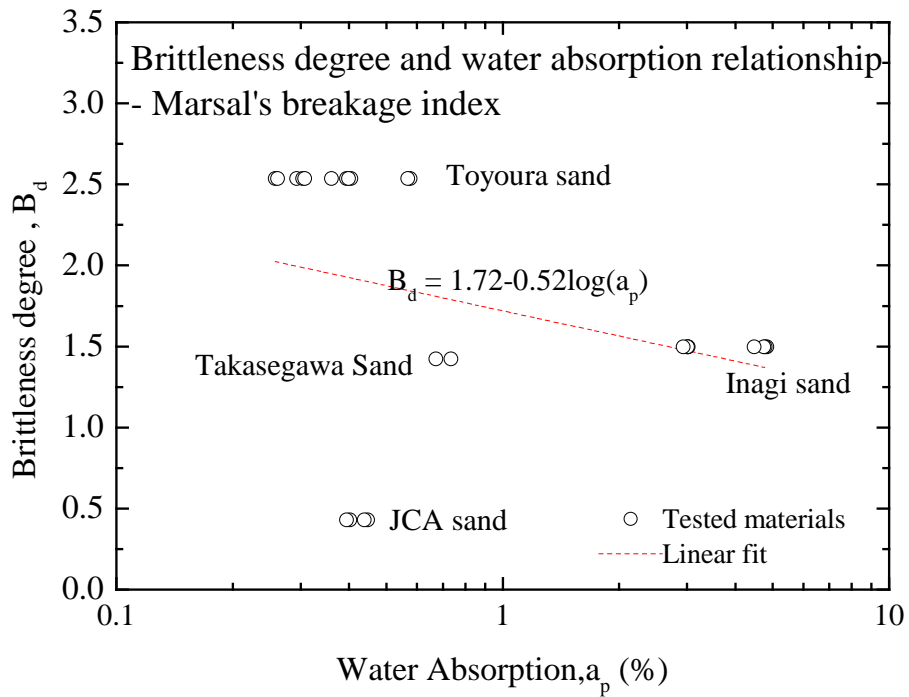


Figure 4.4-7 Brittleness degree and water absorption relationship - Marsal's breakage index

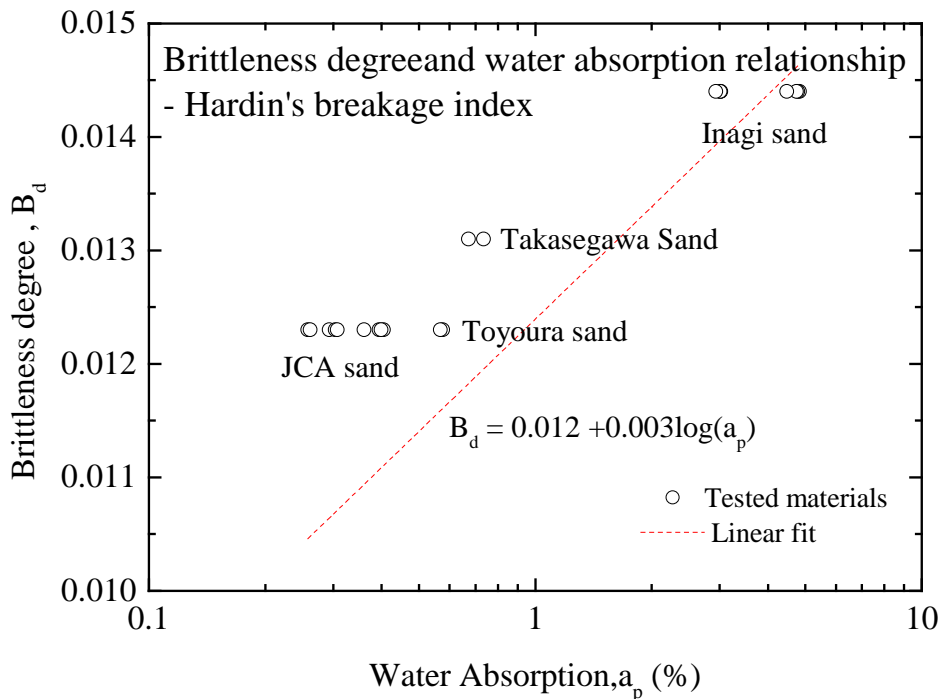


Figure 4.4-8 Brittleness degree and water absorption relationship - Hardin's breakage index

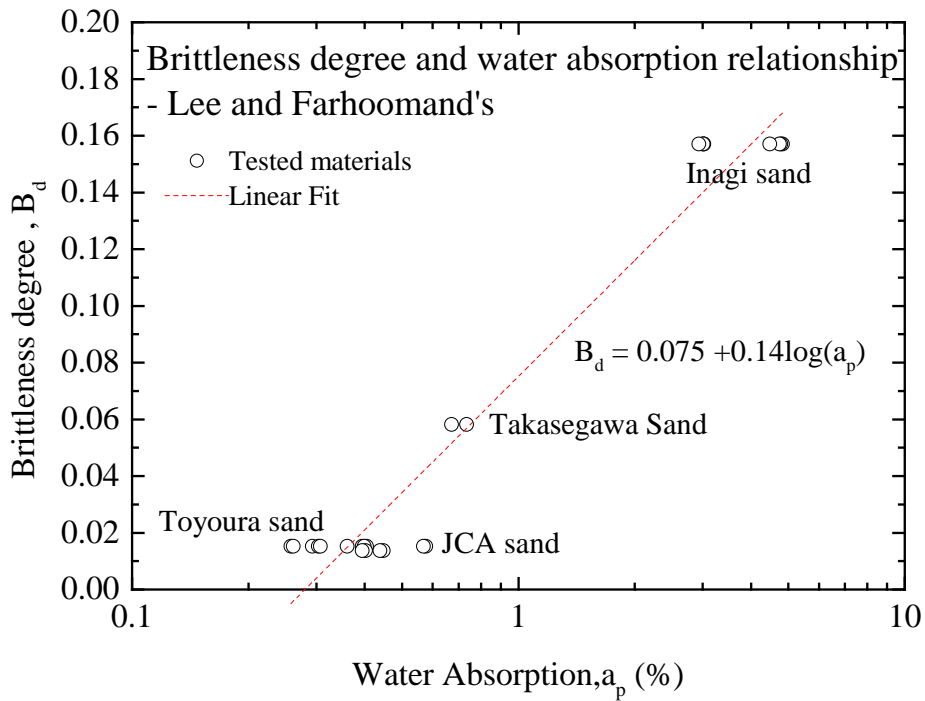


Figure 4.4-9 Brittleness degree and water absorption relationship – Lee and Farhoomand's breakage index

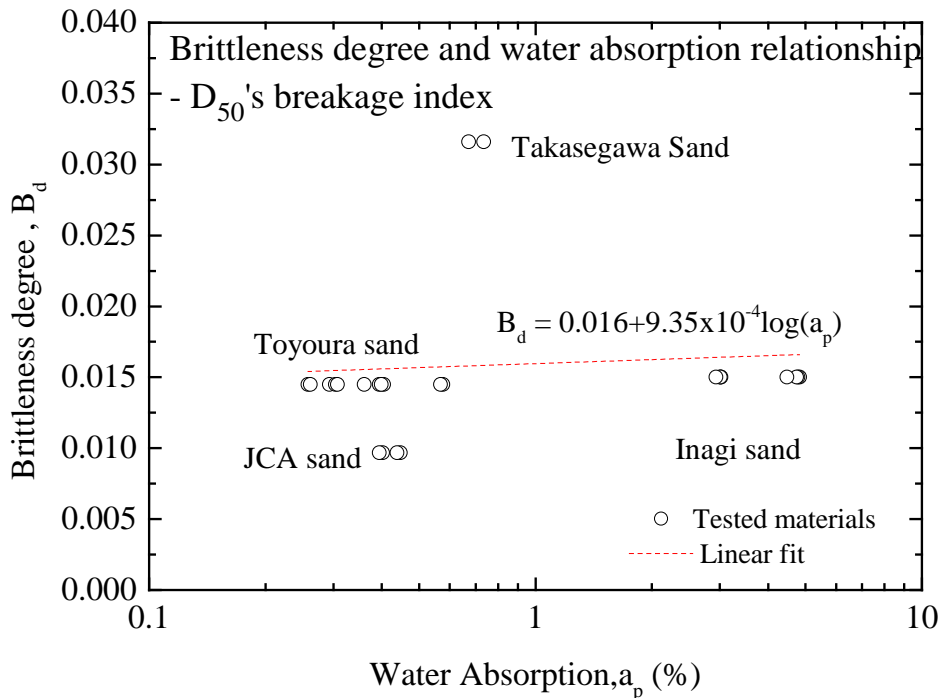


Figure 4.4-10 Brittleness degree and water absorption relationship – D_{50} 's breakage index

A linear dependence of brittleness degree (B_d) for four types with water absorption has been developed in the tests performed. For the range of water absorption values covered the curve, it is evidence that water is essentially stored with particle pores. As water absorption ability increased, brittleness degree tends to increase. It also meant that water absorption ability are involved in the process of particle breakage for four types of sand and given test conditions.

4.6 Summary

Experimental observations revealed that the minimum relative density decreased significantly with slightly increasing water content which can be attributed to the water absorption ability of sands, and as consequence, the sands become more brittle in the present of water, evidencing the phenomenon of water action are involved in the process of particle breakage. Therefore, it is believed that as low water content introduces to sands, if sands have higher ability to absorb liquid, then the crushability of sands increase, resulting in giving rise to an increase in particle breakage. Consequently, the findings can be concluded that the effect of water absorption and water content on particle breakage could be depended on the material properties and its sensitivity to the presence of water. These features can be simulated by a generalize function, $B_d = F(\omega_s, a_p)$, and yet has a simple form in Eq. (4.2) and Eq. (4.3).

To ensure the proposed equation and physical concept has general applicability, brittleness degree (B_d) from CD triaxial tests for different sands are plotted against water content and water absorption as shown in Figures 4.5-1 to 4.5-10. According to the analyzed results, several general trends can be observed. Firstly, a linear dependence of brittleness degree for four types with water absorption has been developed in the tests performed. For the range of water absorption values and water content value covered the curve, water effects of particle breakage were examined. Experimental results from figures revealed that both water content and water absorption ability are involved in the process of particle breakage. The higher water content, the higher B_d of four types of sand. Similar to the effect of water content, as water absorption ability increased, brittleness degree tends to increase. Secondly, to find the most accurate best-fit line I choose to use the process of logarithmic regression. In the case of brittleness degree against water content, the scatter plot has insufficient data points to perform the analysis and the predictions may be inaccurate and largely influenced by random factors. Consequently, a sufficient and manageable volume of data is required for this analysis. Thus, due to sufficient data points through experimental results, water absorption test of fine aggregates can be selected for assessing particle breakage instead of triaxial test.

CHAPTER 5 STUDY ON CONSTITUTIVE MODELS

5.1 General Remarks

Based on the existing constitutive models, the soil strength behavior of sands and intergranular void ratio (e_s) associated with increment of fines content (ΔF_c) is modelled in this chapter. In this model, the relationships among deviator stress, mean effective confining stress, brittleness degree (B_d), fines content (F_c) and intergranular void ratio (e_s) are developed. The stress strain relationships describing both plastic strain and volumetric plastic strain were expressed with theoretical framework of bounding surface hypoplasticity model for sand. The concept of brittleness degree (B_d) which has been discussed in Chapter 4 was introduced by considering increment of fines content (ΔF_c). The increment of fines content (ΔF_c) and intergranular void ratio (e_s) were derived with mathematical functions and incorporated into the model. A comparison of model simulations associated with a certain level of brittleness degree (B_d) was examined, which can describe the breaking behavior of sands. The parameters used to simulate the models obtained from empirical equations and a set of constants determined by Wang et al. (2002) for Toyoura sand.

5.2 Selection of the constitutive model

The most common stress-strain relationships detected from the undrained and drained tests in this study are modelled. With the regression analysis of the test results, mathematical expression are formulated the relationship between deviator stress, and mean effective stress, and axial strain. Moreover, this existing constitutive soil model was selected for modification by introducing extra terms of intergranular void ratio (e_s) and brittleness degree (B_d) that are function of fines content (F_c). Further understanding the effects of brittleness degree of sands contributed to the mean effective stress on appropriate strain for sands both in model simulation and in laboratory.

5.2.1 Modified bounding surface hypoplasticity

Among the reported static and dynamic phenomena leading to particle breakage which described in Chapter 2, for the purpose of modelling the effects of particle breakage on shear response of sands, I adopt the modified bounding surface hypoplasticity model by Wang et al. (2002) due to its capability of simulating the behaviour of sands under undrained and drained tests with basic premises of critical state soil mechanics (Li et al., 1999). In this model, the theoretical summary of the

formulation and model parameters is based on the original papers and dissertations (Dafalia, 1986; Li, 1991; Wang, 1990, Li et al., 1999 and Wang et al. 2002). For more detailed derivation, the readers can refer to these papers of the bounding surface hypoplasticity model.

The model considers the plastic strain increments due to application of stress ratio increments, d_{rji} , and mean stress increment, dp' separately (Wang et al. 2002). According to hypoplasticity theory, the strain increment direction depends on both current state of stress and the stress increment direction. In this approach, the general formulation of the model is defined as (Wang et al. (2002).

$$d\varepsilon_{ij}^e = \frac{d_{s_{ij}}}{2G} + \frac{dp'\delta_{ij}}{3K} \quad (5.1)$$

The elastic strain rates for this model can be similarly decomposed into its volumetric and deviatoric parts where G and K are incremental elastic shear and bulk moduli, respectively.

In the hypoplasticity model, the incremental relationship between the stress and plastic strain is expressed below:

$$d\varepsilon_{ij}^p = \left(\frac{(n_D)_{ij}}{H_r} + \frac{\delta_{ij}}{3K_r} \right) p' (dr_{kl}(n_N)_{kl}) + \left(\frac{r_{ij}}{H_p} + \frac{\delta_{ij}}{3K_p} \right) h(p' - p'_m) \times (d_p') \quad (5.2)$$

in which $r_{ij}=s_{ij}/p'$ is the deviatoric stress ratio, with s_{ij} the deviatroic stress tensor; H_r and K_r =plastic shear and bulk moduli respectively, associated with the tensor of the stress ratio increment d_{rji} . H_p and K_p = plastic shear and bulk moduli, respectively, associate with mean pressure increment, dp ; n_D and n_N =unit vectors that define a deviatory direction and a loading direction. δ_{ij} =unit tensor along the p axis.

In the theory of Wang et al. (2002), the failure surface is given by $R-R_{fg}(\theta)=0$ where R is J/P ; R_f is the stress ratio at failure in compression and $g(\theta)$ interpolates between compression and extension. Wang et al. also defined the loading surface $R-R_{mg}(\theta)=0$ where R_m is a history parameter providing the loading level in terms of R in triaxial compression. A flat-cap surface, $p - p_m = 0$, is proposed for simulating consolidation and rebound.

5.2.2 Intergranular void ratio (e_s)

Recent researches showed that clean sand behavior changes from dilative tendency to contractive tendency with increasing in mean effective stress for same void ratio

(Raman, 2009). Traditionally, void ratio (e) used as an index to predict stress-strain behavior of soil under critical state framework. However, recent literature published that fine particle has an inactive contribution in terms of soil strength if they are less than a certain amount (Kenney, 1977; Troncoso and Verdugo, 1985; Kuerbis et al., 1988). Besides, they also suggested fine particles may simply be occupying void in the sand skeleton and therefore, the measure behavior is controlled by the force chain in sand skeleton. Thevanayagam (1998) defined the intergranular void ratio (e_s) as Equation (5.3), and indicated that $e - p'$ plots of critical state of silty sands converged on the same line regardless of fines content (F_c) up to around 30%. Although Thevanayagam (2002) proposed “equivalent intergranular void ratio” to obtain better fitting of critical state line, I adopt Equation (5.3). When coarse particle to coarse particle contacts dominate soil behaviors, intergranular void ratio (e_s) defines as:

$$e_s = \frac{e + F_c}{1 - F_c} \quad (5.3)$$

where e_s = intergranular void ratio; e = void ratio and F_c = fines content (in decimal) with respect to total dry weight of sands. The concept of intergranular void ratio (e_s) which used in this analysis is inherently assumed that the data points for sand with fines will come to a single trend even for higher fines content (F_c) when they are plotted in $e_s - \log(p')$ space.

A major modification of the constitutive model for sand has to be replace void ratio (e) to intergranular void ratio (e_s). The input parameters are then absorbed the effect of fines and make the model can or cannot be independent of fines content (F_c).

5.2.3 Brittleness degree of soils

In critical state soil mechanics, shearing drives particulate soils towards a state of constant volume and constant shear stress at a constant mean effective stress, term critical state (Roscoe et al., 1958). Theoretically, when particle breakage occurs, the change in grain size distribution curves cannot continue indefinitely; conceptually a final grain size distribution curves where all voids are filled with smaller and smaller particles can be envisioned (McDowell et al., 1996). However, the experimental observation suggested that particle breakage of sand was proportional to the stress and strain input and that magnitude of particle breakage may not have ceased, even after the degree of particle breakage reached steady state. Therefore, for the range of stress, strain levels and degree of particle breakage to this study, it is reasonable to assume that particle breakage do not completely cease at higher stress and continue to very large

strain levels.

In this section, I introduce an alternative way to account for the stress-strain response depending on intergranular void ratio (e_s) and brittleness degree (B_d) of sands. Also, I used brittleness degree of sands to predict ΔF_c parameter form a formulation which is physically reasonable and mathematically consistent with “fines in sand” model. For simplicity, the linear relationship between increment of fines content, ΔF_c , and brittleness degree of sands, B_d , was replaced by the following relationship:

$$dF_c = B_d \frac{\sigma_3'}{p_a} d\varepsilon_1 \quad (5.4)$$

$$e_s = \frac{e + F_c}{1 - F_c} \quad (5.5)$$

$$F_c = f_{c0} + \Delta F_c \quad (5.6)$$

where σ_3' is the minimum principal stress; ε_1 is the maximum principal strain and $p_a = 100$ kPa is atmosphere pressure; F_c is fines content in decimal; the slope B_d is assumed to be dependent on ΔF_c . It was inferred that the selection of appropriate B_d was done by best-fit line process. The key feature of back analysis was the assumption that all points for sand will come to a single trend in $\Delta F_c - (\sigma_3'/p_a) \times d\varepsilon_1$. Each of these parameters for these six formulations is described in the following section.

5.3 Determination of Parameters and input formats

5.3.1 Parameter determination of constitutive model

The constitutive model by Wang et al. (2002) is well documented and verified for Toyoura sand. In addition to the parameters needed for defining critical state, they can be determined from the triaxial tests (Raman, 2009) and empirical equation.

The plastic part of this model consists of flow rule or dilatancy equation, yield function and hardening function (Raman, 2009). Rowe (1962), Nova and Wood (1979) proposed the ratio between the plastic-volumetric-strain increment and the plastic-deviatoric-strain increment for flow rule in p - q space. Wang et al. proposed the constitutive equation for triaxial compression ($\sigma_1 = \sigma_2$) under undrained and monotonic loading condition are described below.

$$dp = -\sqrt{\frac{2}{3}} \left(\frac{p'}{p'_m} \right)^a \left(\frac{\eta}{M_b} \right)^b \frac{M_d - \eta}{(M_b - \eta)^c} \frac{p'}{k_r} d\eta \quad (5.7)$$

$$d\varepsilon_q = \frac{p'}{3} \left(\frac{1}{G} + \frac{2}{H_r} \right) d\eta + \frac{\eta}{3G} dp \quad (5.8)$$

where $p' = (\sigma_1' + 2\sigma_3')/3$ is the mean effective stress, $\varepsilon_q = \varepsilon_1 - \varepsilon_3$ is the deviator strain, $\eta = q/p' = (\sigma_1 - \sigma_3)/p'$ is the deviator stress ratio, and p_m is the preexisting maximum mean pressure. The model parameters, namely, the elastic shear modulus (G), the parameters that define the plastic bulk and shear moduli (k_r and h_r), and the deviator stress ratio at critical state (M) as well as a and b are material constants. The original model used $\zeta = 1$, caused nonzero dilation as the critical state was approach. Whereas, it is proposed that a value of $0 < \zeta < 1$ be used to eliminate dilatancy when failure is approached at large strain.

Wang et al. (2002) proposed to correlate the other two model parameters, namely, the virtual failure stress ratio (M_b) and the dilatancy stress ratio (M_d), with critical state by equations;

$$M_b = M + \beta \left(\sqrt{\frac{p_c}{p'}} - 1 \right) \quad (5.9)$$

$$M_d = M_0 + (M - M_0) \frac{p}{p'_c} \quad (5.10)$$

where p'_c is the effective mean principal stress at critical state, β and M_0 are material constants.

5.3.3 Critical state parameters

The critical state parameter can be obtained from critical state line (Raman, 2009). Mathematically, the *EG-SSL* is defined by the slope of the *EG-SSL*, M , in the q - p' space and the function defining the equation of *EG-SSL* in e_s - $\log(p')$ space. Verdugo and Ishihara (1996) indicated that the critical state lines are not straight line in e - $\log(p')$ space. According to Li et al. (1999), the critical void ratio is dependent on pressure and can be expressed by Eq. 5.11.

$$e_c = e_0 - \lambda_s \left(\frac{p_c}{p_a} \right)^\xi \quad (5.11)$$

Wang et al. (2002) utilized the critical state model of Li et al. (1999) to calculate the value of p'_c for the e , which is formulated as $e = e_0 - \lambda_s (p'_c / p_a)^\xi$ where e_0 , λ_s and ξ are material constants. We replaced the e with e_s in writing a formula for the critical state line (CSL). Then p'_c can be calculated with the following equation:

$$p'_c = p_a \left(\frac{e_0 - e_s}{\lambda_s} \right)^{1/\xi} \quad (5.12)$$

where

$$e_s = \frac{e + F_c}{1 - F_c} \quad (5.13)$$

The increment of fines content (F_c) due to particle breakage of sand during shear deformation is calculated by Equation (5.4), and thus the degree of brittleness (B_d) can be reflected in the modeling of the stress–strain relationship expressed by Equations (5.7) to (5.10) by modeling the critical state line using Equations (5.12) and (5.5).

Thevanayagam (1998) expressed the intergranular void ratio (e_s) using Equation (5.13), and indicated that $e - p'$ plots of the critical state of silty sands converged on the same line regardless of fines content up to around 30%. Although Thevanayagam (2002) proposed an “equivalent intergranular void ratio” to make the CSL fit better, we adopted Equation (5.13) for simplicity.

A unique set of material constants is used in the case study presented in Table 5.3-1 and 5.3-2. The values for this set of constants were determined by Wang et al. (2002) for Toyoura sand. Thus we examined a hypothetical sand with the same nature as Toyoura sand having a brittleness degree (B_d) of zero.

Table 5.3-1 Parameters used in model simulation (Wang et al. 2002)

Initial condition	a	b	G_0	h_r	k_r	M	M_0/M	κ	β
$e_{in}: 0.735-0.907$ $p_{in}: \text{up to } 3000 \text{ kPa}$	0	1.3	200	0.1	0.66	1.25	0.75	0.013	0.05

Table 5.3-2 Constants of critical state line for Toyoura sand (Wang et al. 2002)

e_0	λ_s	ξ
0.934	0.019	0.7

5.3.3 Determination of other parameters

This section discussed about the determination of other model parameters.

1. Parameter a in Eq. 5.7 of model formulation for simulating the effect of over-consolidation ration on volumetric changes. However, because the tests for Toyoura sand were performed under monotonic loading on normally consolidated samples, reasonable model simulations were obtained by simply assuming $a = 0$ (Wang et al. ,2002)

2. Parameter b in Eq. 5.7 controls the slope of effective stress path during contractive

phase of the virgin loading (Wang and Xie, 2014). Parameter b can be obtained by following equation:

$$\frac{tr\epsilon}{tr\epsilon_m} = y \left(b, \frac{R_p}{R_f}, \frac{R}{R_f} \right) y^{-1} \left(b, \frac{R_p}{R_f}, \frac{R_p}{R_f} \right) \quad (5.14)$$

This equation can be used to uniquely determine the constant b by fitting any pair of $J = pR$ and $tr\epsilon$ points. Here, a best fit of the undrained stress path curve for $\eta < M$ yields the value $b = 1.3$ proposed by Wang et al. (2002).

5.4 Comparison of Predicted Results and Measured Results

This section examined a framework in terms of stress-strained response, stress path and the critical state locus in void ratio versus mean effective stress space without changing the input parameters presented by Wang et al. (2002). The framework simulated herein explains that when particle breakage occurs, how breakage effect CSL in e - $\log(p')$ space, and how it contributes to the stress-strain behavior of sands. The framework is based on three assumptions. Firstly, for small amount of fines generated by particle breakage, the measured behavior is controlled by sand skeleton only (use intergranular void ratio (e_s) at low fines content (F_c)). Secondly, particle breakage are capable of either sliding or rolling into the voids and therefore, reducing the specimen's void ratio. Lastly, the degree of particle breakage increases dependency for stress and strain conditions.

5.4.1 Experimental Verification

The data obtained from the experimental program was used to evaluate the predictive ability of bounding surface hypoplasticity model. To provide reliable data for a comprehensive evaluation of whether the constitutive models can use for predicting behavior pattern within different levels of brittleness degree for the framework of CSSM, an experimental program was performed. The test program covered (1) four types of sands; (2) a wide range of confining pressure from 1 MPa to 4MPa; (3) soil particles smaller than 106 μm (equivalent to a No. 140 sieve) were discarded by dry sieving. The selected experimental results for simulation were reached the steady state at the end of triaxial tests. The details of material properties and experimental process for accurate measurement of particle breakage were given in Chapter 3. A unique set of materials parameters obtained from Wang et al. (2002) then used to evaluate the predictive ability of the constitutive models.

For the test cases, the effective stress paths and stress strain response were

simulated by the proposed constitutive model with corresponding parameters as shown in Figure 5.4-1 and 5.4-2. In undrained test, the volume of specimen remains unchanged. The key equations to predict the undrained responses are Eq. 5.7 and Eq. 5.8. Model simulations are compared with experimental results for undrained loading conditions for Toyoura sand, JCA sand and Takasegawa sand. The initial fines content (F_c) is 0 % and for a wide range of mean effective stress from 1MPa to 4MPa. In some cases, it is possible to obtain closed-form analytical expressions by adjusting parameters. However, in order to consistent interpretation of data from the prediction results and measured results, material constant i.e. h_r , k_r , a , b , and G_0 were determined by Wang et al. (2002).

A comparison between simulations and experimental results on sands using constitutive model is shown in Figure 5.4-1 and Figure 5.4-2. With the model, I am capable of reproducing the stress-strain relation and stress paths for different confining stress level. Theoretically, it can be expected from the model that an increasing confining pressure increases the mean effective stress, which leads to a higher deviator stress. As shown in figures, at the end of undrained shearing, the state of stress (p' , q) of specimens, which were consolidated to various confining pressure, lied approximately on a straight line. In other words, irrespective of the confining pressures, the stress states of sand during triaxial shearing moved towards unique (i.e. critical state) state, which were linearly related to each other in the p' - q space.

Although the simulations predicted the stress paths on Toyoura sands reasonably well, the model failed to capture perfectly the stress - strain responses. This is maybe the model does not have a mechanism to properly arrest the increase of q under conditions of undrained dilative shear. Its major drawback is in simulating the behavior of the critical state (i.e. at large strain) (Wang et al., 2002). In this study, the volumetric strain increment is nonzero at the critical state (i.e. at $\eta = M$), which does not conform to the concept of critical state.

Though the prediction in stress - strain responses are limited, the overall spectrum of the prediction is in good agreement with the experimental results. Thus, the model simulation were obtained using a unique set of material constants in conjunction with brittleness degree (B_d) of sands and intergranular void ratio (e_s) can be used to predict undrained behavior of sand with fines content (F_c).

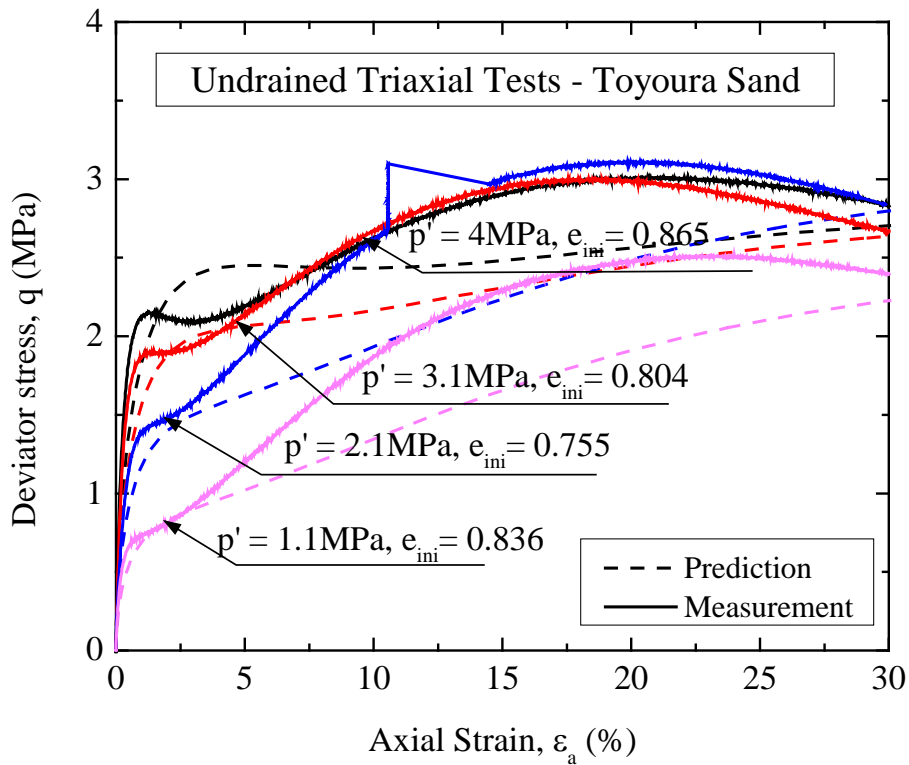


Figure 5.4-1 Comparison between model prediction and test results for stress path on Toyoura sand under different confining pressure

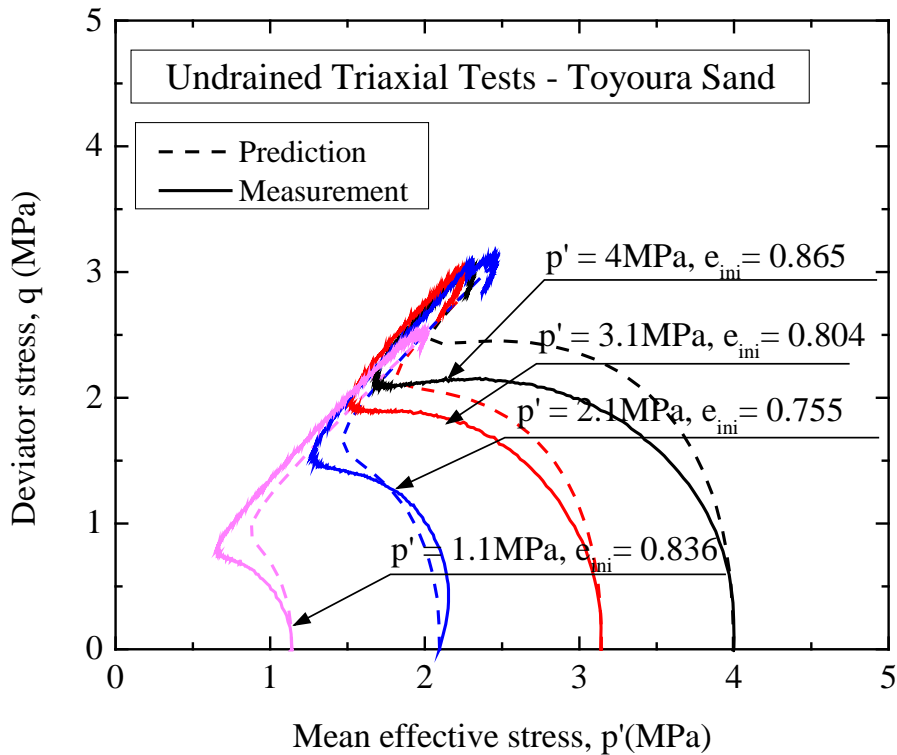


Figure 5.4-2 Comparison between model prediction and test results for stress-strain response on Toyoura sand under different confining pressure

5.4.2 Effect of fines on Monotonic loading behavior

A series of consolidated drained triaxial compression tests were conducted on a sand at various confining pressure and shear deformation up to different axial strain levels. I presented experimental results on the sand and quantified the degree of particle breakage in terms of increment of fines content (ΔF_c). Based on observations from increment of fines content (ΔF_c), I proposed a linear equation to calculate brittleness degree (B_d) associated with stress and strain levels. I then applied to a bounding surface hypoplasticity model for undrained stress-strain behaviour of sandy materials to examine the effect of particle breakage on stiffness and undrained strength behavior of sands. The concept of intergranular void ratio (e_s) was employed to link and correlate brittleness degree (B_d) and stress-strain response in the constitutive model.

5.4.2.1 Numerical Modelling

According to Atkinson (2007), there is a critical state strength at strains of the order of 10% where the soil continues to distort at constant stress and constant volume. ASTM D7181 – 11(2011) pointed out that failure is often taken to correspond to the deviator stress at 15 % axial strain. Ma et al. (2013) mentioned that the large strain observed in triaxial compression test is up to 40 %. Among them, in this research, I obtained the degree of particle breakage by performing triaxial test under a various confining pressure and a maximum axial strain of 40 %. Last but not least, due to linear relationship between B_d and the confining stress levels and axial strain, as particle breakage goes to infinity, the simulations in e_s - $\log(p')$ space at various brittleness degree (B_d) follow a CSL path toward the steady state line a, leading to zero for mean effective stress. Thus, shear strain is limited to 40%.

Therefore, in this simulation, I selected the maximum increment of fines content (ΔF_c) corresponds to a limiting value at $\varepsilon_a = 40\%$. This stimulation covered a wide range of densities under various brittleness degree (B_d). By simulating the models under specified condition, the effect of brittleness degree (B_d) could be examined by the stress-strain and stress path characteristics of sands in undrained shearing. The range of axial strain covered from 0% to 40%. The occurrence of particle breakage during shearing leads to an interesting observation on the difference in stress-strain behavior between models with fines content or without fines content.

Using Eq. (5.4) and the aforementioned concept of brittleness degree (B_d), the increment of fines content (ΔF_c) due to particle breakage of sand during shear

deformation can be approximated. Thus the brittleness degree (B_d) can be reflected to the modelling of stress – strain relationship expressed by Eq. (5.7) to Eq. (5.10) through the modelling of critical state line by Eq. (5.12) and Eq. (5.13). The simulation results discussed in this section on the effect of particle breakage are organized in simulations as detailed below.

Thevanayagam (1998) defined the intergranular void ratio (e_s) as Eq.(5.5), and indicated that $e - p'$ plots of critical state of silty sands converged on the same line regardless of fines content (F_c) up to around 30%. Although Thevanayagam (2002) proposed “equivalent intergranular void ratio” to obtain better fitting of CSL, I adopted Eq. (5.5) for simplicity.

A unique set of material constants, namely, $a = 0$, $b = 1.3$, $G_0 = 200$, $h_r = 0.1$, $M = 1.25$, $M_0/M = 0.75$, $\beta = 0.05$, $e_0 = 0.934$, $\lambda_s = 0.019$ and $\xi = 0.7$ were determined by Wang et al. (2002) for Toyoura sand. This means that I examine imaginal sand which has the same nature as Toyoura sand if brittleness degree (B_d) is zero.

5.4.3.2 Results of Numerical Analyses

Simulations covering a range of brittleness degree (B_d) (0 %, 0.5%, 1%, 2%, 4% and 8%) are presented. The simulated matrix were consolidated to the initial void ratio of 0.7, 0.8 and 0.9 and to mean effective stress of 3MPa, 1Mpa, 0.3MPa, and 0.1Pa. The results of simulation are plotted from Figure 5.4-3 through Figure 5.4-14. Each curve refers to different brittleness degree (B_d). The circular symbol represents the initial condition which are plotted here for reference.

The response of stress strain curve at different brittleness degree (B_d) under various confining pressure are shown in Figure 5.4-3 (a) to Figure 5.4-14 (a) whilst Figure 5.4-3 (b) to Figure 5.4-14 (b) show stress paths, and Figure 5.4-3 (c) to Figure 5.4-14; Figure 5.4-3 (d) to Figure 5.4-14 (d) present $e_s - (p')$; Figure 5.4-3 (e) to Figure 5.4-14 (e) is fines content (F_c)- axial strain (ε_a); finally, fines content (F_c)- mean effective stress (p') is shown in Figure 5.4-3 (f) to Figure 5.4-14 (f).

It is clearly shown from these figures that breakage behavior altered both peak and steady state stress strain response of the each simulation as well as the response of dilation / contraction of stress paths and intergranular void ratio (e_s) –mean effective stress (p') space. To sum, medium dense soils initially showed the same behavior as the loose samples but, after initially exhibiting contractive behavior, the sands averted and began exhibiting dilative behavior.

Furthermore, the behavior of loose sands were subjected to undrained shearing and found that the change in undrained behavior of samples can captured by the change in brittleness degree (B_d). Loose sands with high brittleness degree (B_d) exhibited continuous development of positive pore water pressure to critical state, revealing the tendency to contractive response. A great amount of strain softening took place when the stress path moved toward the critical state points. Therefore, examining the obtained results reveals that peak deviator stress decreased with the brittleness degree (B_d) increasing.

Moreover, dilation behavior of shear strength pronouncedly decreased with the amount of fines content (F_c) increasing. The sands showed a range of softening behavior or dilative behavior that depended on the sand's density and the amount of particle breakage. Particle breakage has obvious effect on the evaluated undrained soil behavior.

Detailed of simulation matrix is presented as follows:

1. Series A: $e_{ini} = 0.7$

In the simulations, the material was consolidated to the same initial void ratio of 0.7 and to mean effective stress of 3MPa, 1MPa, 0.3 MPa and 0.1Mpa. The results of those are shown in Figure 5.4-3, 5-4-4, 5-4-5 and 5-4-6, respectively. The open circular represents the initial condition which are plotted here for reference.

In the case of $p_{ini}' = 3\text{MPa}$, Figure 5.4-3(a) indicated that deviator stress decreased with increasing brittleness (B_d). At low brittleness degree (B_d), i.e. $B_d = 0\%$ and $B_d = 0.5\%$, the model showed that sands were able to sustain a high deviator stress. However, when higher brittleness degree (B_d) were assumed, the model showed an increase in deviator stress to a peak state at a small strain, followed by softening behavior, which was consistent with a trend towards greater compressibility with increasing brittleness degree (B_d).

The stress path in the p' - q space is shown in Figure 5.4-3 (b). At lower brittleness degree (B_d), dilative behavior was predominant and the direction of the stress path moved rapidly to reach the deviator stress ratio at the critical state (M). More brittle sands with higher (B_d) values exhibited continuous development of positive pore water pressure to the critical state, revealing a tendency for contractive response. This implies that higher brittleness degree (B_d) resulted in more contraction and led to a marked reduction in the undrained strength of sand during undrained shearing. Thus, the stress path showed the

role of increasing fines in reducing the mean effective stress and the maximum deviator stress.

Intergranular void ratios (e_s) as defined by Equation 7 are plotted against axial strain in Figure 5.4-3(c). From this figure, I can see that an increase in brittleness degree (B_d) resulted in increased fines content (F_c), which led to increased intergranular void ratio (e_s). These increases were due to the role the fines content played in the upward shift of the CSL in e -log (p') space.

In order to observe the effect of particle breakage on the undrained strength of sands, the CSL in e_s -log (p') space at various brittleness degree (B_d) is plotted in Figure 5.4-3(d). The location of the CSL is strongly dependent on the fines content (F_c). An increase in the amount of fines (F_c) led to an upward shift of the CSL in e_s -log (p') space and consequently to a reduction of the mean effective stress. For example, the curve for $B_d = 8\%$ indicates that the sand sheared at constant volume to the peak, and then progressively moved towards the critical state, exhibiting dilating behavior to softening behavior. Based on the simulation, I can conclude that increased brittleness degree (B_d) precipitates more particle breakage, which leads to an increase in the fines content (F_c) and intergranular void ratio (e_s). When the intergranular void ratio (e_s) increases, pore water pressure develops, causing the undrained strength of the sand to drop.

As shown in Figure 5.4-3(e), the variation of brittleness degree (B_d) due to particle breakage is related to fines content. From this figure, it appeared that fines content (F_c) increased as the brittleness degree (B_d) increased for a given axial strain. Particle breakage continued to increase, leading to increased fines content until the critical state was reached (5.4-3 (f)). In both Figure 5.4-3 (e) and (f), the results also conform that the degree of particle breakage increased with increasing the stress and strain levels.

The effective stresses are plotted in p' - q space are shown in Figure 5.4-3 (b) to Figure 5.4-6 (b). At low confining stress of 0.1 MPa, dilative behavior was predominant and the stress paths moved rapidly to the right from the initial state of test and terminated on the failure line as shown in the figure. As the initial confining pressure was increased, with low brittleness degree (B_d), initially relatively low positive pore pressures were produced and the stress path moved to the right indicating a dilative tendency. As brittleness degree (B_d) increased, the softening behavior predominated and the stress path moved to the left until it reached critical state point. At high confining stress and high brittleness degree (B_d) value, i.e. $p_{ini}' = 3\text{MPa}$, the stress path terminated on the steady state line with large positive pore pressures and mean effective stresses less than the

initial confining pressure indicating softening behavior. The fines content (F_c) was increased due to particle breakage even effective stress decreases. It is noted that the undrained shear behavior is greatly dependent on the particle breakage of sands.

The effect of brittleness degree (B_d) on the location of critical state data are plotted in figures. The results of simulation show that as the brittleness degree (B_d) was low, the sample display dilative behavior; while as the brittleness degree (B_d) was high, the pore water pressure (u_w) increased and the sample displayed softening behavior.

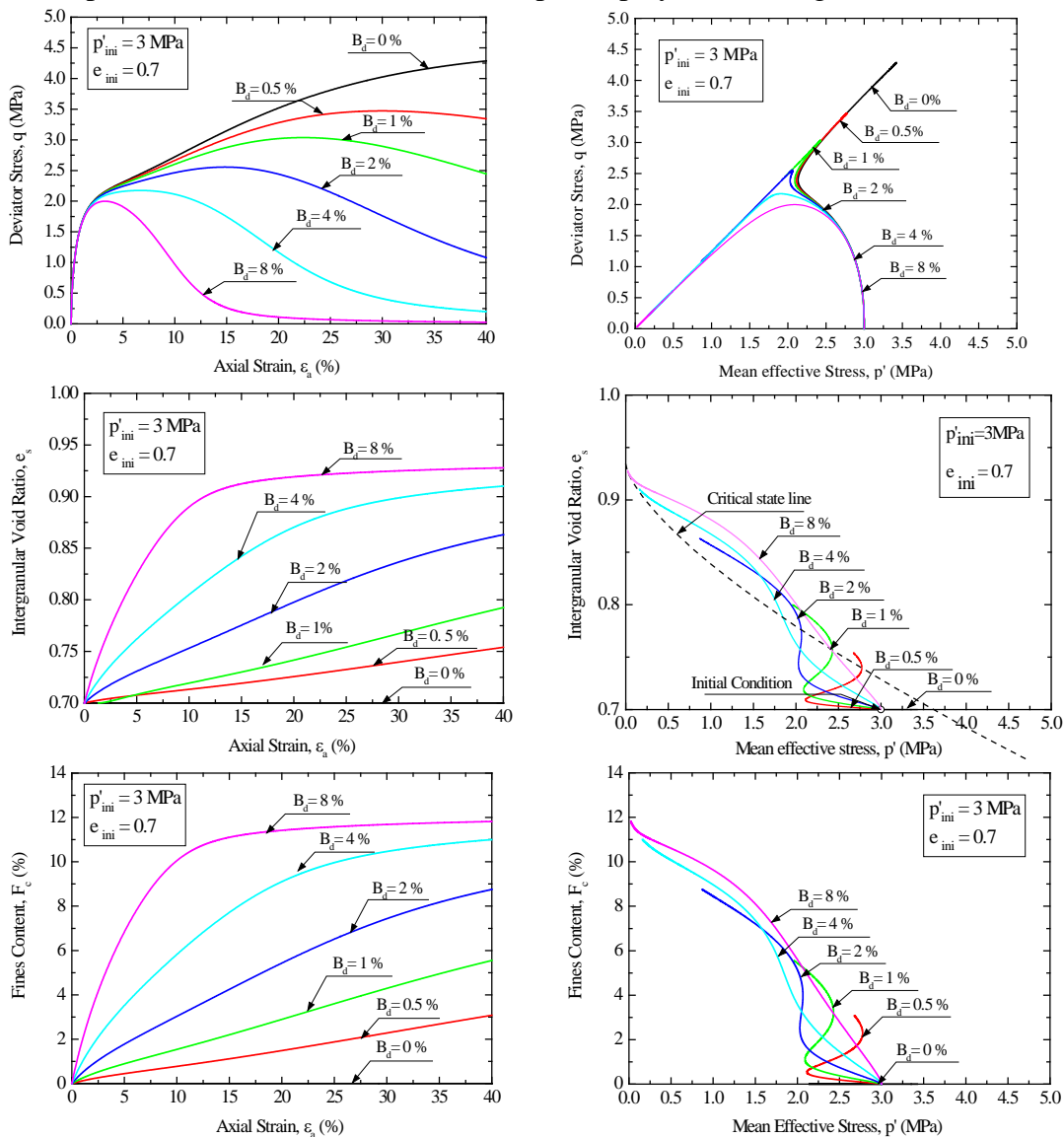


Figure 5.4-3 Simulated Results under various brittleness degree (B_d), for selected value of initial void ratio $e_{ini} = 0.7$ and a confining pressure of 3MPa. (a) stress-strain response; (b) stress path; (c) e_s -axial strain; (d) $e_s - (p')$; (e) fines content- axial strain; (f) fines content- mean effective stress

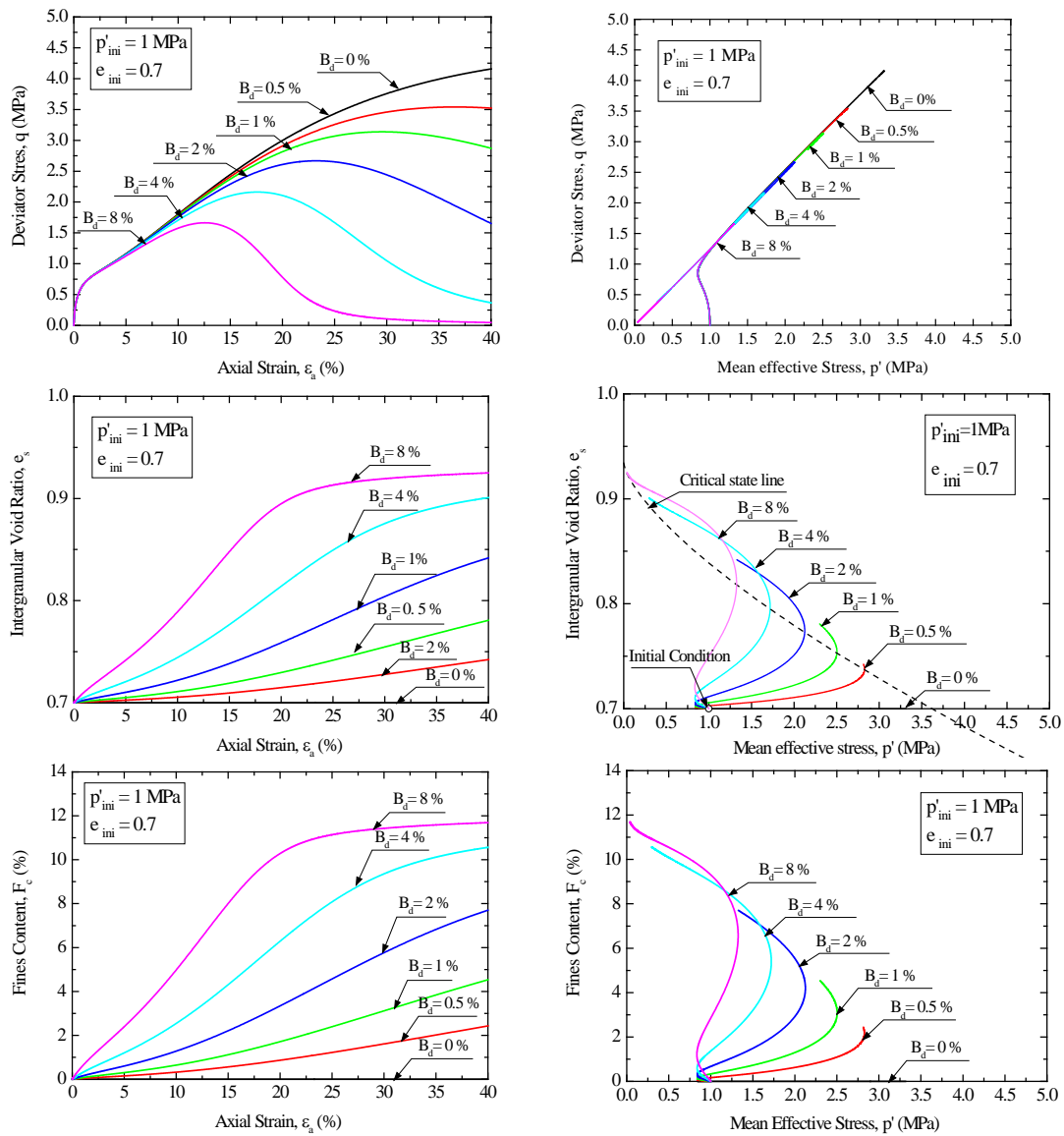


Figure 5.4-4 Simulated Results under various brittleness degree (B_d), for selected value of initial void ratio $e_{ini} = 0.7$ and a confining pressure of 1MPa. (a) stress-strain response; (b) stress path; (c) e_s -axial strain; (d) $e_s - (p')$; (e) fines content- axial strain; (f) fines content- mean effective stress

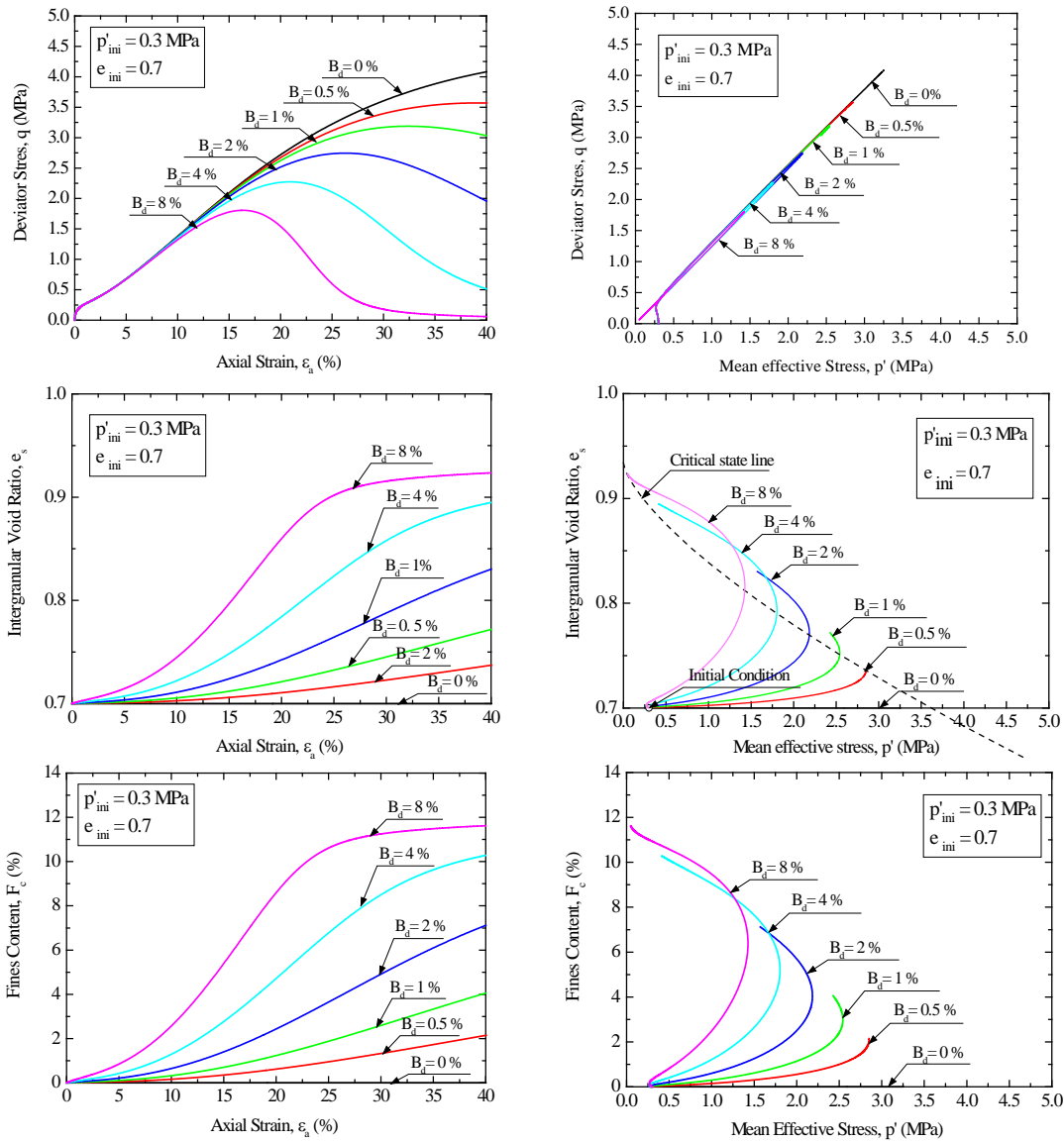


Figure 5.4-5 Simulated Results under various brittleness degree (B_d), for selected value of initial void ratio $e_{ini} = 0.7$ and a confining pressure of 0.3MPa. (a) stress-strain response; (b) stress path; (c) e_s -axial strain; (d) e_s - (p'); (e) fines content-axial strain; (f) fines content- mean effective stress

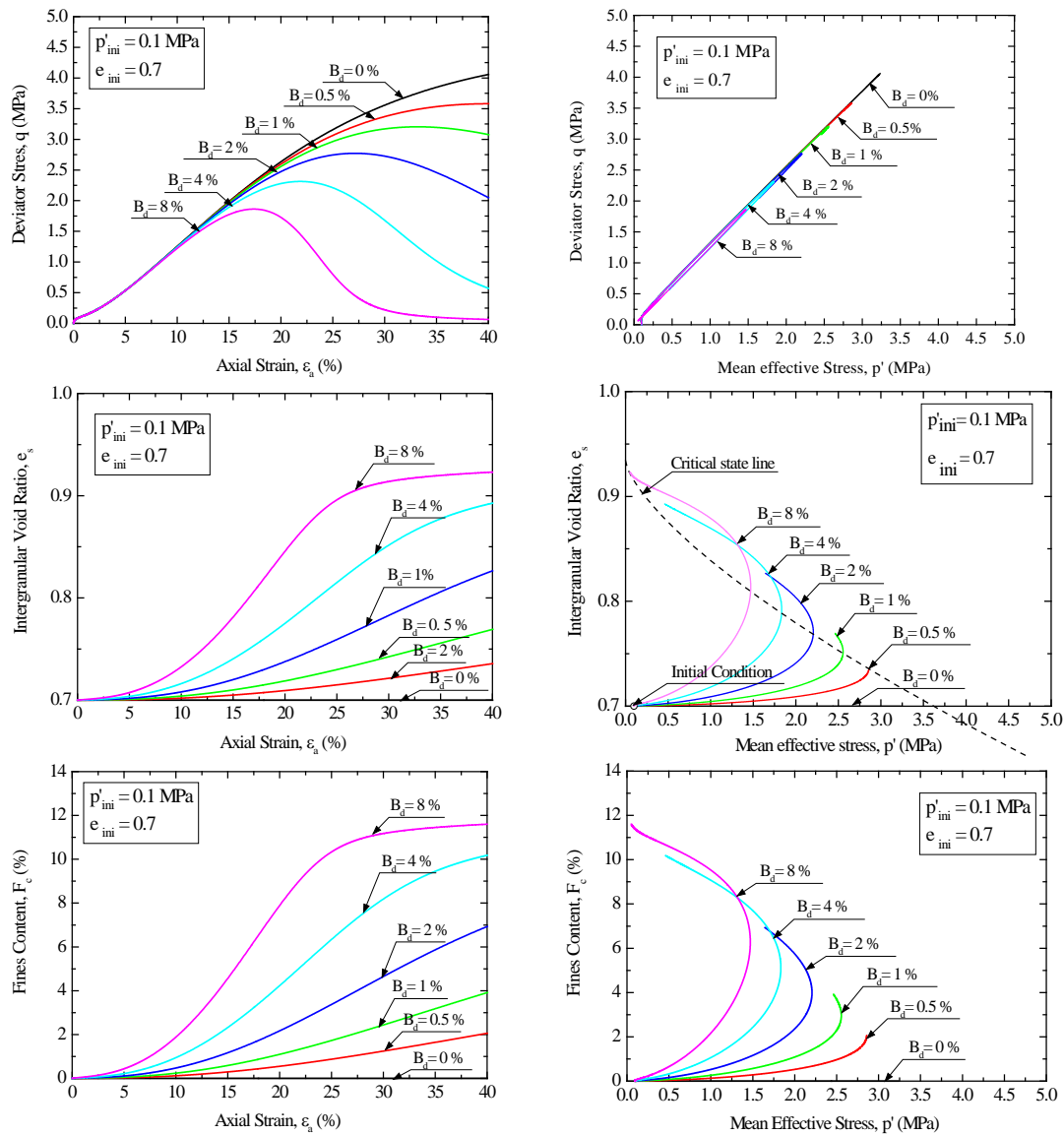


Figure 5.4-6 Simulated Results under various brittleness degree (B_d), for selected value of initial void ratio $e_{ini} = 0.7$ and a confining pressure of 0.1MPa. (a) stress-strain response; (b) stress path; (c) e_s -axial strain; (d) $e_s - (p')$; (e) fines content-axial strain; (f) fines content- mean effective stress

2. Series B: $e_{ini} = 0.8$

The results of series B with mean effective stress of 3MPa, 1MPa, 0.3 MPa and 0.1Mpa are shown in Figure 5.4-7, 5-4-8, 5-4-9 and 5-4-10, respectively.

As shown in Figure 5.4-7 to Figure 5.4-10, the simulation exhibited that at high confining stress, the dense curve behavior with high brittleness degree (B_d) decreased the undrained strength rapidly at a small strain and subsequently decreased until the end of test, which was consistent with a trend towards greater compressibility with increasing

brittleness degree (B_d) values. In the case of stress path, with high confining stress and high brittleness degree (B_d), the stress path showed that gradually turned toward to negative mean effective stress (p') direction and plummeted towards the origin of the stress path space with continuous shearing, and thus, the steady state was attained. This implies that, sands with higher brittleness degree (B_d) are more contractive lead to a marked reduction in undrained strength of sand during undrained shearing.

The effect of brittleness degree (B_d) on the location of critical state data pointed are plotted in figures. As the stress was initiated, particle breakage occurred, sand with higher brittleness degree (B_d) exhibited from dilate behavior gradually towards to a contractive behavior and then moved to critical void ratio. This disappearance of dilation was related to particle breakage occurred during undrained shearing. Therefore, when addition of brittleness degree (B_d) value into sand, a considerable reduction of undrained strength was expected. However, if brittleness degree (B_d) was low, for undrained shearing, the states remained at constant e_s . Undrained strength of sand decreased with increasing brittleness degree (B_d) and towards the critical state line. Therefore, the results of simulation demonstrated that an increase in brittleness degree (B_d) resulted in an increase in intergranular void ratio (e_s) of sand as well as an increase in compressibility.

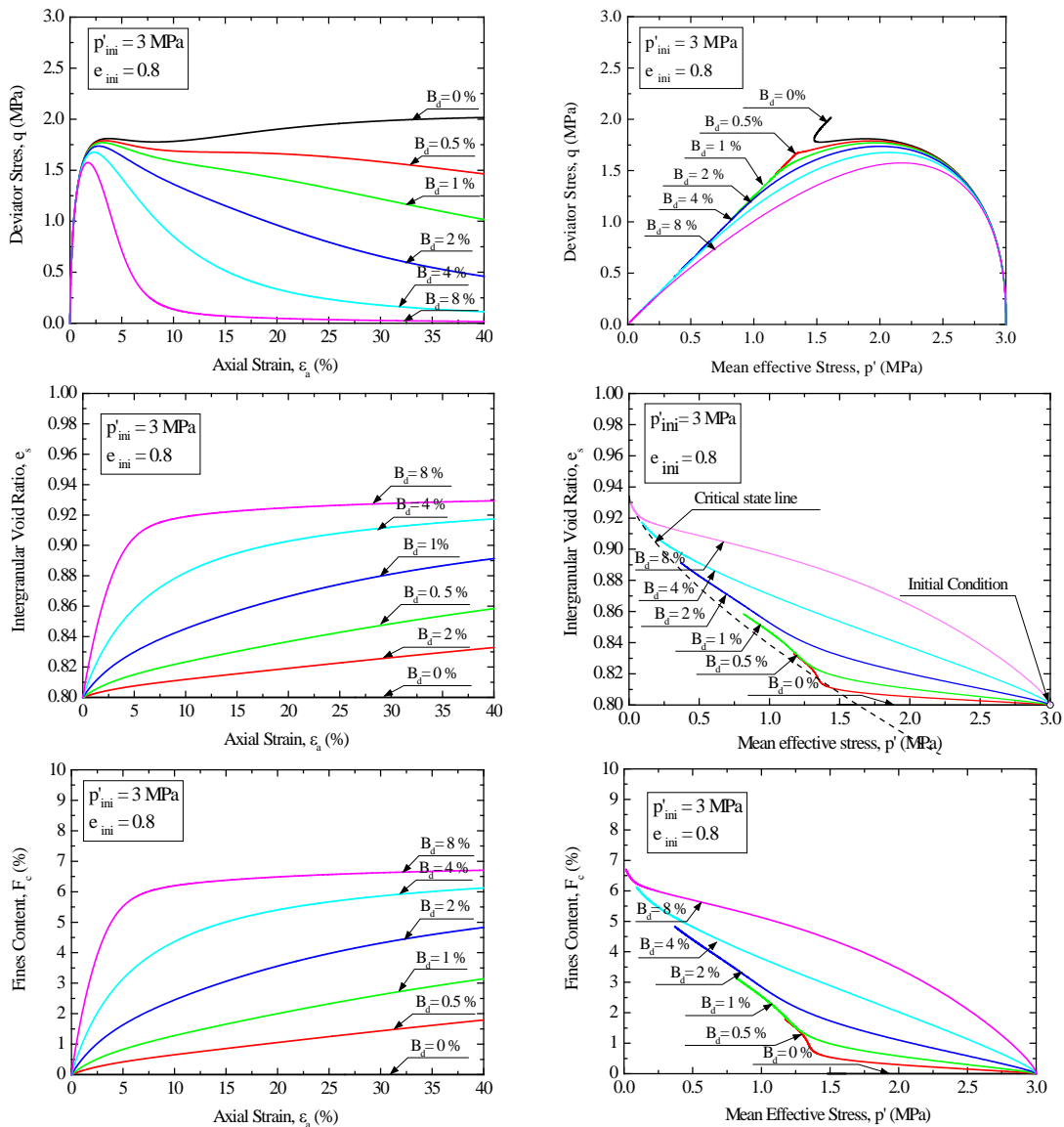


Figure 5.4-7 Simulated Results under various brittleness degree (B_d), for selected value of initial void ratio $e_{ini} = 0.8$ and a confining pressure of 3MPa. (a) stress-strain response; (b) stress path; (c) e_s -axial strain; (d) $e_s - (p')$; (e) fines content- axial strain; (f) fines content- mean effective stress

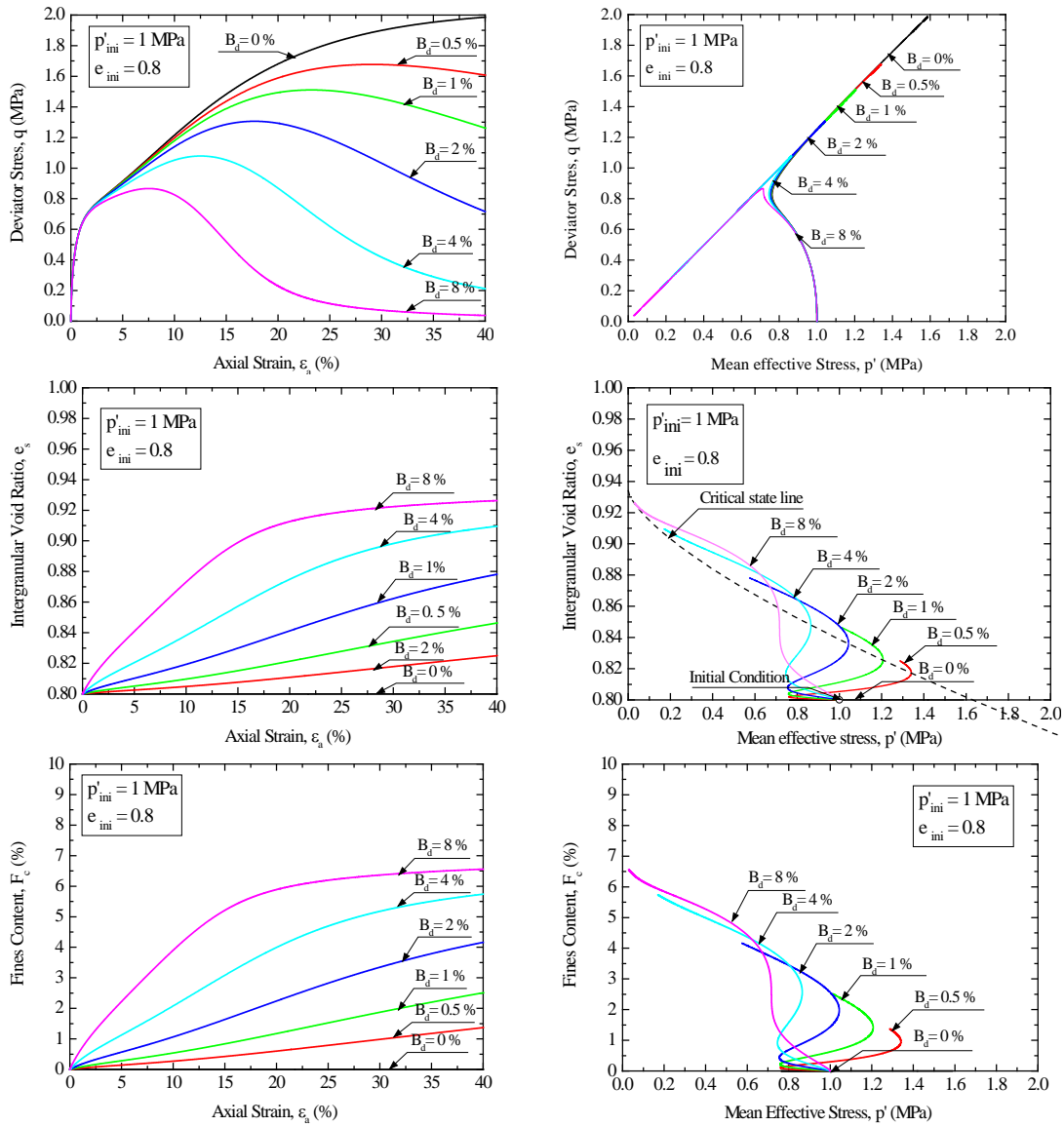


Figure 5.4-8 Simulated Results under various brittleness degree (B_d), for selected value of initial void ratio $e_{ini} = 0.8$ and a confining pressure of 1MPa. (a) stress-strain response; (b) stress path; (c) e_s -axial strain; (d) $e_s - (p')$; (e) fines content- axial strain; (f) fines content- mean effective stress

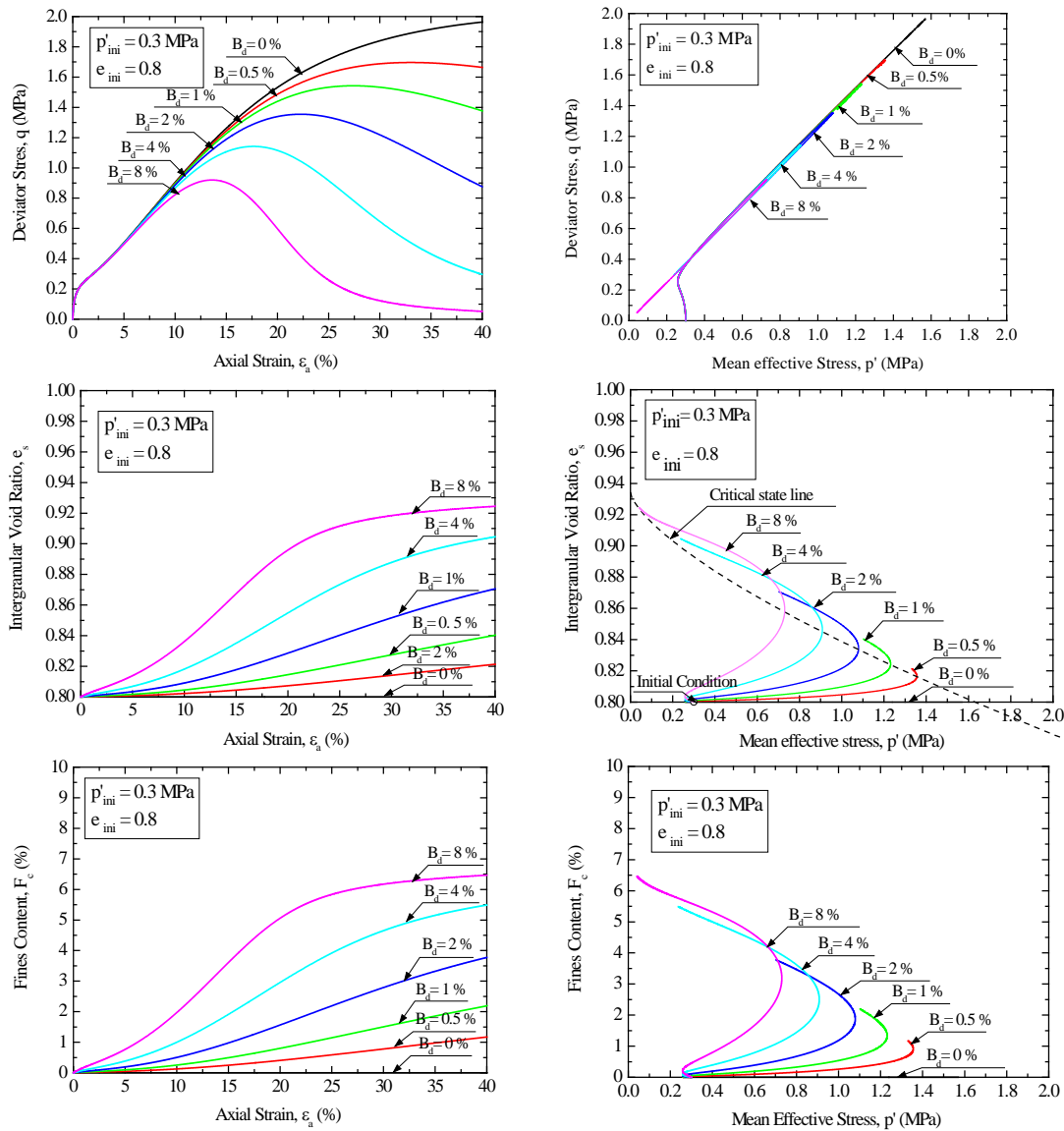


Figure 5.4-9 Simulated Results under various brittleness degree (B_d), for selected value of initial void ratio $e_{ini} = 0.8$ and a confining pressure of 0.3MPa. (a) stress-strain response; (b) stress path; (c) e_s -axial strain; (d) $e_s - (p')$; (e) fines content-axial strain; (f) fines content- mean effective stress

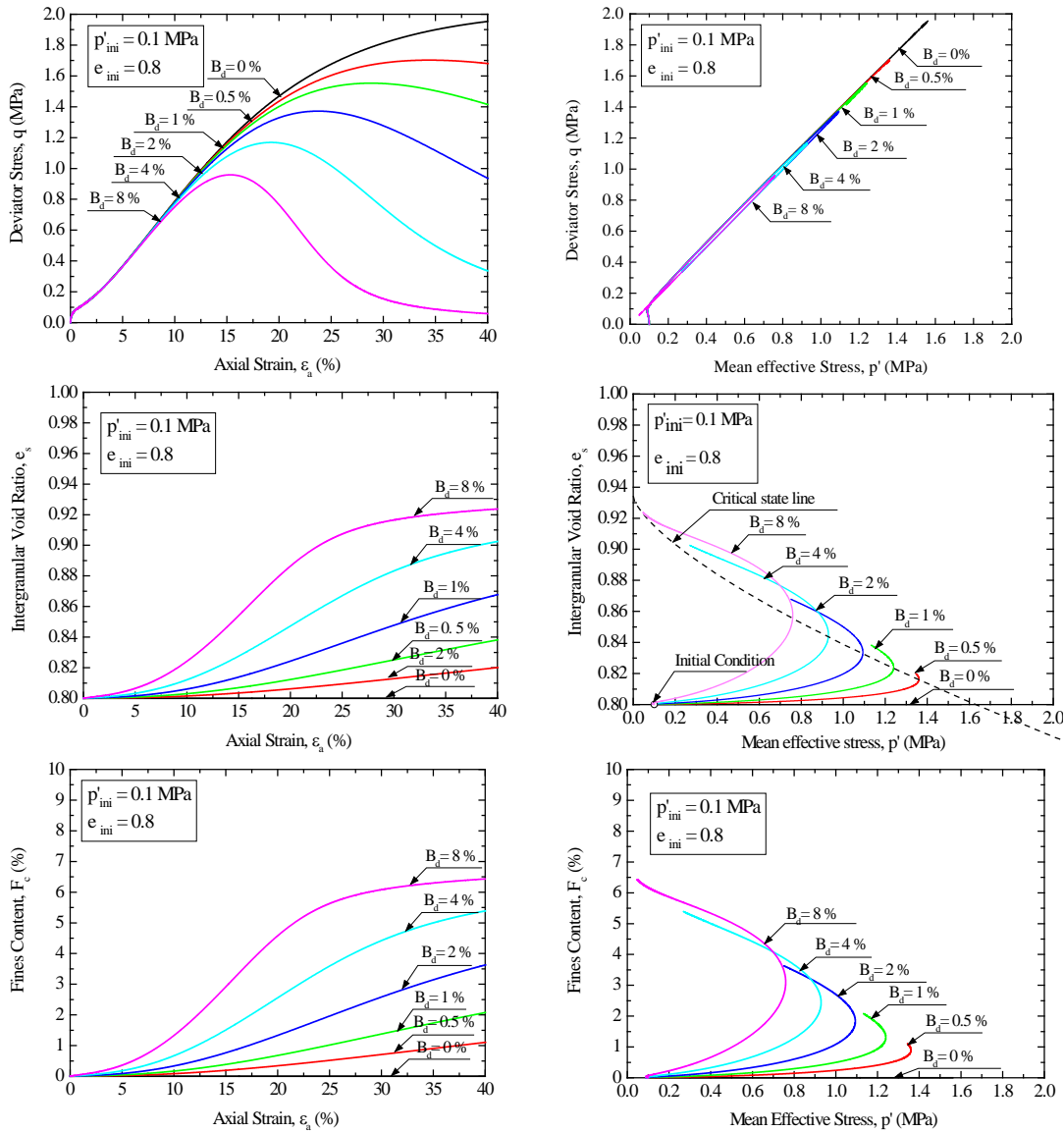


Figure 5.4-10 Simulated Results under various brittleness degree (B_d), for selected value of initial void ratio $e_{ini} = 0.8$ and a confining pressure of 0.1MPa. (a) stress-strain response; (b) stress path; (c) e_s -axial strain; (d) $e_s - (p')$; (e) fines content-axial strain; (f) fines content- mean effective stress

3. Series C: $e_{ini} = 0.9$

In contrast to the simulation aforementioned, there is an evolution approaching liquefaction for simulation with initial void ratio (e_{ini}) of 0.9 with mean effective stress of 3MPa, 1MPa, 0.3 MPa and 0.1MPa which have been observed in Figure 5.4-11 to Figure 5.4-14, respectively.

The overall behavior of this loose sand behavior in stress- strain response and stress path is strongly influenced by variation of brittleness degree (B_d). With higher brittleness

degree (B_d), the result of stress-strain response revealed that an increase in brittleness degree (B_d) led to decrease the deviator stress of sand. The peak deviator stress was reached at very low strain level, followed by a distinct reduction in the deviator stress and level off at large strain. The simulations also showed that there were an enormous decrease in effective stress throughout the modelling. The stress paths directed towards the origin of the q - p' space after reaching their respective peak deviator stress states as shown in Figure 5.4-11(b).

The critical data points were plotted in Figure 5.4-11(c). Sand with higher brittleness degree (B_d) exhibited that an increase in brittleness degree (B_d) resulted in an increase in intergranular void ratio (e_s) of sand as well as an increase in compressibility.

Thus, to interpret this loose sand simulation under high confining pressure and various brittleness degree (B_d), initially very loose samples liquefied because of the continued increase in pore water pressure and the corresponding decrease in effective stress and shear resistance.

However, at confining pressure of 0.3 MPa, for sand with high brittleness degree (B_d), i.e., $B_d = 8\%$, which liquefied, there was also continuous to the fully softened condition. On the other hand, for the sand with low brittleness degree (B_d), i.e., $B_d = 4\%$, the simulation showed that liquefaction was averted after maximum deviator stress by a decrease in pore water pressure and thus an increase in effective stress and undrained strength. Sand with lower brittleness degree (B_d) had a tendency to dilate shortly after the initial maximum deviator stress was reached, and a significant decrease in pore water pressure produced major increase in effective stress and undrained strength. This description also can be applied to confining stress of 0.1 MPa (Figure 5.4-14). Thus, to interpret this loose sand simulation under high confining pressure and various brittleness degree (B_d), initially very loose samples liquefied because of the continued increase in pore water pressure and the corresponding decrease in effective stress and shear resistance. This should be taken as proving high brittleness degrees (B_d) induce liquefaction potential.

Overall, when the brittleness degree (B_d) was low, the sample displayed dilative behavior; while as the brittleness degree (B_d) was high, the pore water pressure increased and the sample displayed softening behavior. Therefore, it can be expected a considerable reduction of undrained strength.

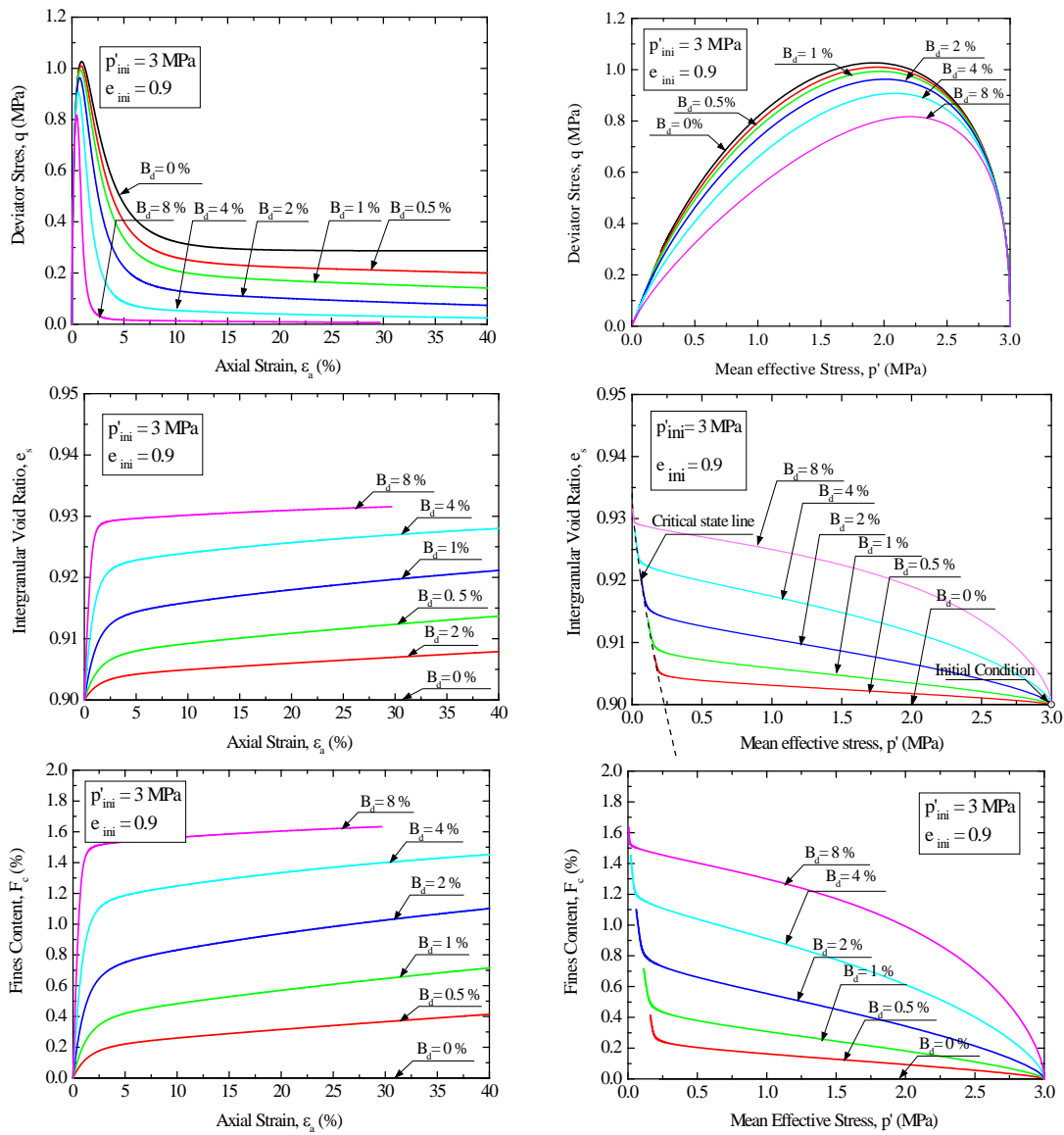


Figure 5.4-11 Simulated Results under various brittleness degree (B_d), for selected value of initial void ratio $e_{ini} = 0.9$ and a confining pressure of 3MPa. (a) stress-strain response; (b) stress path; (c) e_s -axial strain; (d) $e_s - (p')$; (e) fines content- axial strain; (f) fines content- mean effective stress

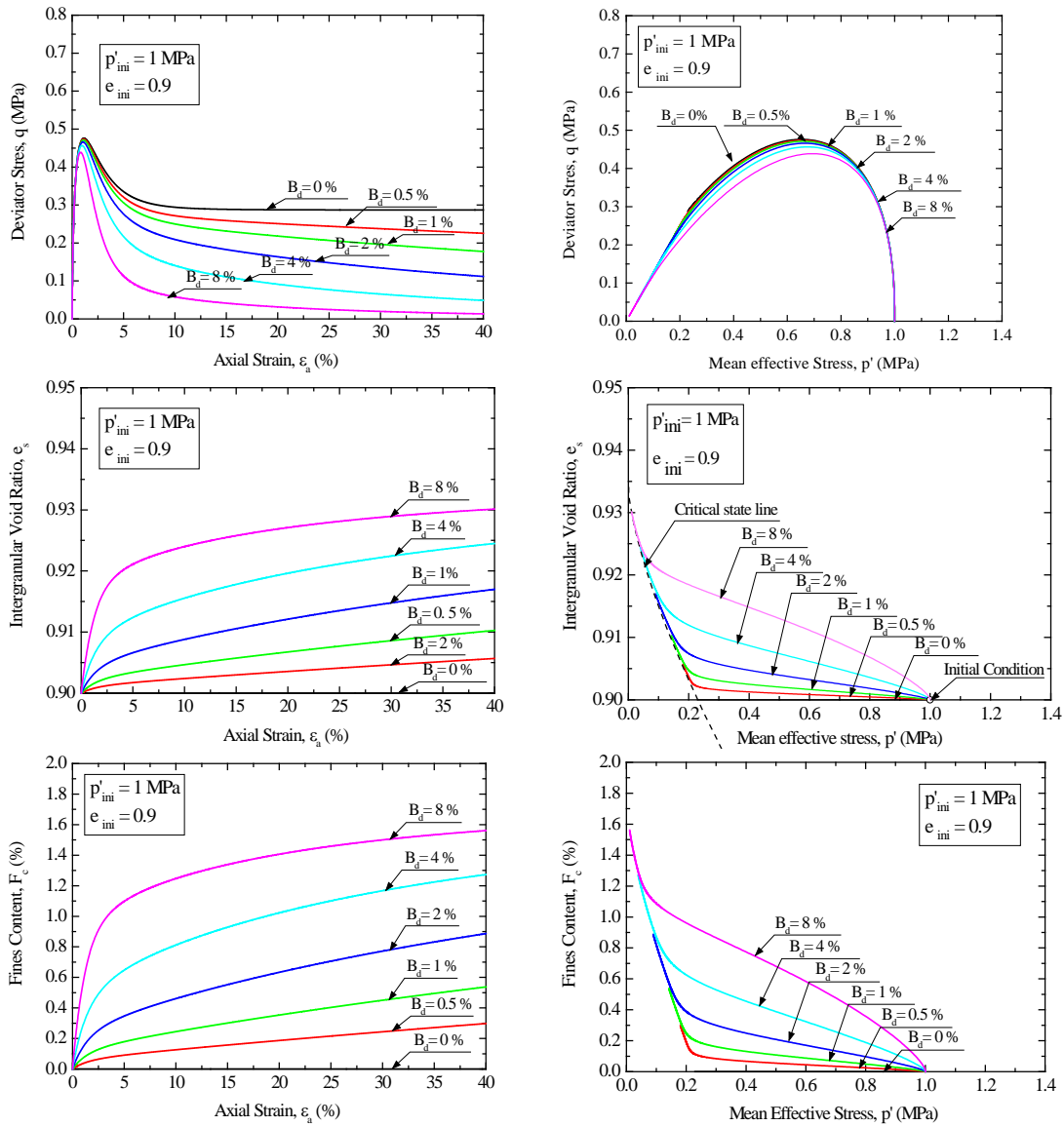


Figure 5.4-12 Simulated Results under various brittleness degree (B_d), for selected value of initial void ratio $e_{ini} = 0.9$ and a confining pressure of 1MPa. (a) stress-strain response; (b) stress path; (c) e_s -axial strain; (d) $e_s - (p')$; (e) fines content- axial strain; (f) fines content- mean effective stress

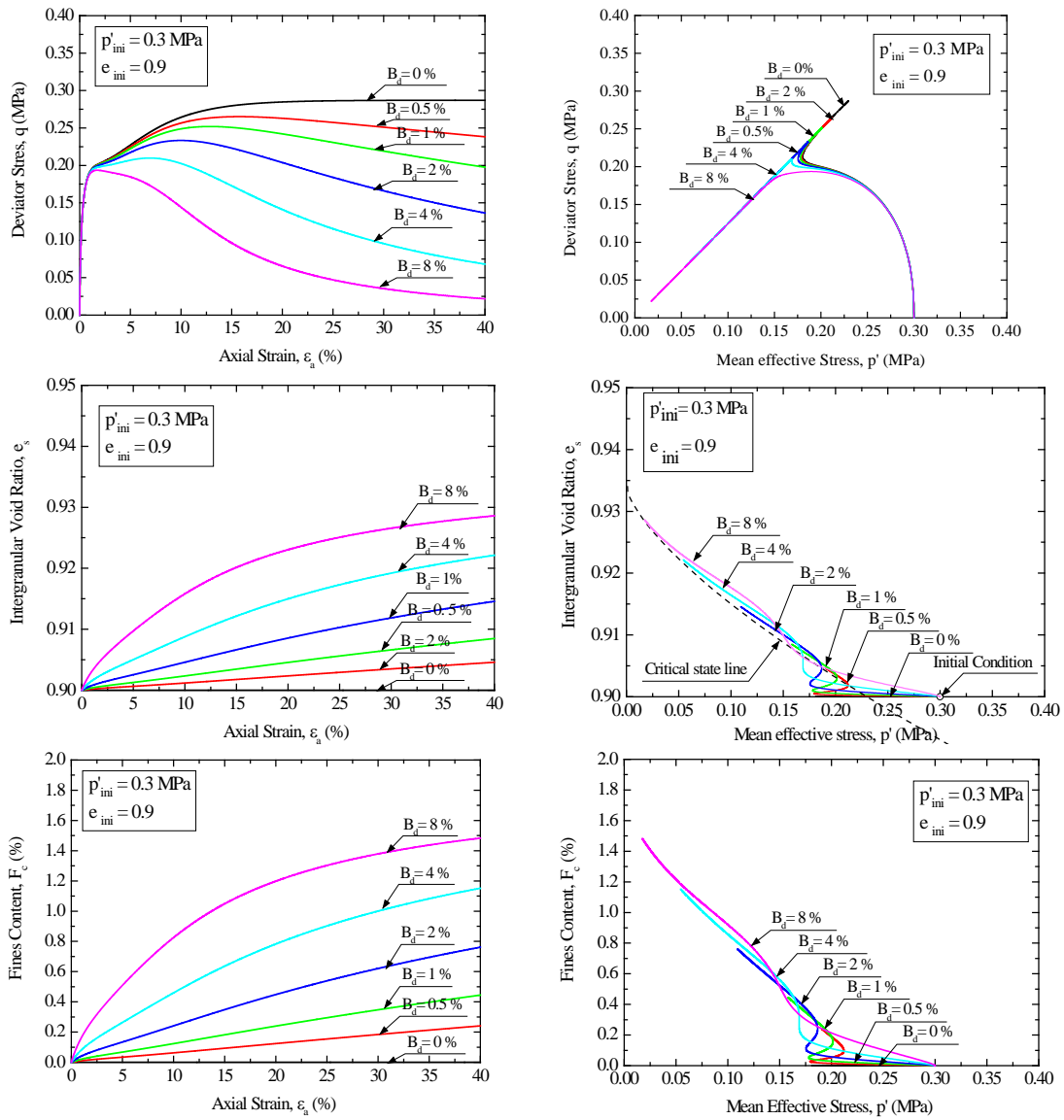


Figure 5.4-13 Simulated Results under various brittleness degree (B_d), for selected value of initial void ratio $e_{ini} = 0.9$ and a confining pressure of 0.3MPa. (a) stress-strain response; (b) stress path; (c) e_s -axial strain; (d) $e_s - (p')$; (e) fines content-axial strain; (f) fines content- mean effective stress

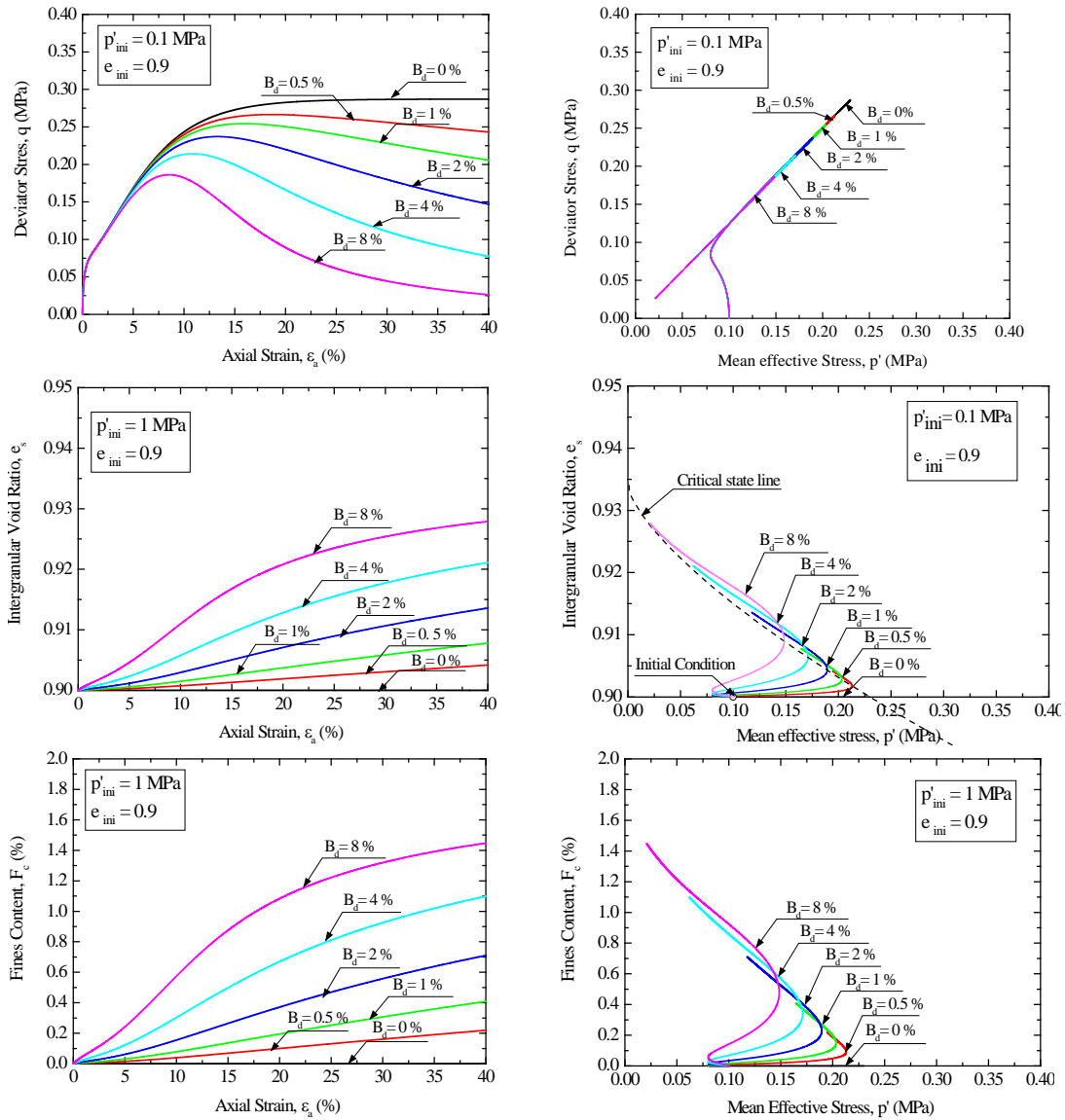


Figure 5.4-14 Simulated Results under various brittleness degree (B_d), for selected value of initial void ratio $e_{ini} = 0.9$ and a confining pressure of 0.1MPa. (a) stress-strain response; (b) stress path; (c) e_s -axial strain; (d) $e_s - (p')$; (e) fines content-axial strain; (f) fines content- mean effective stress

5.5 Summery

A bounding surface hypoplasticity model accounting for the influence of particle breakage was performed, which included the constitutive equations controlling brittleness degree (B_d). Using the set of determined parameters (Table 5.3-1 and Table 5.3-2) proposed by Wang et al. (2002), all comparisons between the experimental data and the numerical simulations demonstrated that the model reproduced with good agreement.

To examine the effect of particle breakage on stiffness and undrained strength behavior of sandy materials, the increment of fines content (ΔF_c), brittleness degree (B_d), and intergranular void ratio (e_s) are simulated to stress-strain response, stress paths and critical state void ratio in the model. The constitutive model with the same set of material constants covered a wide range of densities under various brittleness degrees (B_d). The following summaries are the outcome of this simulation.

1. With respect to the fines content (F_c), the concept of intergranular void ratio (e_s) is suggested to substitute the void ratio to define the initial state of granular soils in this study. According to the results of simulation, when particle breakage occurs, it reveals an increase in fines content (F_c) resulted in an increase in the intergranular void ratio (e_s) as well as an increase in compressibility.
2. The overall behavior of sand behavior in stress- strain response and stress path is strongly influenced by variation of brittleness degree (B_d). When particle breakage occurs during undrained shearing, sand with fines manifested higher compressibility during undrained shearing and initiated the volume change. As more and more particle breakage occurs, the initial void ratio moves upward to critical state line and then achieved higher intergranular void ratio (e_s) than clean sand ($B_d = 0\%$) in the simulation.
3. With low brittleness degree (B_d), dense sand possesses initially little contractive tendency and then shows dilative tendency in $q - p'$ stress path and the stress path traces towards high mean effective stress and ultimately it reaches to the steady state line. Further, increase in brittleness degree (B_d) causes decrease in deviator stress. However, loose sand reveals that softening behavior of strength with high brittleness degree (B_d).
4. With high brittleness degree (B_d), the peak deviator stress is reached at very low strain level, followed by a distinct reduction in the deviator stress and required considerably larger axial strain to reach critical state. The simulation also shows that there is an enormous decrease in effective stress throughout the simulation, the stress path turns gradually toward to negative p' direction at respective q and plummet towards the origin of the stress path with continuous shearing until the end of simulation, and thus, the steady state is attained. Therefore, it infers that brittleness degree (B_d) leads to change in the shape of stress path and reduce in maximum deviator stress.
5. According to Lade and Yamamuro (1997), they showed that liquefaction is enhanced

by the presence of fines and the liquefaction potential increases with an increase of fines content (F_c). Regarding to the Eq. (5.4), the fines content (F_c) increased with increasing brittleness degree (B_d). The behavior of stress-strain response and stress paths of four pairs of simulations indicates that the interaction between fines content (F_c) and sand create more compressible than sand without particle breakage. It can be inferred that the presence of fines content (F_c) in the sand has influence on static liquefaction potential of sand during the period of ground shaking.

5. The results of model simulation exhibit significant reduction of stiffness and undrained strength of sandy materials due to increase of the potential of particle breakage. Therefore, it is noted that the undrained shear behavior is greatly dependent on the particle breakage and the effect of particle breakage for engineering judgement in practice cannot be negligible.
6. Due to the limitations in modelling, particle breakage may be incomplete because of the limitation of axial strains, i.e., the steady state of deformation would be difficult to be reached, especially for those sand in medium or dense state. In fact, in many cases, such as some landslides, the shearing behavior may involve runout of several meters to tens of kilometers. Therefore, quite large shear displacement is needed to examine these failure phenomena where shearing resistance may decrease along with shear displacement.

CHAPTER 6 CONCLUSIONS

6.1 General

Geotechnical structures such as tunnel, earth dams, bridge, abutments, retaining structures, slope, etc., have been discussed to deform and settle due to particle breakage. In practice, when particle breakage occurs due to changes in stress, it can cause change in the original physical properties of soils, alter the stiffness and strength of a soil, compress the volume of materials, and finally leads to practical problems occurred. Therefore, it is important to be able to identify and quantify the effects of particle breakage on these engineering properties.

In this dissertation, I performed a total of 129 CD triaxial tests, 12 undrained triaxial tests, and grain size distribution of original sand prior to shear and after shear. Furthermore, I carried out 68 maximum density test and 83 minimum density tests for selected sands to examine the sensitivity of water content, as well as water absorption tests of fine aggregates. Moreover, I examined the experimental results of stress-strain relationship and degree of particle breakage corresponding to Marsal, Hardin, Lee & Farhoomands and D_{50} as well as increment of fines content (ΔF_c) on four types of sand.

Based on my observations, I proposed a linear equation to calculate the brittleness degree (B_d) associated with various stress and strain levels. I then applied the findings to a bounding surface hypoplasticity model for undrained stress-strain behavior of sandy materials to examine the effect of brittleness on particle breakage. The concept of intergranular void ratio (e_s) was employed to link and correlate brittleness degree (B_d) with stress-strain response in the constitutive model. The main results can be summarized as following sections

6.2 Summary and Conclusions

The main results and conclusions drawn from this thesis are summarized below.

1. Summary behavior of four sands in Laboratory test

- (1) The CD triaxial test results indicated that the maximum deviator stress of either stiff or weak particles increases with increasing initial confining pressure. Under the same axial strain, stiff particles have a higher deviator stress than brittle particles.
- (2) Within the range of confining pressures investigated, the stress-strain relations of Toyoura sand and JCA sand showed a stiff response at small strain level; while both

Takasegawa sand and Inagi sand showed contractive response followed by dilative behavior. The contractive response was more significant at higher confining pressure.

- (3) Within the level of confining pressure used in the tests, particle breakage in sands occurred during shearing stage of triaxial test more than the consolidation stage. In addition, the degree of particle breakage increased with the stress and strain levels.
- (4) The effect of particle shape for the angular materials is more significant than that on the rounded materials.
- (5) To examine the degree of particle breakage, I adopted Marsal's breakage index, Hardin's breakage index, Lee and Farhoomad's breakage Index, D_{50} , and the increment of fines content (ΔF_c). Having compared the various methods, the particle breakage proposed by Marsal indicates that when the grain size distribution curve of materials falls into narrow range, it tends to be greatest amount of particles retained on one or two sieve size interval to be used in calculation the degree of particle breakage. Contrarily, when the grain size distribution curve of materials is wide-range, it tends to be very little materials left for comparison on the original sieves. In addition to Marsal's method, even though Hardin's breakage index is based on consideration of the entire grain size distribution, it ignored silt-size particle in calculation. Therefore, the materials which contained or induced a great amount of finer particles after shearing would not be appropriate to adopt in this method. Both Lee and Farhoomad's breakage index and D_{50} 's breakage index were measured criteria related to particle size scale. Quantifying particle breakage should prevent inaccurate estimation of both numerator and the denominator of equation. Any errors in judgments of the denominator of equation have a greater impact on particle breakage estimation because errors in the denominator can amplify particle breakage index.
- (6) I examined the degree of particle breakage in terms of Marsal's, Hardin's, Lee & Farhoomand's, D_{50} 's breakage indices, and increment of fines content (ΔF_c). It can be concluded that the degree of particle breakage of sands during shear deformation has linear relationship with confining stress and axial strain level.
- (7) I conducted a series of consolidated drained triaxial compression test on sand under a wide range of confining stress and strain levels. I then adopted the fines content (F_c) as an index to quantify the magnitude of particle breakage. From experimental results, I found that degree of particle breakage has linear relationship with stress levels and

axial strains so that a linear equation based on fines content (F_c) and brittleness degree (B_d) associated with stress and strain levels is then proposed as $dF_c = B_d (\sigma_3'/p_a) \times d\varepsilon_1$.

- (8) Experimental results of stress-strain relationship and particle breakage corresponding to increment of fines content (ΔF_c) on four types of sand showed that the amount of particle breakage continued to very large strains even when the steady state for four sands was reached at higher stress levels. This implies that the amount of particle breakage at steady state was independent of the path taken to reach it but is depended on the magnitude of stress levels and axial strains.
- (9) Experimental observations revealed that the minimum density decreased significantly with slightly increasing water content which can be attributed to the water absorption ability of material, and as consequence, the material becomes more brittle in the present of water, evidencing the phenomenon of water action are involved in the process of particle breakage. Therefore, it is believed that if soils have higher ability to absorb liquid, the potential of crushability of which is higher, resulting in giving rise to an increase in particle breakage. Consequently, the findings can be concluded that the effect of water absorption and water content on particle breakage could be depended on the material properties and its sensitivity to the presence of water.
- (9) To find more efficient and less time-consuming approaches to evaluate the particle breakage, I presented a relevant mechanism between particle breakage and water effects. I examined the relationship between brittleness degrees of soils, minimum and maximum densities of soils, and water content as well as water absorption ability. It is implied that the higher the increment of water content, the higher brittleness degree (B_d) of soils at a given relative density. The higher the water absorption ability, the higher the brittleness degree (B_d) is.

2. Summary in numerical model simulations

- (1) Prediction of brittleness degree by water absorption was proposed. It is suggested that brittleness degree of soils account for various breakage indices is linearly related to the logarithm of water absorption through material parameters.
- (2) A constitutive model was modified in conjunction of brittleness degree (B_d) and intergranular void ratio (e_s) and used to simulate the undrained behavior of sand. With the higher brittleness degree (B_d), the results of simulation demonstrated that a

trend from dilate behavior gradually towards to a contractive behavior and eventually moves to critical void ratio. Consequently, an increase in brittleness degree (B_d) resulted in an increase in intergranular void ratio (e_s) as well as an increase in compressibility.

- (3) When the brittleness degree (B_d) is low, the sample displays dilative behavior; while as the brittleness degree (B_d) is high, the pore water pressure increases and the sample displays softening behavior. Therefore, it can be expected a considerable reduction of undrained strength.
- (4) It is clearly shown from these figures that breakage behavior alters both peak and steady state stress strain response of the each simulation as well as the response of dilation / contraction of stress paths and intergranular void ratio (e_s) –mean effective stress (p') space.
- (6) The results of model simulation exhibited significant reduction of undrained strength of sands due to increase of the potential of particle breakage. Therefore, it is noted that the undrained shear behavior is greatly dependent on the particle breakage and the effect of particle breakage for engineering judgement in practice cannot be negligible.

I studied the influence of particle breakage and then I confirmed that significant reduction of stiffness and undrained strength of sandy materials due to increase of particle breakage. These theoretical findings are complemented by experimental activity on real datasets, showing the cheap and quick experiments such as density test and water absorption test can be carried out to investigate the particle breakage and the brittleness of particles should be carefully and properly considered in engineering practice.

6.3 Recommendations for Future Research

1. Triaxial test is most well-known approach to evaluate the particle breakage phenomenon. In this dissertation, I have already examined two handful methods to assess the particle breakage which are the methods of minimum and maximum density of soils and water absorption of fine aggregates. More fundamental and less-time consuming experimentations are encouraged to investigate the particle breakage development.
2. The experimental result for clean sands presented in this dissertation are in limited scope as it only discussed about “fines in sand” model at the maximum increment of

finer content (ΔF_c) corresponds to a limiting value at $\varepsilon_a = 40\%$. Thus, the following recommendations can be made for future research.

- (1) The experimentation and theoretical development of the dissertation is limited to $\varepsilon_a = 40\%$. In some cases, particle breakage may be incomplete due to the limitation of axial strains, i.e., the steady state of deformation would be difficult, especially for those sand in medium or dense state. In fact, in many cases, such as some landslides, the shearing behavior may involve runout of several meters to tens of kilometers. Therefore, quite large shear displacement is needed to examine these failure phenomena where shearing resistance may decrease along shear displacement. Therefore, this limitation can be extended to larger axial strain by introducing new parameters.
- (2) Many attempts have been made to find various relationships for different parameters and some types of constitutive models for studying the behavior of particulate media, i.e. time, energy, and hydraulic conductivity, etc.
- (3) In this dissertation, the experimentation theoretical development of the dissertation was focus on the effect of particle breakage with clean sands. The effect of fines types, the effect of fines shape, the amount of fines content (F_c), and the link between monotonic and cyclic loading behavior for sand with fines should need further study.
- (4) A constitutive model was modified in conjunction of e_s and it was evaluated for sand with fines. It could be interesting to modify a constitutive model in conjunction with inter-fines void ratio, e_f and to evaluate the model prediction with experimental results. The comparison between these two models and model parameters might highlight some unknown attributes of the framework.

References

1. Aghaei Araei, A., Soroush, A. and Rayhani, M.H.T. (2010). "Large-scale triaxial testing and numerical modeling of rounded and angular rock materials," *Scientia Iranica, Transaction A: Civil Engineering*, 169-83.
2. Agung, M.W., Sassa, K., Fukuoka, H., and Wang, G. (2004). "Evolution of shear-zone structure in undrained ring-shear tests," *Landslides*, 1: 101–112.
3. Anandarajah, A. (2008). "Modeling liquefaction by a multimechanism model," *Journal of Geotechnical and Geoenvironmental Engineering*, 134(7), 949–959.
4. Arulanandan, K., Li, X. S., and Sivathasan, K. (2000). "Numerical simulation of liquefaction-induced deformations," *Journal of Geotechnical and Geoenvironmental Engineering*, 126(7), 657–666.
5. ASTM D7181 (2011). "Standard Test Method for Consolidated Drained Triaxial Compression Test for Soils," *Annual Book of ASTM Standards*, ASTM International, West Conshohocken, PA.
6. Atkinson, J. (2007). "The mechanics of soils and foundations," Second Edition, Taylor & McGraw-Hill, London. 122.
7. Been, K. and Jefferies, M. G. (1985). "A state parameter of sands," *Geotechnique, England*, 35(2), 99–112.
8. Bishop, A.W. (1966). "The strength of soils as engineering materials," *Geotechnique*, 16: 89–130.
9. Bouckovalas, G. D., Andrianopoulos, K. I., and Apadimitriou, A. G. (2003). "A critical state interpretation for the cyclic liquefaction resistance of silty sands," *Soil Dynamic Earthquake Engineering*, 23(2), 115–125.
10. Chester, J.S., Lenz, S.C., Chester, F.M., and Lang, R.A. (2004). "Mechanisms of compactions of quartz sand at diagenetic conditions," *Earth and Planetary Science Letters*, 220(3–4): 435–451.
11. Huang, C. W., Yoshimine, M., Inoue, M., Yamada, D.(2012), "Measurements of pore water pressure in a ground, temperature and rainfall at a slope failure in mountainous area", 5th Taiwan-Japan Joint Workshop on Geotechnical Hazards from Large Earthquakes and Heavy Rainfall, SV 13-SV 18.

12. Coop, M.R. (1990). "The mechanics of uncemented carbonate sands," *Geotechnique*, 40: 607–626.
13. Chuhan, F.A., Kjeldstad, A., Bjorlykke, K., and Hoeg, K. (2002). "Porosity loss in sand by grain crushing — experimental evidence and relevance to reservoir quality," *Marine and Petroleum Geology*, 19: 39–53.
14. Coop, M.R., and Lee, I.K. (1993). "The behavior of granular soils at high stresses," In *Predictive soil mechanics*. Edited by G.T. Housbly and A.N. Schofield. Thomas Telford, London, U.K. pp. 186 –198.
15. Coop, M.R., Sorensen, K.K., Bodas-Freitas, T., Georgoutsos, G. (2004). "Particle breakage during shearing of a carbonate sand," *Geotechnique*, 54(3):157–163.
16. Dafalias, Y. F., Popov, E. P. (1975). "A model of nonlinearly hardening materials for complex loading," *Acta Mechanica* 21, 173–192.
17. Dafalias, Y. F. (1986). "Bounding surface plasticity: I. Mathematical foundation and hypoplasticity," *Journal of Engineering Mechanics*, 112(9), 966–987.
18. Dafalias, Y. F., and Manzari, M. T. (2004). "Simple plasticity sand model accounting for fabric change effect," *Journal of Engineering Mechanics*, 130(6), 622–634.
19. Das, B. M. (2002). "Principles of Geotechnical Engineering," Fifth Edition, Brooks/Cole, Pacific Grove, CA. 83-108, 664–668.
20. Elgamal, A., Yang, Z., Parra, E., and Ragheb, A. (2003). "Modeling of cyclic mobility in saturated cohesionless soils," *International Journal of Plasticity*, 19(6), 883–905.
21. Erzin, Y., Yilmaz, I. (2008). "Case study of crushing resistance of Anatolian sands at lower and higher density," *Bulletin of Engineering Geology and The Environment*, 67:71 –77.
22. Fedaa, J. (2002). "Notes on the effect of grain crushing on the granular soil behavior," *Engineering Geology*, 63(1–2): 93–98.
23. Fukumoto T. (1992). "Particle breakage characteristics of granular soils," *Soils and Foundations*, 32(1), 26–40.
24. Georgiannou, V. N., Hight, D. W. & Burland, J. B. (1990). "The undrained behavior of clayey sands in triaxial compression and Extension," *Geotechnique*, 40, No. 3, 431–449.
25. Gerolymos, N. and Gazetas, G. (2007). "A model for grain-crushing-induced landslides—Application to Nikawa, Kobe 1995," *Soil Dynamics and Earthquake Engineering*, 27, 803–817.
26. Ghanbari, A., Sadeghpour, A.H., Mohamadzadeh, H. and Mohamadzadeh, M. (2008). "An experimental study on the behavior of rockfill material using large scale tests,"

- Electronic Journal of Geotechnical Engineering, 13, Bundle G. 1–16.
27. Hagerty, M.M., Hite, D.R., Ulrich, C.R., Hagerty, D.J. (1993). "One dimensional high pressure compression of granular media," *ASCE Journal of Geotechnical Engineering*, 119(1):1–18.
 28. Hall, E.B., and Gordon, B.B. (1963). "Triaxial testing with large-scale pressure equipment," In *Proceedings of the Symposium on Laboratory Shear Testing of Soils*, Ottawa, Ont., 9–11 September 1963. ASTM STP 361. American Society for Testing and Materials, West Conshohocken, Pa. 315–328.
 29. Hardin, B.O. (1985). "Crushing of soil particles," *ASCE Journal of Geotechnical Engineering*, 11(10):1177–1192.
 30. Hattori, T., Kitagawa, R., Seto, K., Sokobiki, H., and Kusakabe, O. (1998). "Field investigation of weathering in Hiroshima granite," *Journal of Geotechnical Engineering*, *Proceedings of the Japanese Society of Civil Engineers*, 589(III-42): 359–368.
 31. Hall, E.B., and Gordon, B.B. (1963). "Triaxial testing with large-scale pressure equipment," In *Proceedings of the Symposium on Laboratory Shear Testing of Soils*, Ottawa, Ont., 9–11 September 1963. ASTM STP 361. American Society for Testing and Materials, West Conshohocken, Pa., 315–328.
 32. Indraratna, B. and Salim, W. (2002). "Modelling of Particle Breakage of Coarse Aggregates Incorporating Strength and Dilatancy," *Geotechnical Engineering*, *Proceedings of Inst. of Civil Engineers*, UK, Vol. 155(4), 24–252.
 33. Indraratna B. and Salim W. (2003). "Deformation and degradation mechanics of recycled ballast stabilised with geosynthetics," *Soils and Foundations*, 43, No. 4, 35–46.
 34. Inoue, M. (2000). "発電用貯水池における流入土砂の予測と制御に関する研究," Ph.D. Thesis, University of Kyoto, Kyoto, Japan.
 35. Japanese Industrial Standards Committee (2006). "Method of test for density and water absorption of fine aggregates," JIS A1109–2006.
 36. Japanese Geotechnical Society (2009). "Test method for minimum and maximum densities of sands," JGS 0161–2009.
 37. Japanese Geotechnical Society (2009). "Method for consolidated-drained triaxial compression test on soils," JGS 0524–2009.
 38. Japanese Geotechnical Society (2009). "Test method for density of soil particles," JGS 0111–2009.
 39. Japanese Geotechnical Society (2009). "Test method for particle size distribution of soils," JGS 0131–2009.

40. Kenney, T. C. (1977). "Residual strength of mineral mixtures," Proceedings of the 9th International Conference on Soil Mechanics and Foundation Engineering, 1, 155–160.
41. Krieg, R. D. (1975). "A practical two surface plasticity theory," *Journal of Applied Mechanics* 42, Trans. ASME 97 (Series E), 641–646.
42. Kuerbis, R., Negussey, D., and Vaid, Y. P. (1988). "Effect of gradation and fines content on the undrained response of sand." *Hydraulic fill structure (GSP 21)*, ASCE, New York, 330–345.
43. Lade, P.V., Yamamuro, J.A., Bopp, P.A. (1996). "Significance of particle crushing in granular materials," *ASCE Journal of Geotechnical Engineering*, 122(4):309–316.
44. Lade, P.V. and Yamamuro, J.A. (1997). "Effects of Nonplastic Fines on Static Liquefaction of Sands," *Canadian Geotechnical Journal*, 34, 918–928.
45. Lee, K.L and Farhoomand, I. (1967). "Compressibility and crushing of granular soil in anisotropic triaxial compression," *Canadian Geotechnical Journal* 4(1):68–86.
46. Leslie D.D. (1963). "Large scale triaxial tests on gravelly soils," Proceedings of the second Pan-American conference on SMFE, vol. 1, Brazil, 181–202.
47. Leung, C.F., Lee, F.H., and Yet, N.S. (1996). "The role of particle breakage in pile creep in sand," *Canadian Geotechnical Journal*, 33(6): 888–898.
48. Li, X. S., Wang, Z. L., and Shen, C. K. (1992). "SUMDES: A nonlinear procedure for response analysis of horizontally-layered sites subjected to multi-directional earthquake loading," Department of Civil Engineering, University of California, Davis, CA.
49. Li, X. S., and Wang, Y. (1998). "Linear representation of steady-state line for sand," *Journal of Geotechnical and Geoenvironmental Engineering*, 124(12), 1215–1217.
50. Li, X. S., Shen, C. K., and Wang, Z. L. (1998). "Fully coupled inelastic site response analysis for 1986 Lotung earthquake," *Journal of Geotechnical and Geoenvironmental Engineering*, 124(7), 560–573.
51. Li, X. S., Dafalias, Y. F., and Wang, Z. L. (1999). "State-dependent dilatancy in critical-state constitutive modelling of sand," *Canadian Geotechnical Journal*, 36(4), 599–611.
52. Li, X. S. (2002). "A sand model with state-dependent dilatancy," *Geotechnique*, 52(3), 173–186.
53. Lobo-Guerrero, S., Vallejo, L.E. (2005). "Crushing a weak granular material: experimental numerical analyses," *Geotechnique*, 55(3):245–249.
54. Lobo-Guerrero, S. (2006). "Evaluation of crushing in granular materials using the discrete element method and fractal theory," Ph.D. thesis, University of Pittsburgh,

Pittsburgh, Pa.

55. Mandl, G., de Jong, L. N. J. and Maltha, A. (1977). "Shear zones in granular material-an experimental study of their structure and mechanical genesis," *Rock Mechanics* 9, 95– 144.
56. Manzari, M. T., and Dafalias, Y. F. (1997). "A critical state two-surface plasticity model for sands." *Geotechnique*, England, 47(2): 255–272.
57. Marsal, R.J. (1967). "Large-scale testing of rockfill materials," *Journal of the Soil Mechanics and Foundations Division*, 93(2): 27–43.
58. McDowell, G.R., Bolton, M.D., and Robertson, D. (1996). "The fractal crushing of granular materials," *International Journal of mechanics and physics of solids*, 44(12): 2079–2102.
59. McDowell, G.R., Bolton, M.D. (1998). "On the micromechanics of crushable aggregates," *Geotechnique*, 48(5):667–679.
60. McDowell, G.R., and Khan, J.J. (2003). "Creep of granular materials," *Granular Matter*, 5(3): 115–120.
61. Melboucil, B., Bahar, R., Cambou, B. (2008). "Study of the behavior of schist grains under crushing," *Bulletin of Engineering Geology and The Environment*, 67(2):209–218.
62. Mesri, G., and Vardhanabhuti, B. (2009). "Compression of granular materials," *Canadian Geotechnical Journal*, 46: 369–392.
63. Miura, N., and Yamanouchi, T. (1975). "Effect of water on the behavior of a quartz-rich sand under high stresses," *Soils and Foundations*, 15, No.4, 23–34.
64. Miura, N., and O'Hara, S. (1979). "Particle-crushing of a decomposed granite soil under shear stresses," *Soils and Foundations*, 19(3): 1–14.
65. Miura, N. (1985). "Point resistance of piles in sand," In *Proceedings of the 11th International Conference on Soil Mechanics and Foundation Engineering*, San Francisco, Calif., 12–16 August 1985. A.A. Balkema, Rotterdam, the Netherlands. Vol. 3, pp. 1445–1448.
66. Mitchell, J. K. (1976). "Fundamental of soil behavior," 1st edition, John Wiley & Sons, Inc.
67. Nakata, T., Miura S. and Kawamura, S. (1998). "Particle breakage and its evaluation of volcanic coarse-grained soils," *Proceeding of International Symposium on Problematic Soils*, Sendai, Japan, Vol.2, 145–148.
68. Nakata, Y., Hyde, A.F.L., Hyodo, M., Murata, H. (1999). "A probabilistic approach to sand particle crushing in the triaxial test," *Geotechnique* ,49(5) :567–83.
69. Nakata, Y., Kato, Y., Hyodo, M., Hyde, A.F.L., and Murata, M. (2001a). "one–

- dimensional compression behavior of uniformly graded sand related to single particle crushing strength," *Soils and Foundations*, 41: 39–51.
70. Nakata, Y., Hyodo, M., Hyde, A.F.L., Kato, Y., and Murata, H. (2001b). "Microscopic particle crushing of sand subjected to high pressure one – dimensional compression," *Soils and Foundations*, 41: 69–82.
 71. Nakata, Y., Hyodo, M., Murata, H., Hyde, A.F.L., and Ham, T.G. (2003). "Effect of water on particle breakage for decomposed granite soils," In *Deformation characteristics of geomaterials*. Edited by H. Di Benedetto, T. Doanh, H. Geoffroy, and C. Sauze´at. Taylor & Francis, London, 701–705.
 72. Nakata, Y., Bolton, M.D., and Cheng, Y.P. (2005). "Relating particle characteristics to macro behavior of DEM crushable material," In *Powders and grains*. Taylor & Francis Group, London, 1387–1391.
 73. Ni, Q., Tan, T. S., Dasari, G. R., and Hight, D. W. (2004). "Contribution of fines to the compressive strength of mixed soils," *Géotechnique*, 54(9):561–569.
 74. Nobari, E.S., and J.M. Duncan (1972). "Effect of reservoir filling on stresses and movements in earth and rockfill dams," Berkley: University of California, 165.
 75. Nova, R. and D. Wood (1979). "A constitutive model for sand in triaxial compression," *International Journal for Numerical and Analytical Methods in Geomechanics*, 3:277–299.
 76. Ohta, H., Yoshikoshi, H., Mori, Y., Yonetani, S., Itho, M., and Ishiguro, T. (2001). "Behavior of rockfill dam during construction," In *Proceedings of the 15th International Conference on Soil Mechanics and Geotechnical Engineering, Istanbul, Turkey, 27–31 August 2001*. A.A. Balkema, Rotterdam, the Netherlands. Vol. 2, pp. 1227–1231.
 77. Oldecop, L. A. and Alonso, E. E. (2001). "A model for rockfill compressibility," *Ge´otechnique*, 51, No. 2, 127–139.
 78. Ovando-Shelley, E. and Perez, B. E. (1997). "Undrained behavior of clayey sands in load controlled triaxial tests," *Ge´otechnique*, 47, 1, 91–111.
 79. Park, S. S., and Byrne, P. M. (2004). "Practical constitutive model for soil liquefaction," *Proc., 9th International Symposium on Numerical Models in Geomechanics (NUMOG IX)*, Taylor and Francis, London, 181–186.
 80. Pestana, J.M., and Whittle, A.J. (1995). "Compression model for cohesionless soils," *Ge´otechnique*, 45: 611–631.
 81. Pitman, T. D., Robertson, P. K. and Sego, D. C. (1994). "Influence of fines on the collapse of loose sands," *Canadian Geotechnical Journal*, Ottawa, Canada, 31, 728–739.

82. Prevost, J. H. (1981). "DYNA FLOW: A nonlinear transient finite element analysis program," Rep. No. 81-SM-1, Dept. of Civil Engineering, Princeton Univ., Princeton, NJ.
83. Rahim, A. (1989). "Effect of morphology and mineralogy on compressibility of sands," Ph.D. thesis, Indian Institute of Technology Kanpur, Kanpur, India.
84. Rahman, Md. Mizanur (2009). "Modelling the influence of fines on liquefaction behavior," Ph.D. thesis, The University of New South Wales at Australian Defense Force Academy, Australian.
85. Roscoe, K. H., Schofield, A. N. and Wroth, M. A. (1958). "On the yielding of soils," *Geotechnique*, 8, 22–53.
86. Rowe, P. W. (1962). "The stress-dilatancy relation for static equilibrium of an assembly of particles in contact," *Proceedings of the Royal Society, London*, A269, 500–527.
87. Sadrekarimi, A., Ghalandarzadeh, A., and Sadrekarimi, J. (2008). "Static and dynamic behavior of hunchbacked gravity quay walls," *Journal of Soil Dynamics and Earthquake Engineering*, 28(2): 99–117.
88. Sadrekarimi, A. and Olson, S. (2010). "Particle damage observed in ring shear tests on sands," *Canadian Geotechnical Journal*, 47: 497–515.
89. Kawabe, S., Sutoh, M. & Tatsuoka, F. (2011). Several factors affecting the viscous property of sand, *Deformation Characteristics of Geomaterials*: 646-653.
90. Takei, M., Kusakabe, O., and Hayashi, T. (2001). "Time-dependent behavior of crushable materials in one-dimensional compression test." *Soils and Foundations*, 41(1): 97–121.
91. Taiebat, M., and Dafalias, Y. F. (2008). "SANISAND: Simple anisotropic sand plasticity model," *International Journal of Numerical Models in Geomechanics*, 32(8), 915–948.
92. Tarantino, A., Hyde, A.F.L. (2005). "An experimental investigation of work dissipation in crushable materials," *Geotechnique*, 55(8): 575–584.
93. Thevanayagam S. (1998). "Effect of fines and confining stress on undrained shear strength of silty sands," *Journal of Geotechnical and Geoenvironmental Engineering*, 124(6):479–491.
94. Thevanayagam, S. and Shenthan, T., Mohan (2000). "Intergranular state variables and stress-strain behavior of silty sands," *Geotechnique* 50, No. 1, 1–23.
95. Thevanayagam, S., Shenthan, T., Mohan, S., and Liang, J. (2002). "Undrained fragility of clean sands, silty sands, and sandy silts," *Journal of Geotechnical and Geoenvironmental Engineering*, 128(10), 849–859.

96. Troncoso, J.H. & Verdugo .R. (1985). "Silt content and dynamic behavior of tailing sand," Proceeding of 11th JCSMFE, Balkema, Rotterdam, the Netherlands, 1311-1314.
97. Valdes, J.R., Caban, B. (2006). "Monitoring the hydraulic conductivity of crushing sands," *Geotechnical Test Journal*, 29(4):322–329.
98. Verdugo, R., and Ishihara, K. (1996). "The steady-state of sandy soils," *Soils and Foundation*, 36(2), 81–91.
99. Vesic, A. S., and Barksdale, R. D. (1963). "Discussion: shear strength at high pressures Lab. Shear Testing of Soils," *ASTM STP 361*, ASTM. Ottawa, Canada. 301–305.
100. Wang, Z. L., Dafalias, Y. F., and Shen, C. K. (1990). "Bounding surface hypoplasticity model for sand," *Journal of Engineering Mechanics*, 116(5), 983–1001.
101. Wang, Z. L., and Makdisi, F. I. (1999). "Implementation a bounding surface hypoplasticity model for sand into the FLAC program," *FLAC and numerical modeling in geomechanics*, Balkema, Rotterdam, Netherlands, 483–490.
102. Wang, Z.L., Dafalias, Y.F., Li, X.S., and Makdisi, F.I. (2002). "State pressure index for modelling sand behavior," *Journal of Geotechnical and Geoenvironmental Engineering*, ASCE, 128(6): 511–519.
103. Wang, G. and Xie, Y. (2014). "Modified Bounding Surface Hypoplasticity Model for Sands under Cyclic Loading," *Journal of Engineering Mechanics*, 140(1), 91–101.
104. Wood, D. M., Belkheir, K. and Liu, D. F. (1994). "Strain softening and state parameter for sand modelling," *Geotechnique*, England, 44(2), 335–339.
105. Woodward, P, K. (2001). "Advanced numerical modelling of granular soils," *Advanced numerical applications and plasticity in geomechanics*, CISM courses and lectures NO.426 international centre for mechanical sciences, 277–291.
106. Yamamuro, J. A. and Lade, P. V. (1993). "Effects of strain rate on instability of granular soils," *Geotechnical Testing Journal*, 16(3), 304–313.
107. Yamamuro, J.A., and Lade, P.V. (1996). "Drained sand behavior in axisymmetric test at high pressures," *Journal of Geotechnical and Geoenvironmental Engineering*, ASCE, 122: 109–119.
108. Yang, Z. H., Elgamal, A., and Parra, E. (2003). "Computational model for cyclic mobility and associated shear deformation," *Journal of Geotechnical and Geoenvironmental Engineering*, 129(12), 1119–1127.
109. Yang, S. L., Sandven R., and Grande, L. (2006). "Steady state lines of sands- silt

- mixtures," *Canadian Geotechnical Journal*, 43, 1213–1219.
110. Ma, H.L., Yang, C.H., Liu, J.F., Chen, J.W. (2013). "The influence of cyclic loading on deformation of rock salt," *Rock Characterization, Modelling and Engineering Design Methods*, 63–68.
 111. Yasufuku, N., and Hyde, A.F.L. (1995). "Pile end-bearing capacity in crushable sands," *Geotechnique*, 45(4): 663–676.
 112. Yin, Z. Y., Chang, C., and Hicher, P. (2010). "Micromechanical modelling for effect of inherent anisotropy on cyclic behavior of sand," *International Journal of Solids and Structure*, 47(14–15), 1933–1951.
 113. Yin, Z. Y. and Chang, C. (2013). "Stress-dilatancy behavior for sand under loading and unloading conditions," *Journal for Numerical and Analytical Methods in Geomechanics*, 37(8), 855–870.
 114. Zienkiewicz, O. C., Chan, A. H. C., Pastor, M., Schrefler, B. A., and Shiomi, T. (1999). "Computational geomechanics: With special reference to earthquake engineering," Wiley, New York.
 115. Zlatovic, S., and Ishihara, K. (1995). "On the influence of nonplastic fines on residual strength," 1st International Conference on Earthquake Geotechnical Engineering, Rotterdam, The Netherlands. 239–244.